Gravitational waves from neutron stars:
detection prospects and inferences for two distinct types of remnants

Lectures 1 & 2 - Binary neutron star mergers

José Antonio Font
Universitat de València
www.uv.es/virgogroup

Outline

- Motivation
- Gravitational wave astronomy (LVK detections)
- BNS signals: GW170817 & GW190425
- Modellisation of BNS waveforms
- Detection prospects and inferences:
  - Inspiral
  - Early postmerger
  - Late postmerger

- Few remarks on topics untouched

Motivation

Fields impacted from the study of BNS mergers:

- Gravitational wave physics: among strongest source.
- Neutron star properties: laboratory to study high-density matter; key to decipher NS properties (e.g. radius and EoS).
- GRB physics: central engine of short gamma-ray bursts. BNS merger GRB association.
- Nucleosynthesis of heavy elements: kilonova emission due to the radioactive decay of by-products of the r-processed matter from the material ejected in the merger.
- Cosmology: measure of Hubble parameter with GW information (BNS as standard sirens).

Most of the above firmly supported by the one single multi-messenger observation of GW170817.

Motivation

Fields impacted from the study of BNS mergers:

- Gravitational wave physics: among strongest source.
- Neutron star properties: laboratory to study high-density matter; key to decipher NS properties (e.g. radius and EoS).
- GRB physics: central engine of short gamma-ray bursts. BNS merger GRB association.
- Nucleosynthesis of heavy elements: kilonova emission due to the radioactive decay of by-products of the r-processed matter from the material ejected in the merger.
- Cosmology: measure of Hubble parameter with GW information (BNS as standard sirens).

Most of the above firmly supported by the one single multi-messenger observation of GW170817.

Gravitational-wave spectrum

Adapted from: Romano, J.D., Cornish, N.J.
Living Rev Relativ 20, 2 (2017).
https://doi.org/10.1007/s41114-017-0004-1

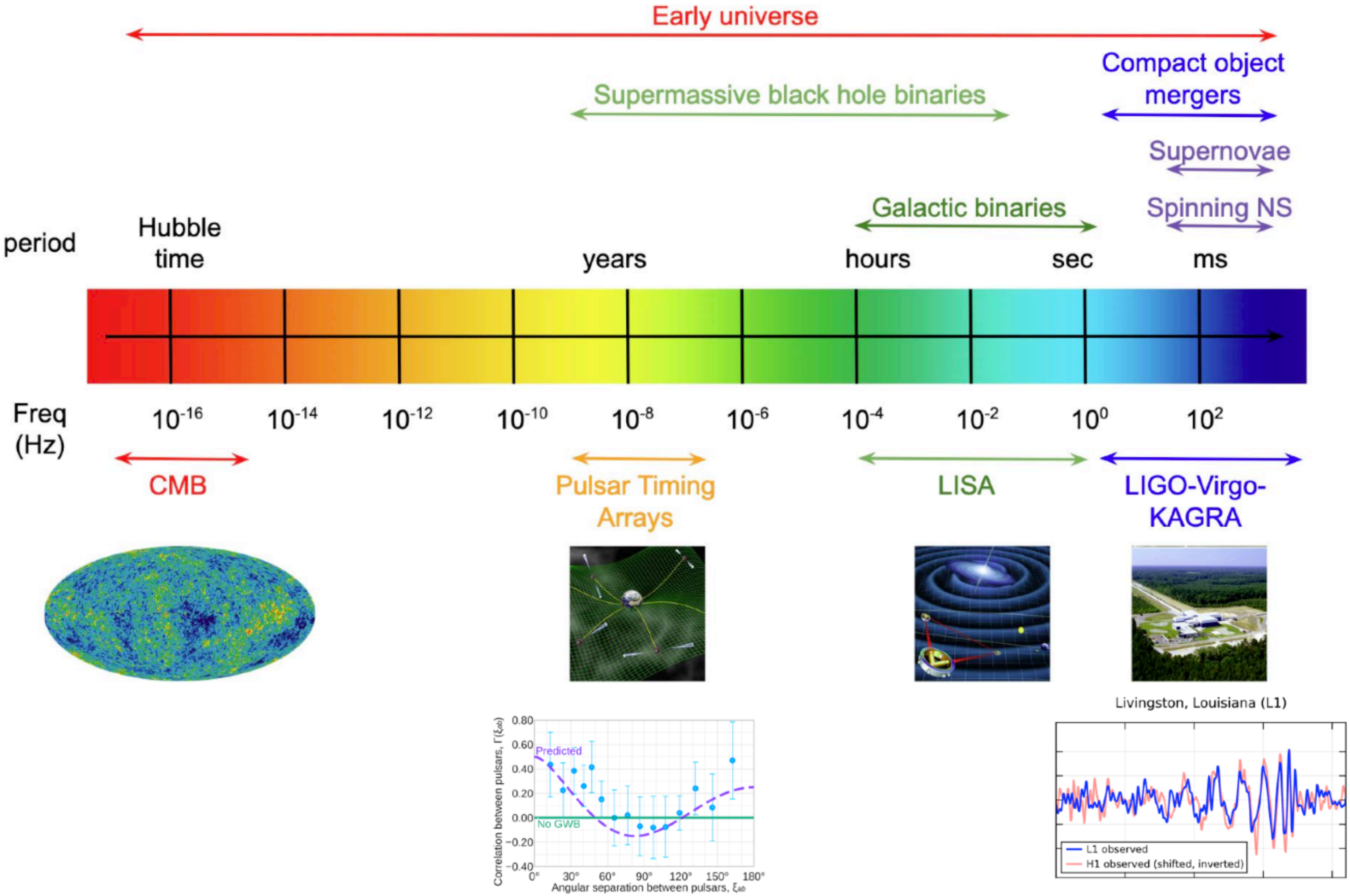

June 2023 (NANOGrav, EPTA, PPTA, InPTA, CPTA)

September 2015 (LIGO)

Gravitational-wave spectrum

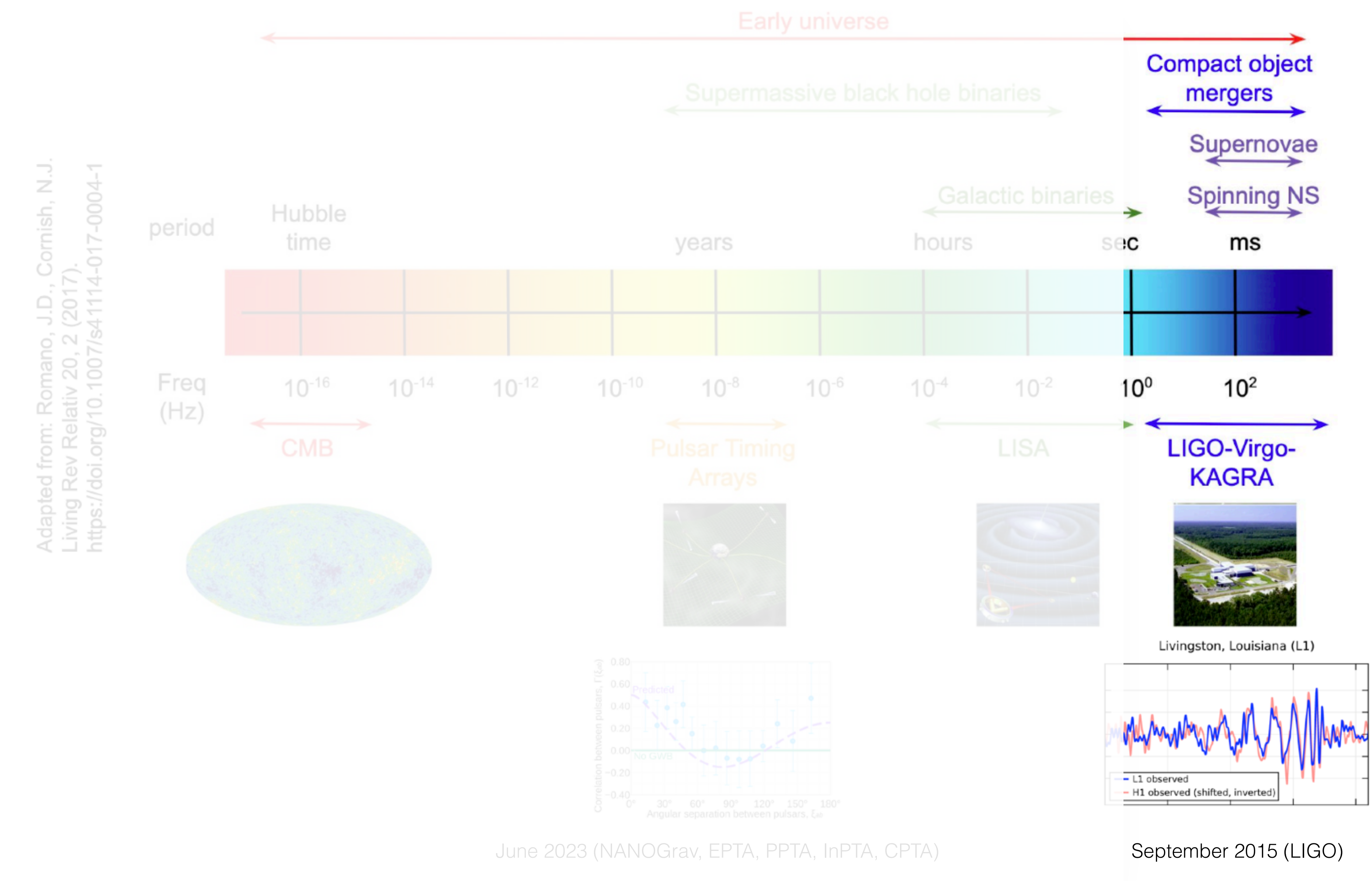

Gravitational waves: present-day detectability region

Prime astrophysical sources of GW: compact objects (neutron stars and black holes) with matter at relativistic speeds.

$$\mathcal{L} \sim \varepsilon^2 \frac{c^5}{G} \left(\frac{R}{R_S}\right)^{-2} \left(\frac{v}{c}\right)^6 \qquad \mathcal{L} \sim 10^{59} \mathrm{erg\ s}^{-1} \sim 10^{25} \mathcal{L}_\odot \sim 10^{51} \mathrm{W}$$

Gravitational radiation

$$f \leq \frac{c^3}{4\pi G M} \sim 10^4 \left(\frac{M}{M_\odot}\right)^{-1} \mathrm{Hz}$$

within the audible range

$$[20\,\mathrm{Hz}, 20\,\mathrm{kHz}]$$

Electromagnetic radiation

$$f \geq 10^7\,\mathrm{Hz}$$

visible light: $f \sim 10^{11}\,\mathrm{Hz}$

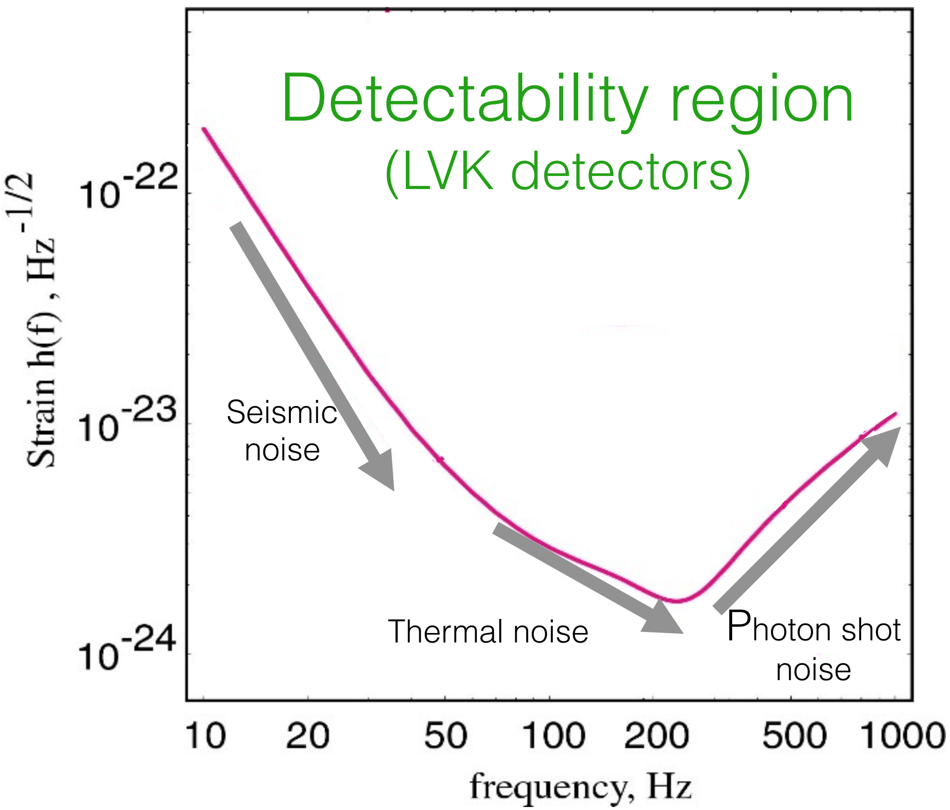

Orbital evolution B1913+16

Orbital evolution of the Hulse-Taylor binary pulsar agrees with that of a compact binary system that emits gravitational radiation according to GR.

(1993)

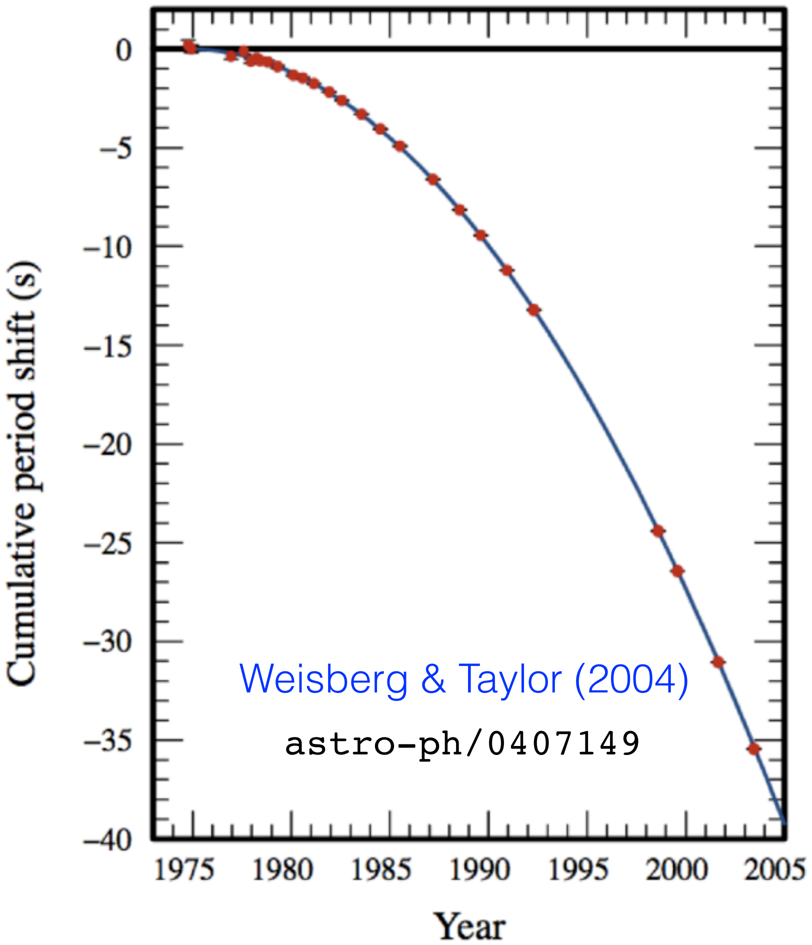

$$t_{\rm coal} = \frac{5}{256}\frac{c^5}{G^3}\frac{(l_0^{\rm in})^4}{\mu M^2}$$

$$\approx 1542 \times 10^6 \text{ years}$$

See also Burgay et al (2003) for results on PSR J0737-3039

Galactic compact BNS systems observed

Examples of Galactic BNS that will merge within a Hubble time (13.7 Gyr)

Lorimer (2008)

System	P(day)	e	$M_1(M_{sun})$	$M_2(M_{sun})$	$M(M_{sun})$	$\tau_{\rm GW}(10^8 {\rm yr})$
B1913+16	0,323	0,617	1.39	1.44	2.83	2.45
B1534+12	0,421	0,274	1.33	1.35	2.69	22.5
B2127+11C	0,335	0,681	1.35	1.36	2.71	2.2
J0737-3039	0,102	0,088	1.35	1.24	2.58	0.85
J1756-2251	0,320	0,180	1.31	1.26	2.58	1.69
J1906-0746	0,166	0,085	1.25	1.37	2.62	3.0

$$\tau_{\rm GW} = \frac{5}{64}\frac{a^4}{\mu M^2} = 2.2\times 10^8 q^{-1}(1+q)^{-1}\left(\frac{a}{R_\odot}\right)^4\left(\frac{M_1}{1.4M_\odot}\right)^{-3} \; {\rm yr}$$

[according to lowest-order dissipative contribution from GR (2.5PN level); both NSs point masses.]

A global GW detector network

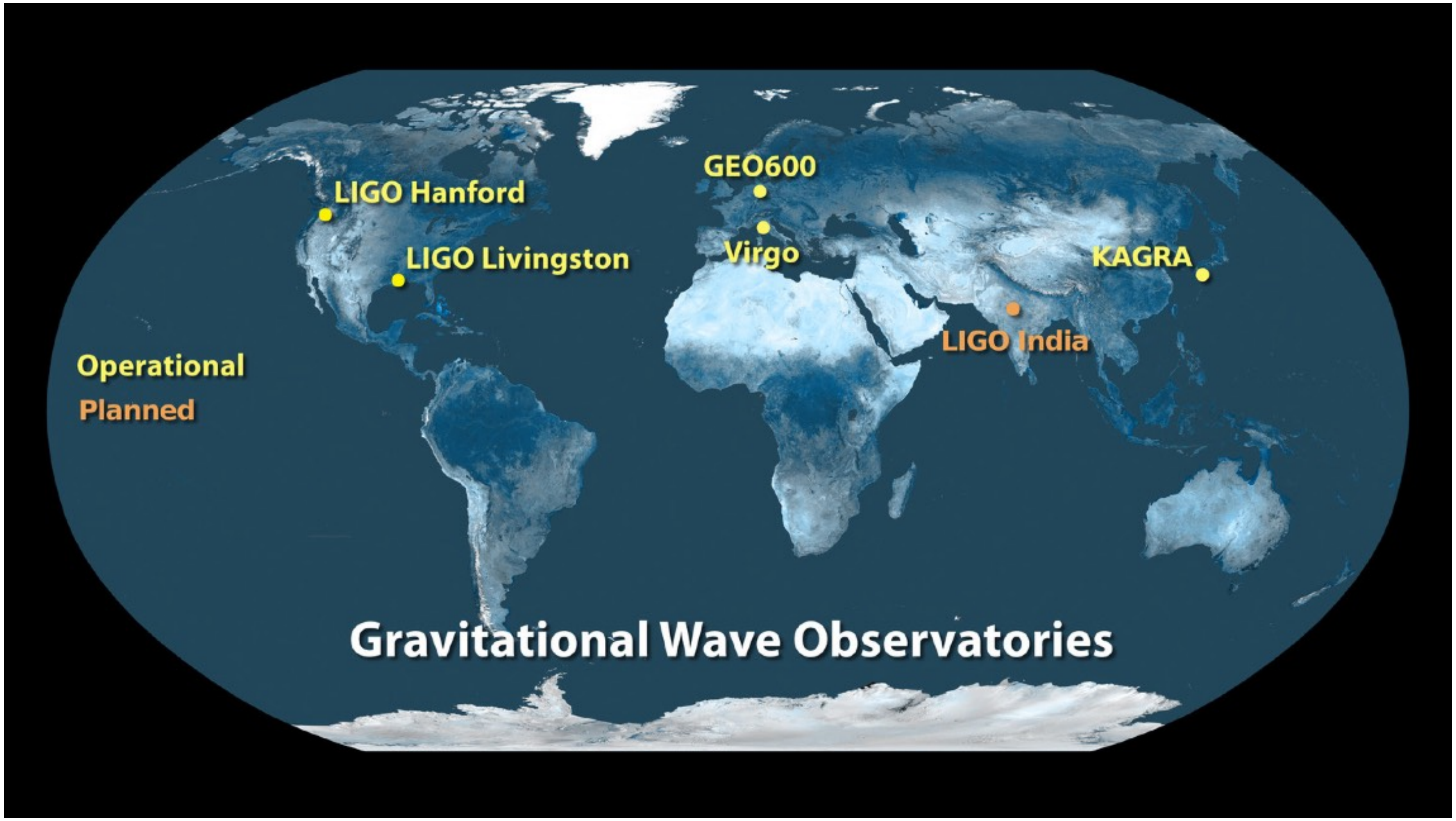

- km-scale interferometers
- sensitive to GWs between a few Hz to a few kHz
- simultaneous detection increases detection confidence
- improved sky localisation and polarization

Observing timeline

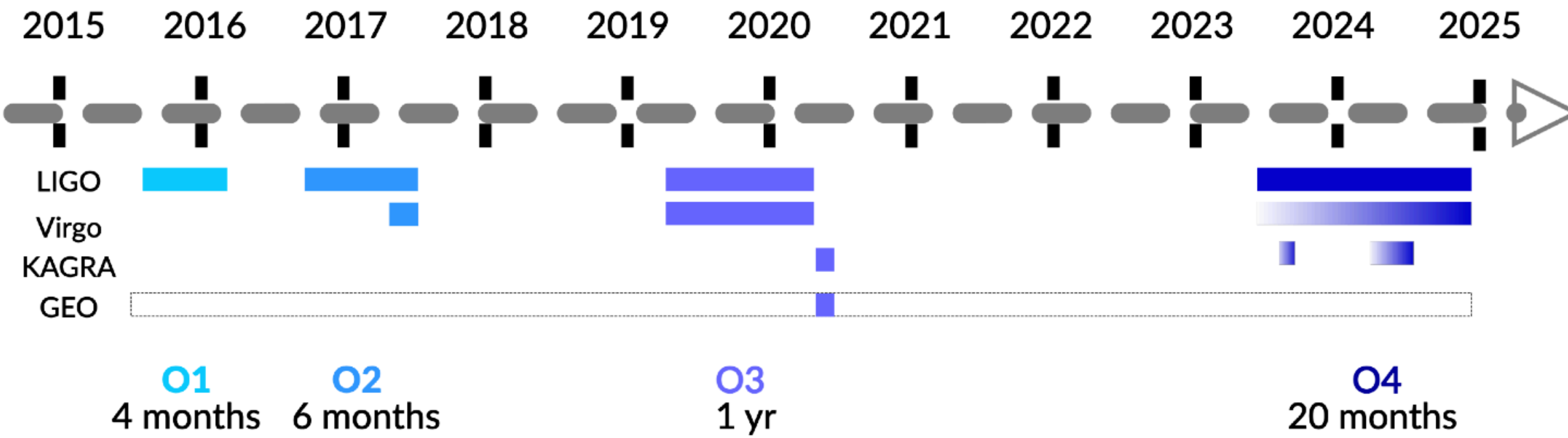

More details at: https://observing.docs.ligo.org/plan/

All data is **public**: Gravitational Wave Open Science Center (www.gw-openscience.org)

Detectors' sensitivities and BNS range during O3

Sensitivities during O3
(2019-2020)

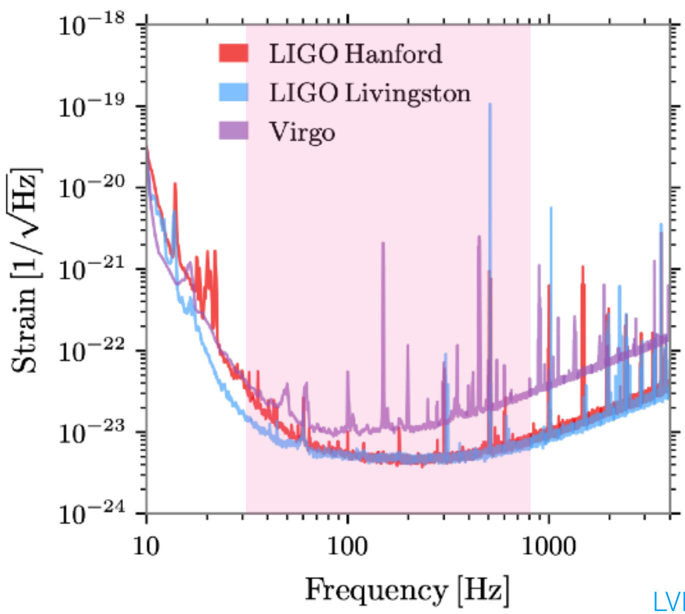

Distance range to BNS mergers
(averaged over sky position and inclination)

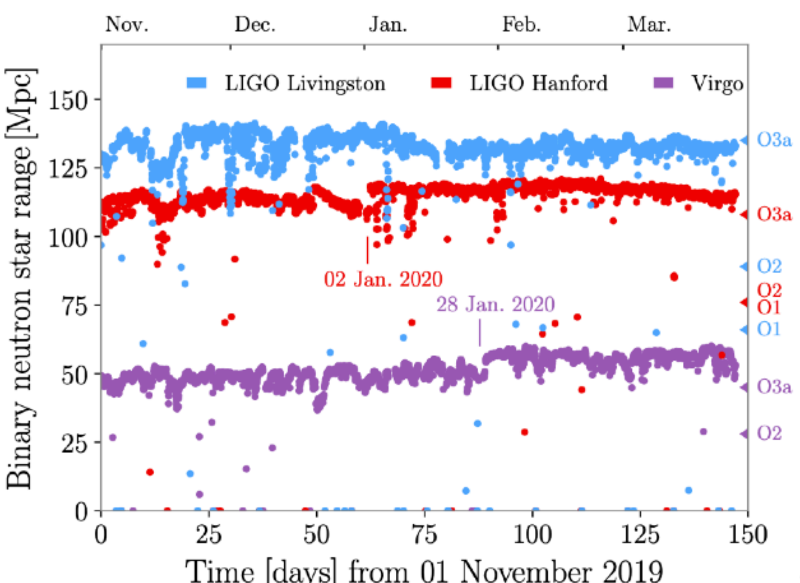

L1: 135 Mpc
H1: 115 Mpc
V1: 50 Mpc

LVK arXiv:2111.03606

1 parsec = 3.26 ly
= 31 x 10^{12} km

Observing timeline

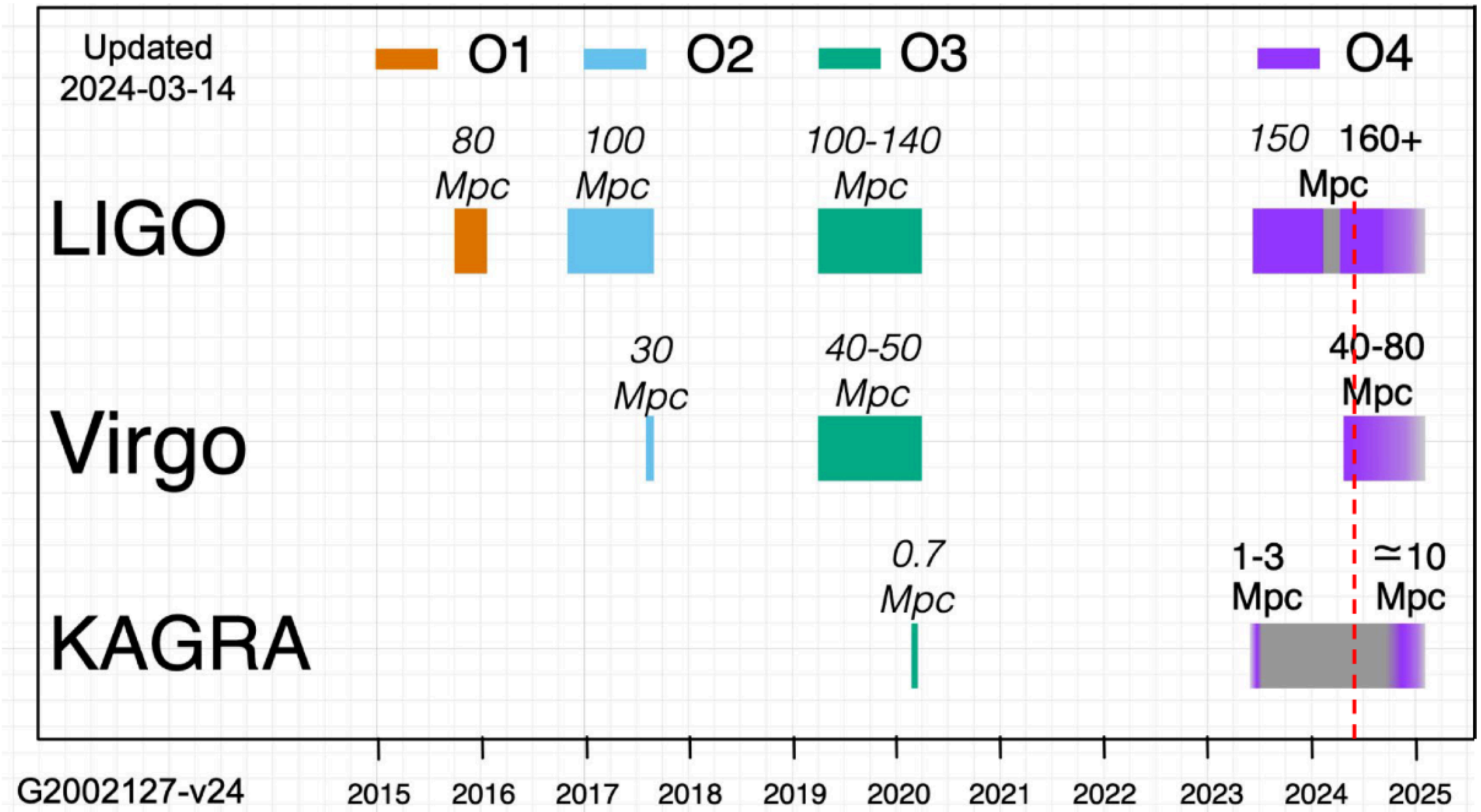

More details at: https://observing.docs.ligo.org/plan/

GW observations

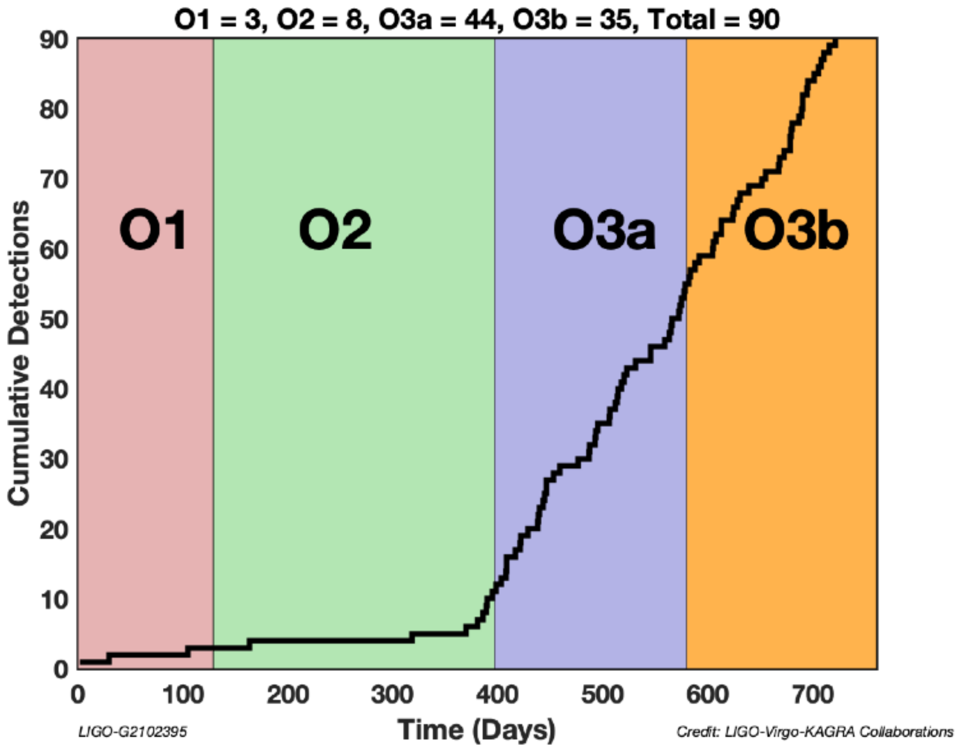

GWTC-1:

11 GW events from O1 & O2

Including GW150914 & GW170817

GWTC-2 & GWTC-2.1:

44 new GW events (O3a)

GWTC-3:

35 new GW events (O3b)

O3 detection rate ~ 1 event every 5 days

GW observations

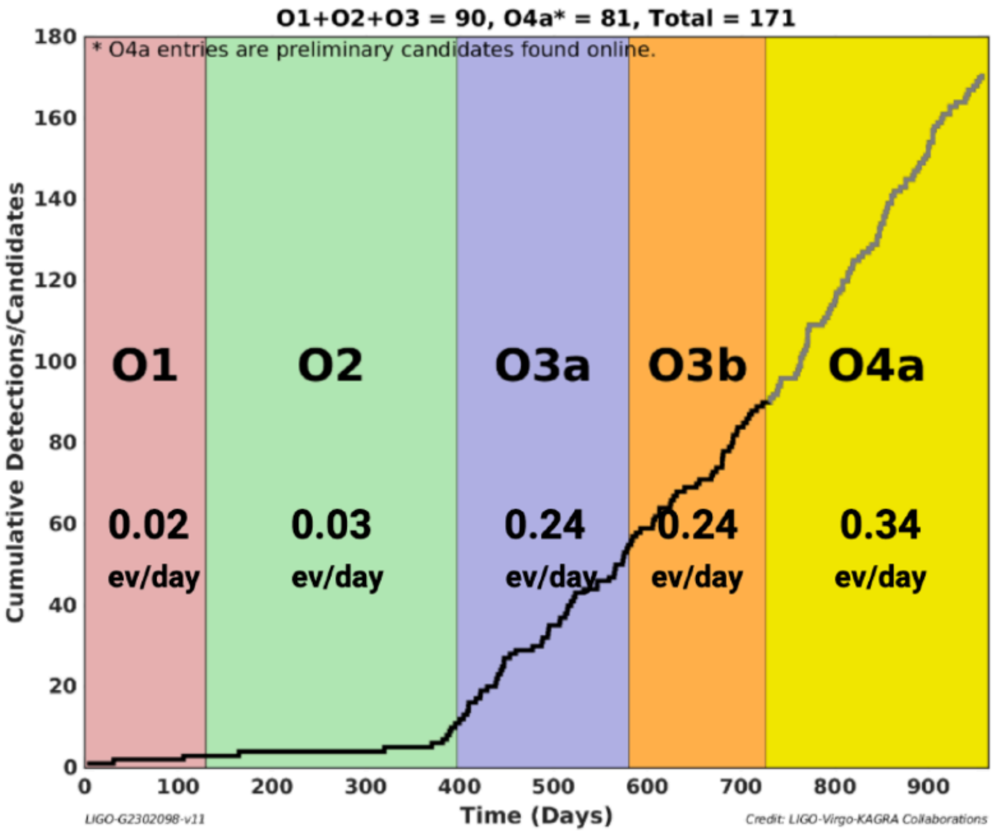

O4a significant detection candidates: 81 (92 total, 11 retracted)

[O4a entries are preliminary candidates found online]

GW observations (O1-O3)

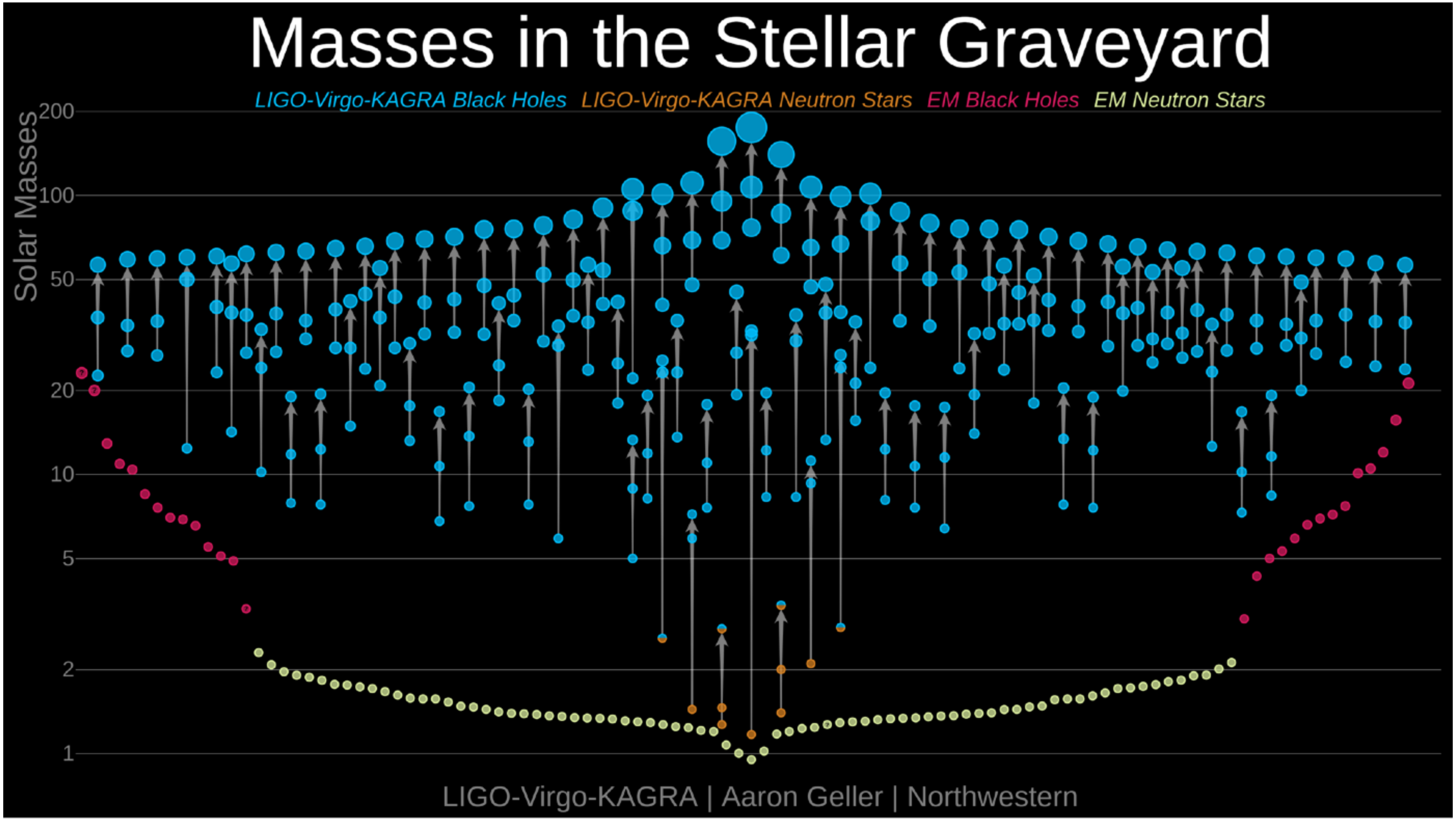

All events through end of O3 with p_astro > 0.5

GW observations (O1-O3)

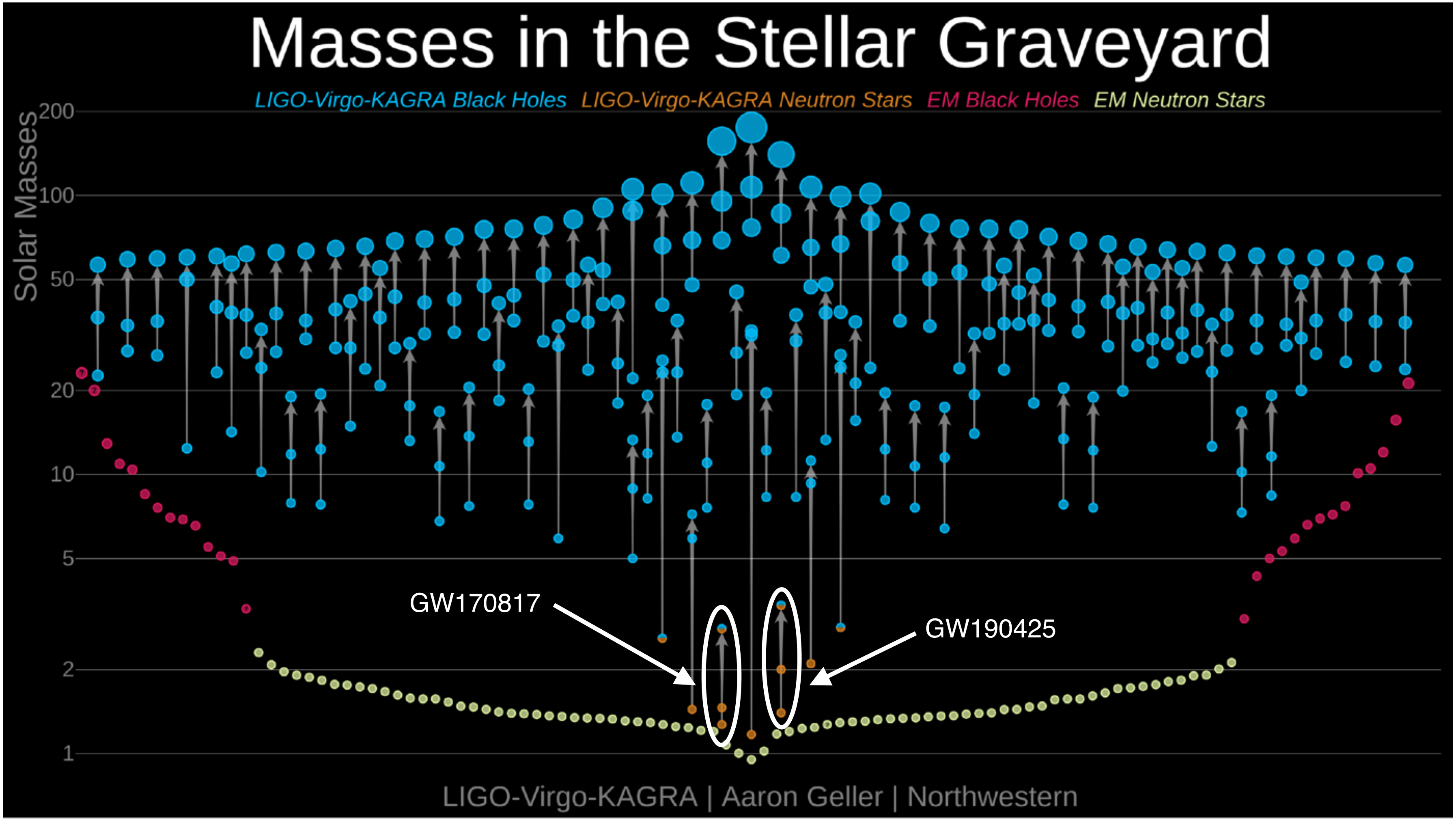

All events through end of O3 with p_astro > 0.5

LVK BNS mergers - GW170817

GW170817 & GRB170817A & AT2017gfo

Dozens of EM follow-up observations: **multi-messenger astronomy**

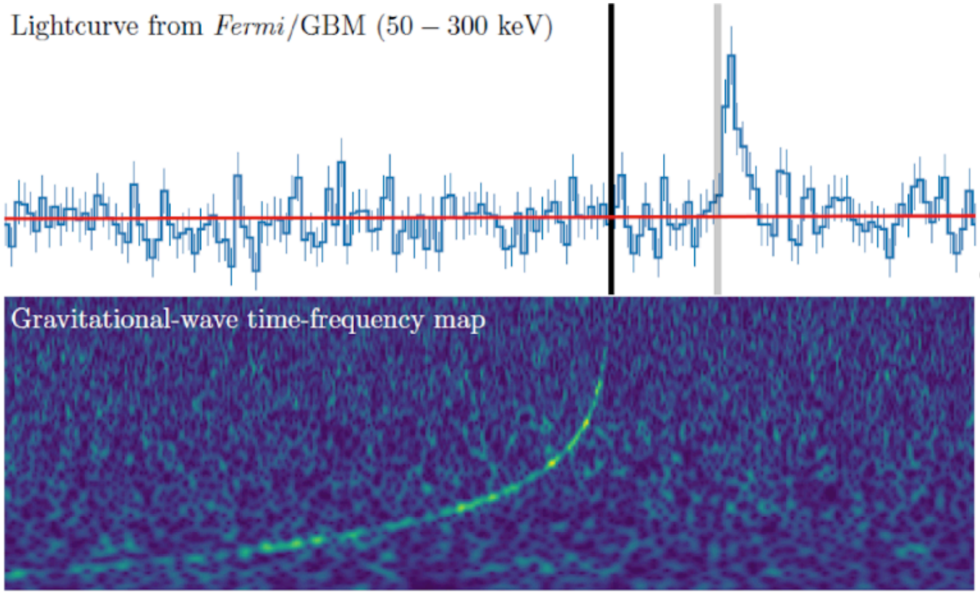

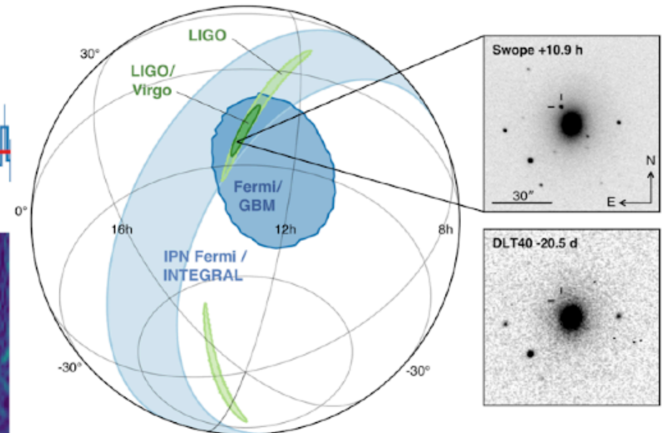

Large impact in astrophysics, cosmology, and nuclear physics:

- BNS/sGRB association
- Support for the kilonova model, heavy element nucleosynthesis
- Measurement of H_0 (BNS as standard siren)
- Constraints on EOS of high-density matter (tidal deformability)

Zoom on the kilonova in NGC 4993

Does the kilonova model work for GW170817?

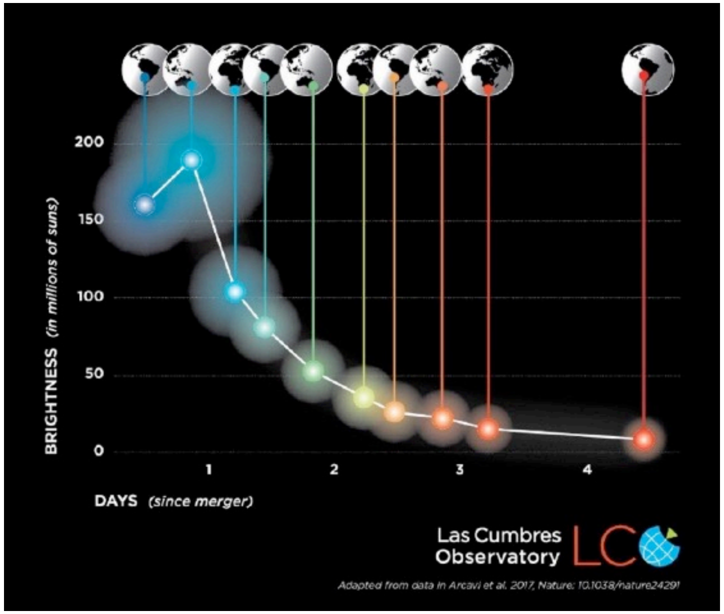

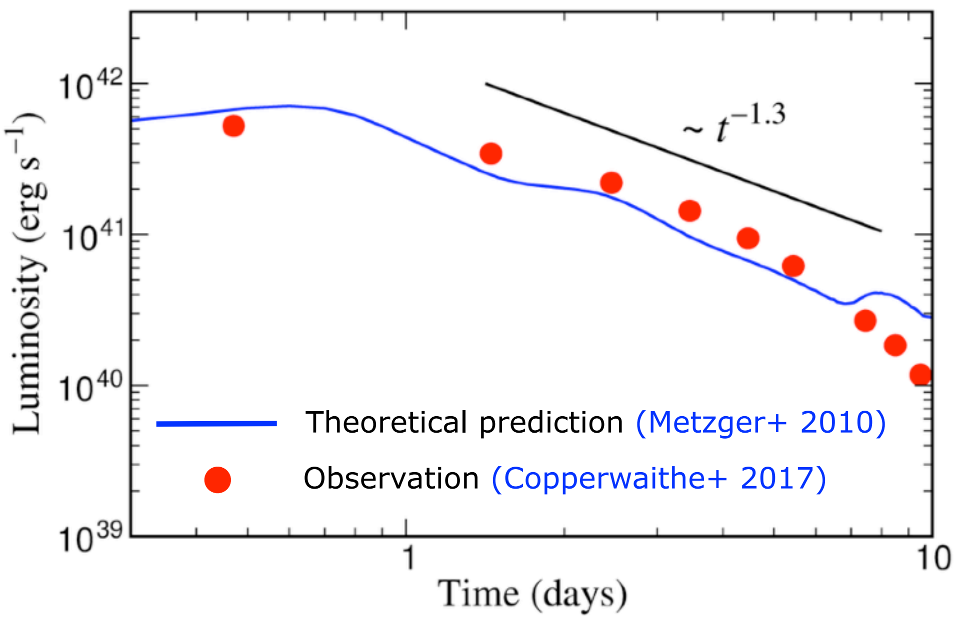

Temporal evolution of the kilonova determined by radiactive decay of nuclei. Two components:

Blue: dominated by light elements (Z < 50)

Red: presence of de lanthanides (Z = 57-71) and/or actinides (Z = 89-103)

GW170817
0.06 solar masses ejected → 10x Earth mass of gold
50x Earth mass of platinum
5x Earth mass of uranium

LVK BNS mergers - GW190425

GW190425: Observation of a Compact Binary Coalescence with Total Mass ~ 3.4 $M_\odot$
(LVC, ApJL, 892:L3, 2020)

Most likely 2nd BNS merger after GW170817 (BBH or NSBH cannot be ruled out)

2 interferometer detection: L1 + Virgo (poor sky localisation; no EM counterpart)

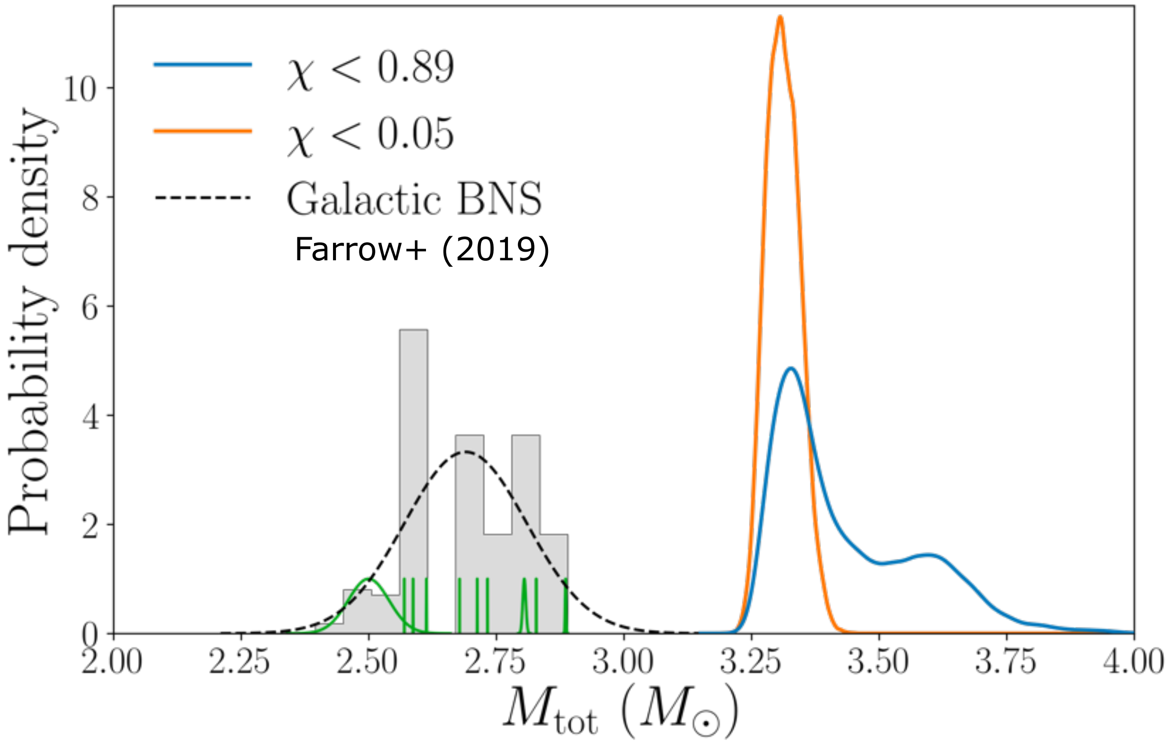

Total mass larger than any known system so far. A new population?

LIGO-Virgo-KAGRA physics program

Transient GW signals

Compact Binary Coalescences (CBC)
modelled

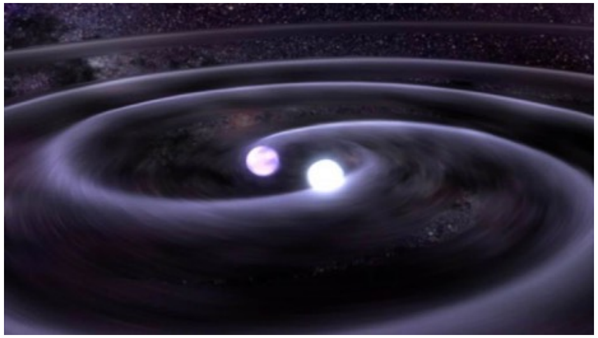

Bursts (e.g. supernovae) unmodelled

Long(er) duration GW signals

Continuous waves
(e.g. rotating neutron stars)

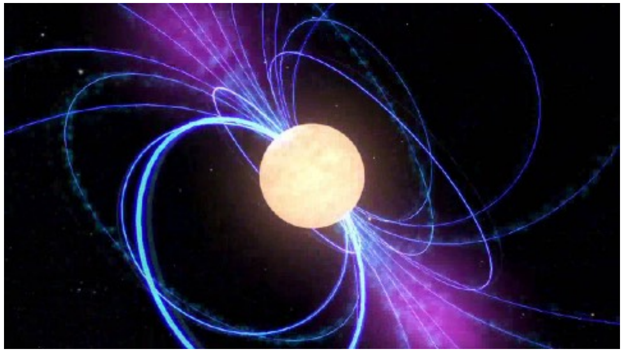

Stochastic GW background

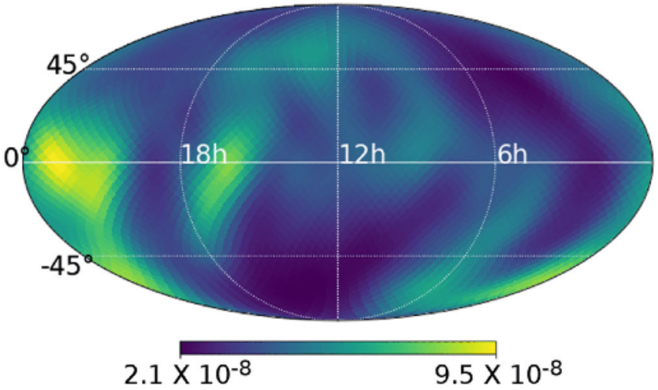

LIGO-Virgo-KAGRA physics program

Transient GW signals

Compact Binary Coalescences (CBC) modelled

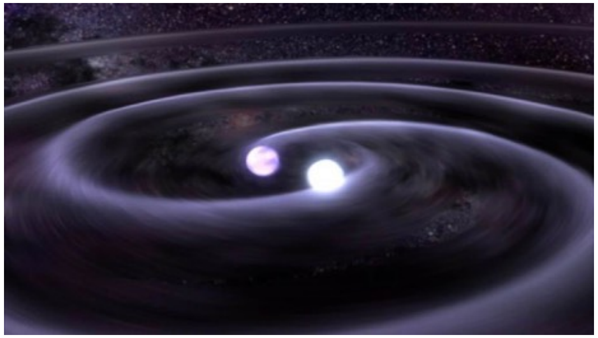

Bursts (e.g. supernovae) unmodelled

Long(er) duration GW signals

Continuous waves (e.g. rotating neutron stars)

Stochastic GW background

GW observations

All events detected so far are consistent with **compact binary coalescences**.

Signal "chirps" in the sensitivity band of the detector.

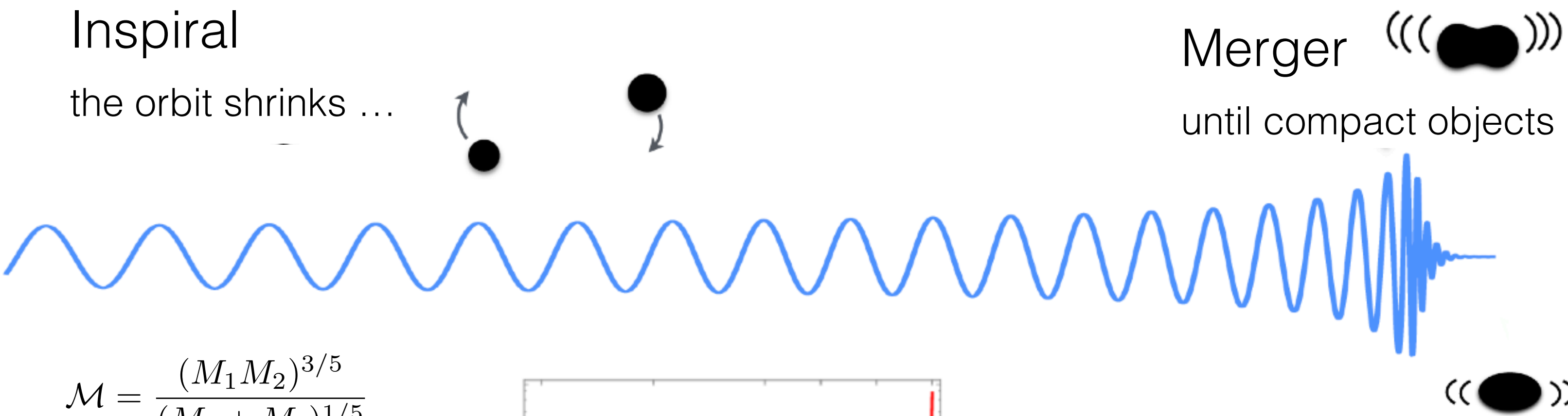

$$\mathcal{M} = \frac{(M_1 M_2)^{3/5}}{(M_1 + M_2)^{1/5}}$$

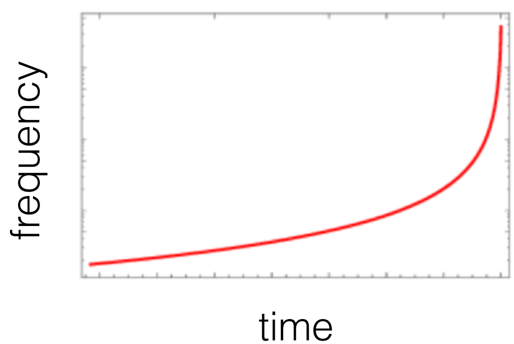

Ringdown

and form a single black hole

Until merger, B1913+16 will be emitting a distinctive "chirp" gravitational wave signal, a universal waveform for all coalescing, quasi-circular binary systems.

CBC sources - modelled sources

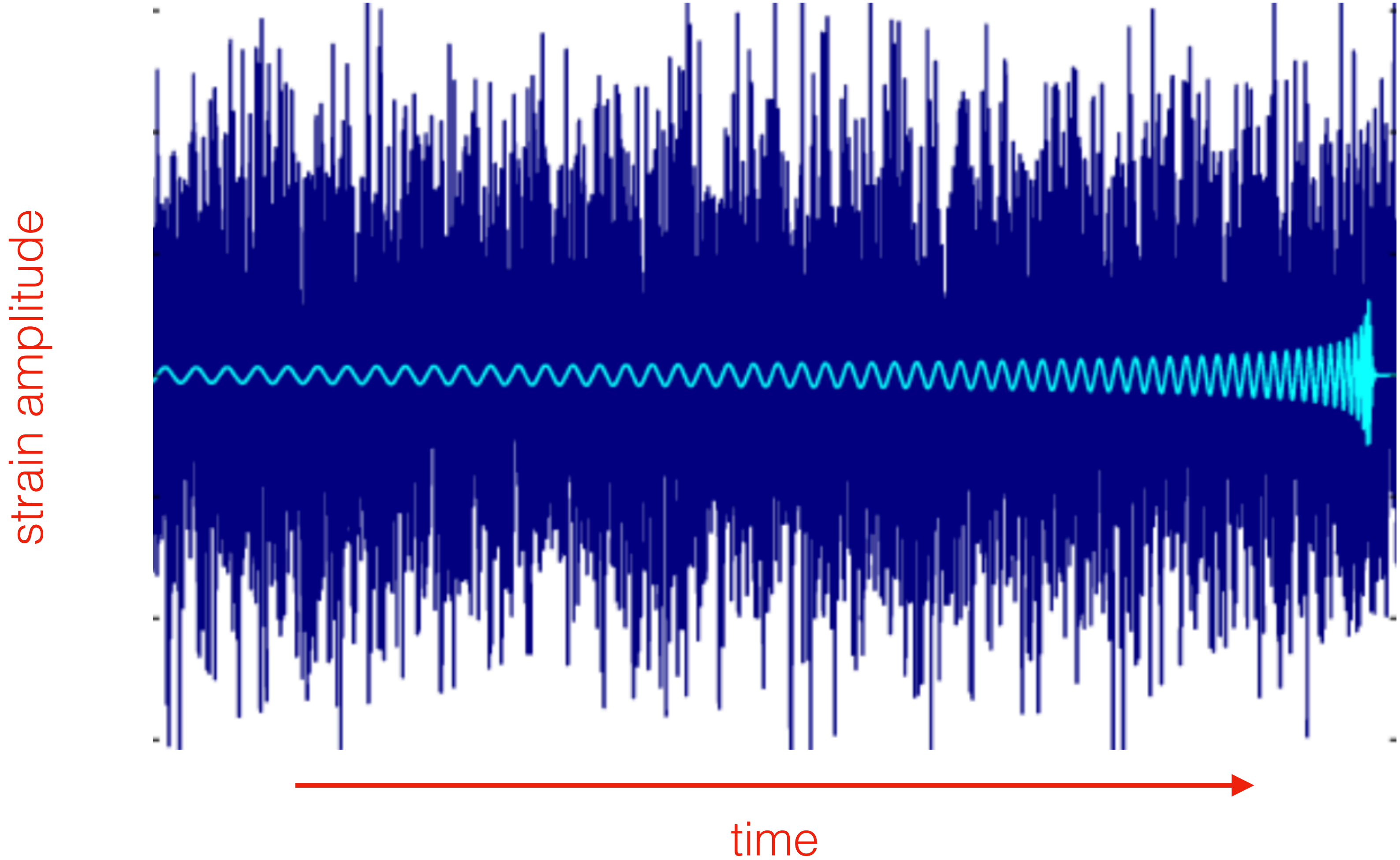

GW signal buried into noise. To dig the signal out, searches are based on **matched-filtering** using template banks from GR.

CBC waveform modelling

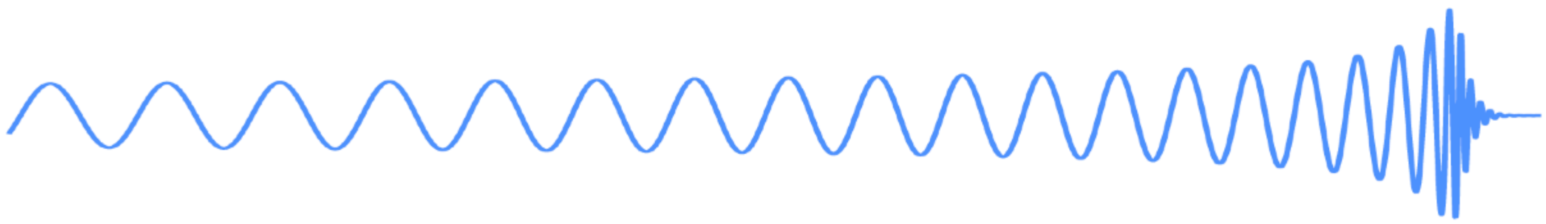

Huge amounts of template waveform banks required for both **detection** and **parameter estimation**. Banks **incomplete** in some regions of the parameter space (large mass ratio, precession, non QC orbits, …).

Numerical relativity is our best tool to model CBC waveforms. **But**: incomplete physics, insufficient resolution, memory and computer power limitations. Very expensive.

Synergy between numerical relativity and analytical relativity fundamental.

Machine Learning can help complete template banks, aid searches and PE.

Aspects to improve:

- increase mass ratio and harmonic content
- decrease WF systematics
- non-QC binaries (eccentricity, dynamical captures, hyperbolic encounters)
- WF models for exotic compact objects?
- WF models beyond GR?

BNS mergers

Before merger $(20\,\mathrm{Hz} < \nu <\sim \mathrm{kHz})$ After merger $(\nu >\sim \mathrm{kHz})$

post-Newtonian / EOB Numerical Relativity

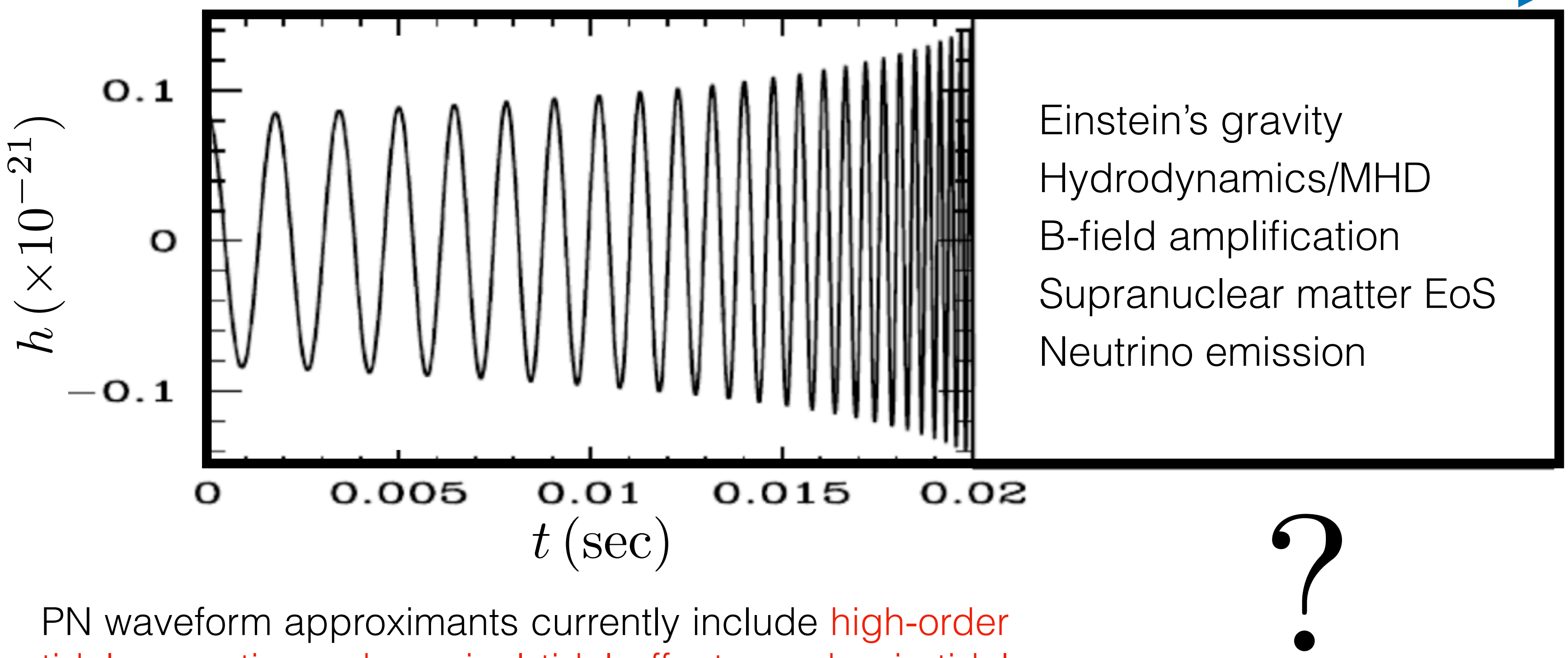

PN waveform approximants currently include high-order tidal corrections, dynamical tidal effects, and spin-tidal couplings.

Present-day tidal waveform models for BNS mergers are mostly based on the EOB approach.

Post-merger waveform is the current frontier

NR waveform approximants - A challenging numerical problem

Mathematically & Physically:

- **strong gravitational fields**
- matter motion with **relativistic speeds**
- **shock waves**
- **strong magnetic fields**
- **Nuclear physics:** EoS, radiation transport, nuclear reaction networks

Numerically:

- intrinsic **multidimensional** character
- inherent issues in Einstein's gravity: **coordinate degrees of freedom** and **curvature singularities** (BH formation)
- **spatial scales:** near zone vs wave zone

Computationally:

- Time-dependent problem: Major resources needed in terms of memory and CPU. Large parameter space. **Supercomputers.**

Despite difficulties, major progress achieved during ~ **last 25 years** in NR simulations of BNS mergers.

Numerical Relativity: Our basic theoretical model

- **Einstein's field equations** $$R_{\mu\nu} - \frac{1}{2} g_{\mu\nu} = 8\pi T_{\mu\nu}$$

Formulations: BSSN, Z4, GHF (hyperbolicity).
Methods: high-order finite differencing, (pseudo-)spectral methods.

- **Hydrodynamics equations** $$\nabla_\mu T^{\mu\nu} = 0 \qquad \nabla_\mu (\rho u^\mu) = 0$$

Flux-Conservative hyperbolic formulations ("Valencia").
Methods: high-order shock-capturing finite volume.

Current frontier:

- initial data (eccentric orbits, spins, precession)
- microphysics for tabulated thermal EOS
- magnetic fields (KHI, MRI, amplification, jet formation)
- dissipative (non ideal) fluids
- neutrino radiation transport (full Boltzmann, M1)
- nucleosynthesis (nuclear reaction network)

Most simulations: hybrid (piece polytropic + ideal gas) EoS; few include tabulated thermal EoS, neutrino effects, MHD (B-field amplification), and viscosity.

Example: Computational Relativity (CoRe) collaboration's public database of GWs from BNS mergers. (www.computational-relativity.org)

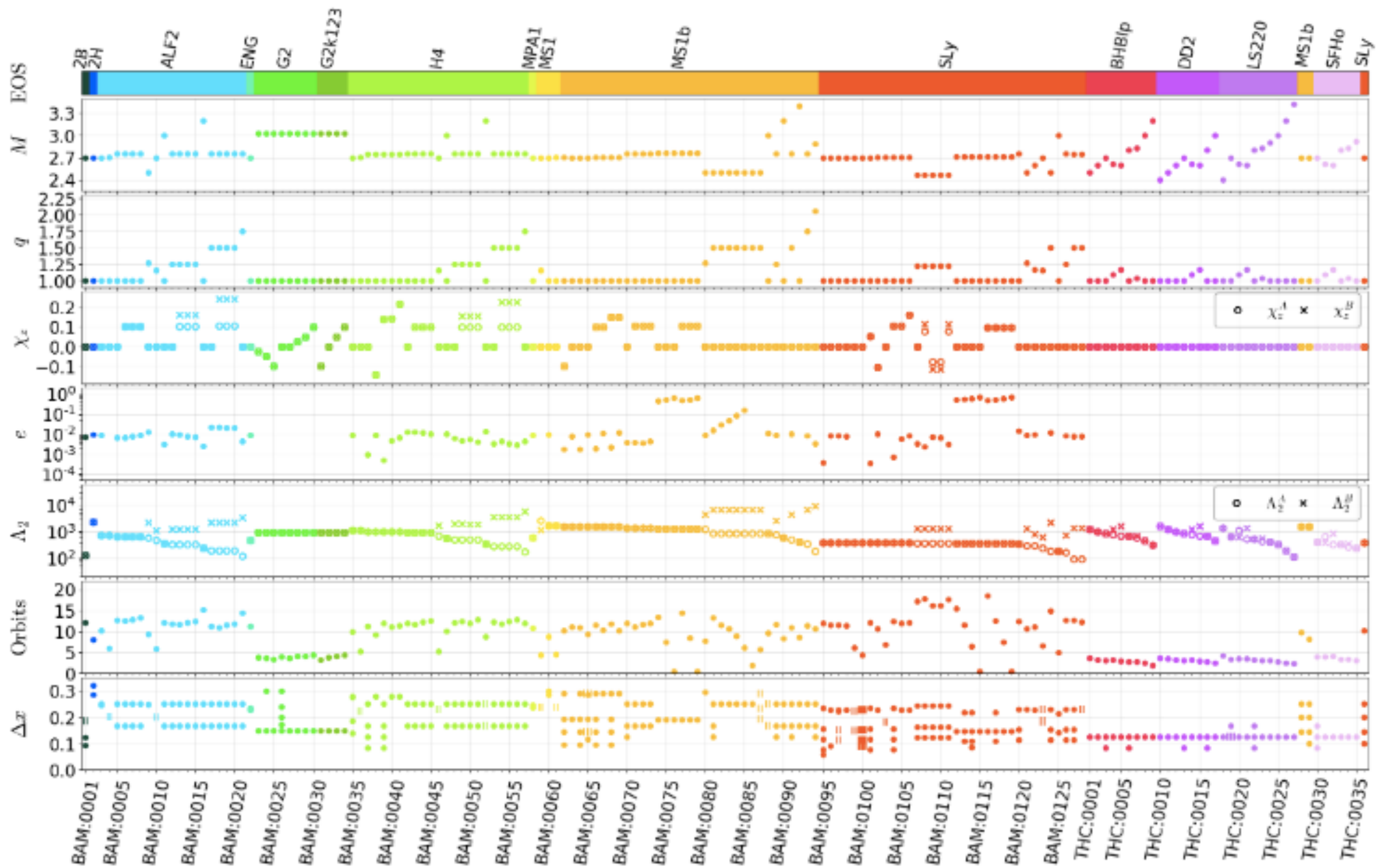

367 waveforms, 150 million CPU-hours on supercomputers

NR waveforms fundamental to validate LIGO-Virgo PE pipelines

Dietrich+ 2018
1806.01625

CoRe BNS database (www.computational-relativity.org)

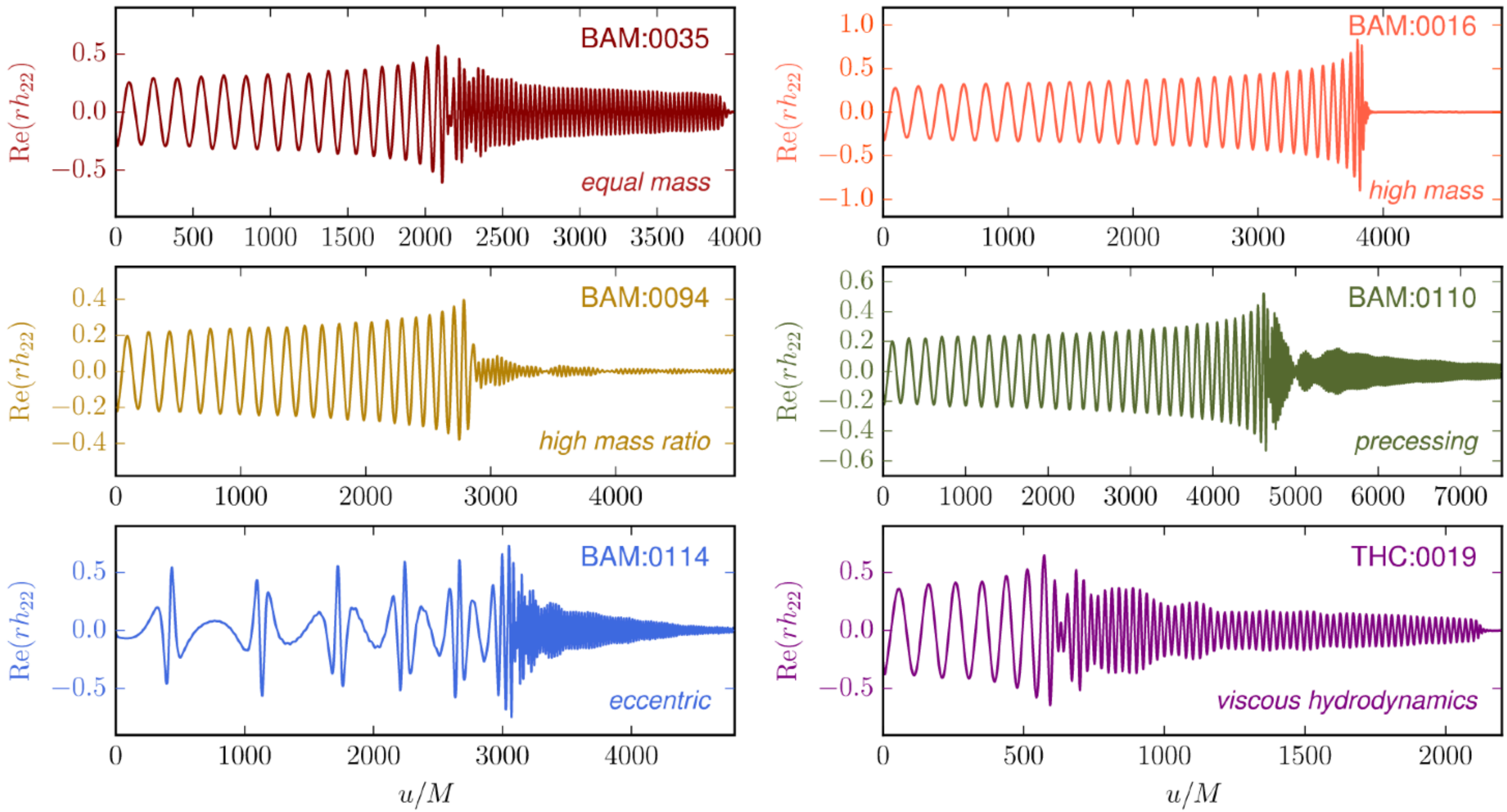

Dietrich+ 2018
1806.01625

2nd release of the database (590 waveforms)
González+ 2023
2210.16366

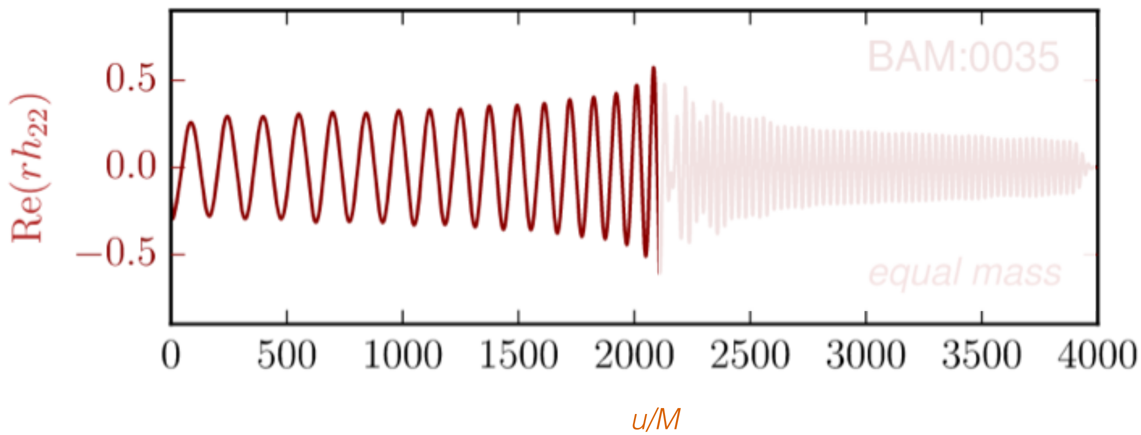

(Late) inspiral

Tidal deformability and measurability of NS properties

NS in binary systems produce mutual tidal stresses that deform the metric around the star in an EoS-dependent manner, through the **tidal deformability parameter**.

$$\Lambda = \frac{2}{3} k_2 \left(\frac{R}{M} \right)^5$$

k_2 quadrupolar Love number

Both R and k_2 are fixed for a given stellar mass M by the EoS ($k_2 \simeq 0.05$–0.15 for realistic neutron stars; $k_2=0$ for BHs).

The tidal deformability parameter describes the degree to which a local metric suffers quadrupole deformations when in the tidal field of a companion.

Large tidal effects on BNS mergers observed in numerical simulations of late inspiral.

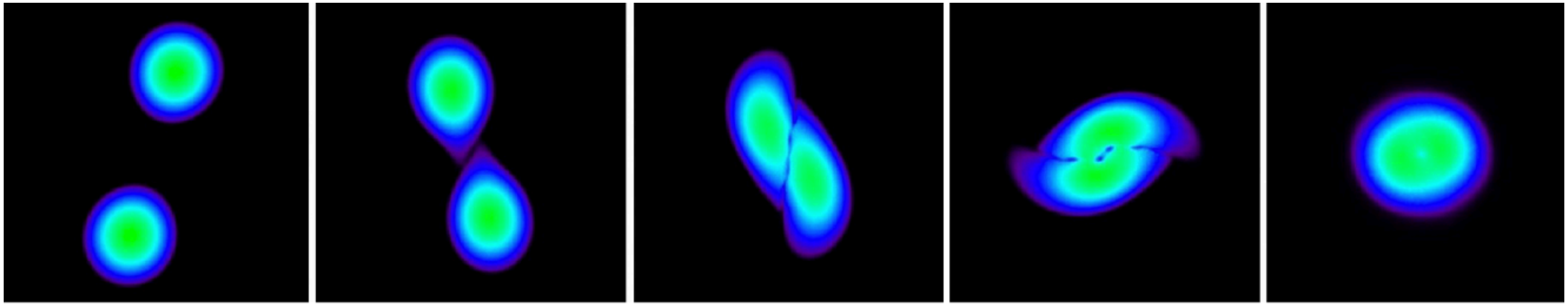

(cf. Bauswein)

It determines the $(\ell, m) = (2, 0)$ departure of the asymptotic metric from spherical symmetry and the departure of **waveform phase evolution** from point-particle form.

Tidal deformability and measurability of NS properties

Orbital phase evolution affected by tidal deformability, as GW frequency increases. Effect becomes significant above f_{GW}~600 Hz (only last orbits before merger), potentially observable.

Inspiral **accelerated** compared to point-particle inspiral for larger Lambda.

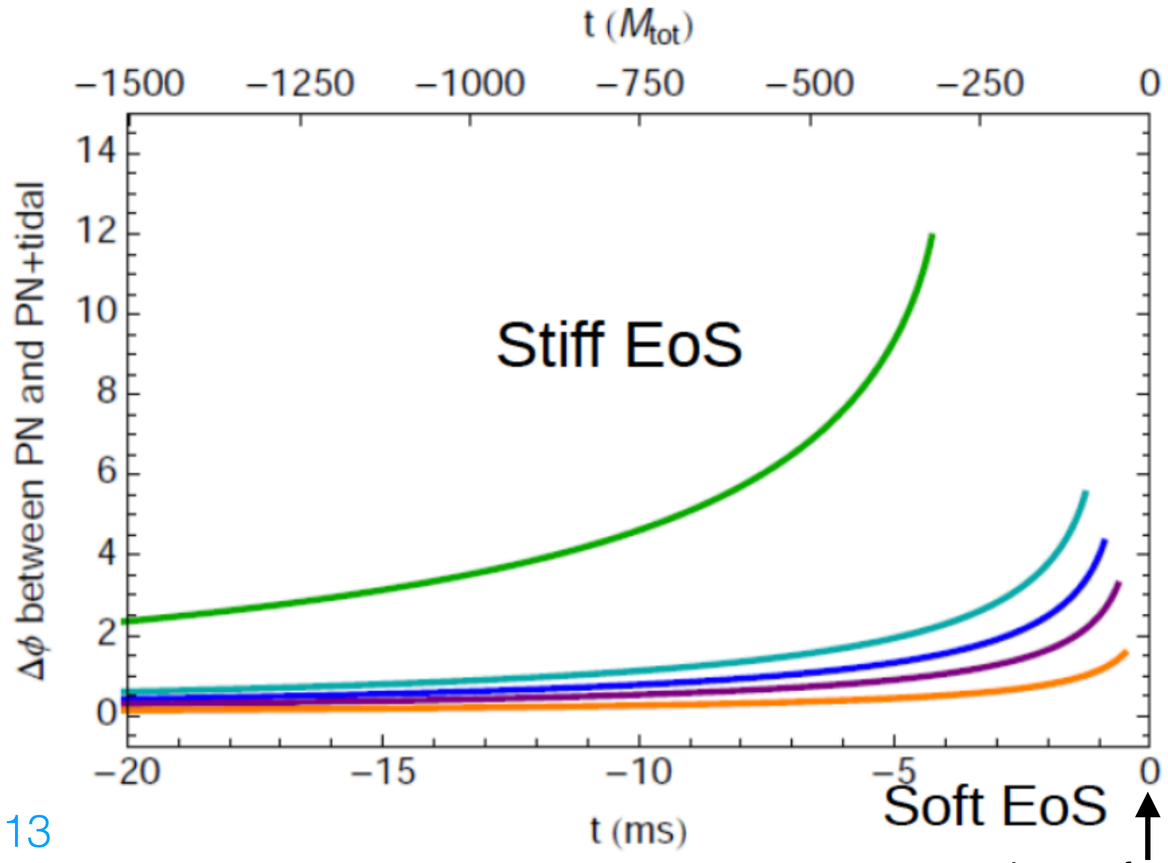

Read+ 2013

merger time of point particle

Tidal deformability and measurability of NS properties

Read+ (2013): systematic investigation of inspiral using extended set of EOS and multiple-code effort (SACRA & Whisky) to generate NR waveforms. Goal: improve data-analysis estimates of the measurability of matter effects in BNSs.

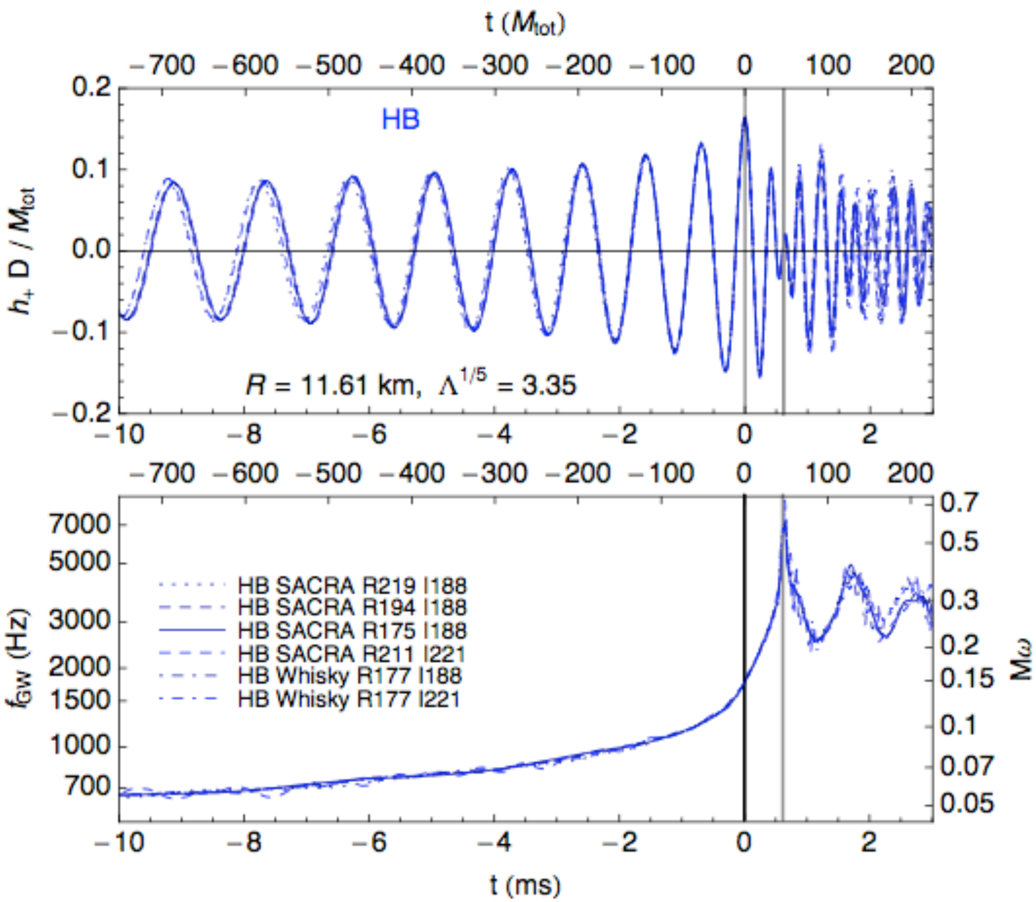

Tidal deformability and measurability of NS properties

Λ effectively characterizes properties of the star at the peak of the GW amplitude at the end of the inspiral phase.

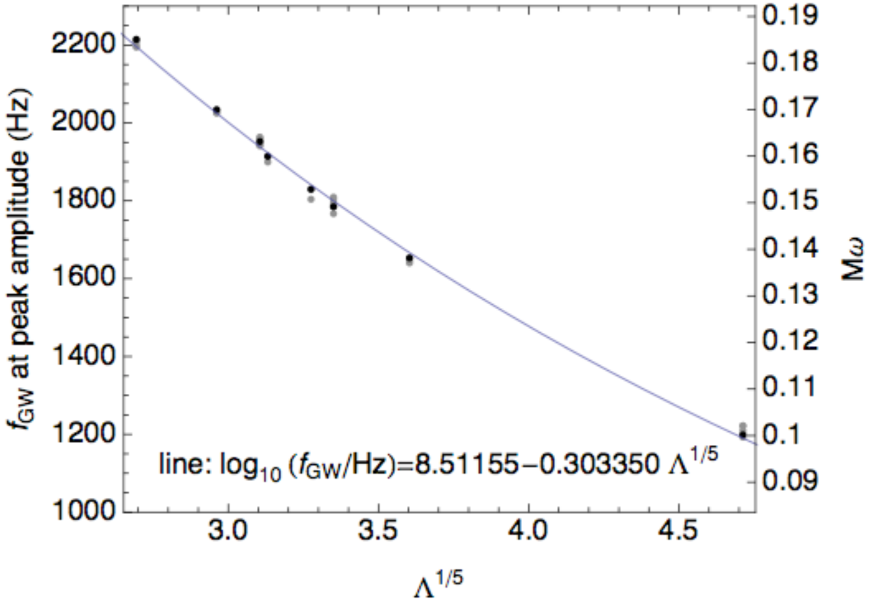

Quasi-universal relation found between peak GW frequency at merger and tidal deformability.

Tidal deformability and radii scale tightly but not perfectly.

Quasi-universality implies that once f_{GW} at peak amplitude is measured, so is the tidal deformability, hence I, M/R. **Procedure:** (1) f_{GW} and component masses measured from inspiral GW signal. (2) quasi-universal relation yields values of component Lambdas; (3) analytic relation between Lambda and R yields individual radii.

With a single source at ~100 Mpc, the NS radius or Λ could be constrained to about 10%.

Constraining the NS radius & EoS with GW170817

Properties of GW source inferred by matching the data with predicted waveforms.

Frequency domain post-Newtonian waveform model.

Bayesian analysis in the frequency range 30–2048 Hz.

Source-frame chirp mass constrained to be ~$1.186 M_\odot$

Estimates of component masses affected by degeneracy between mass ratio and aligned spin components. Assumptions made on admissible values of spins.

Low-spin prior (consistent with observed population) yield component masses $M_1 \in (1.36, 1.60) M_\odot$ and $M_2 \in (1.17, 1.36) M_\odot$.

A single function Λ(m) computed from the static l=2 perturbation of a TOV solution.

Posterior distribution of tidal deformabilities

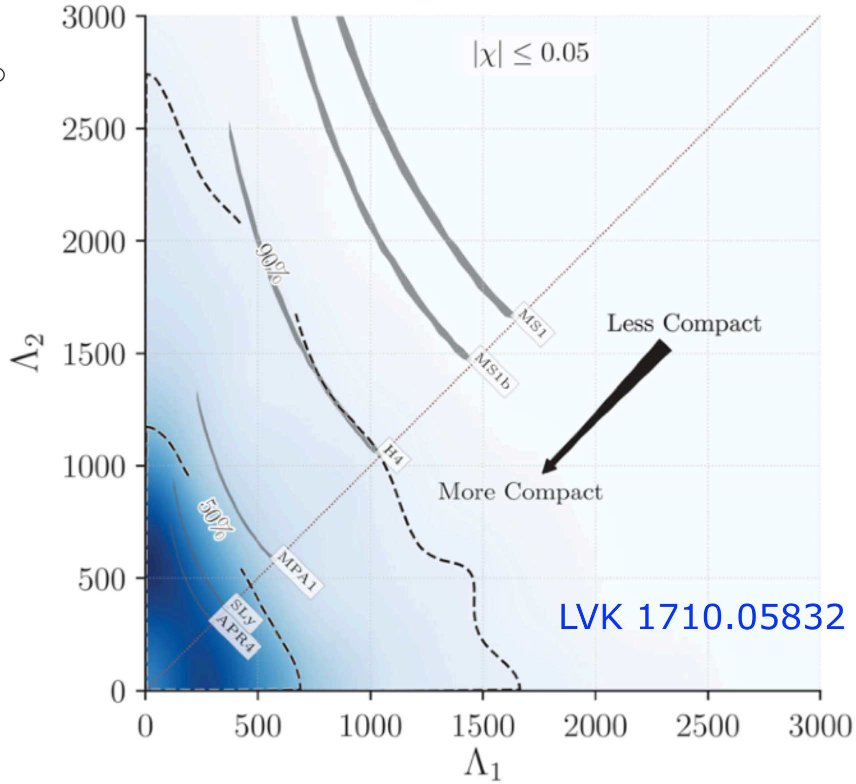

LVK 1710.05832

LVK constraints on Λ_1 and Λ_2 **disfavor (stiff) EoS** that predict less compact stars, such as MS1 and MS1b, since mass range recovered generates Λ values outside the 90% probability region. Consistent with radius constraints from X-ray observations of neutron stars.

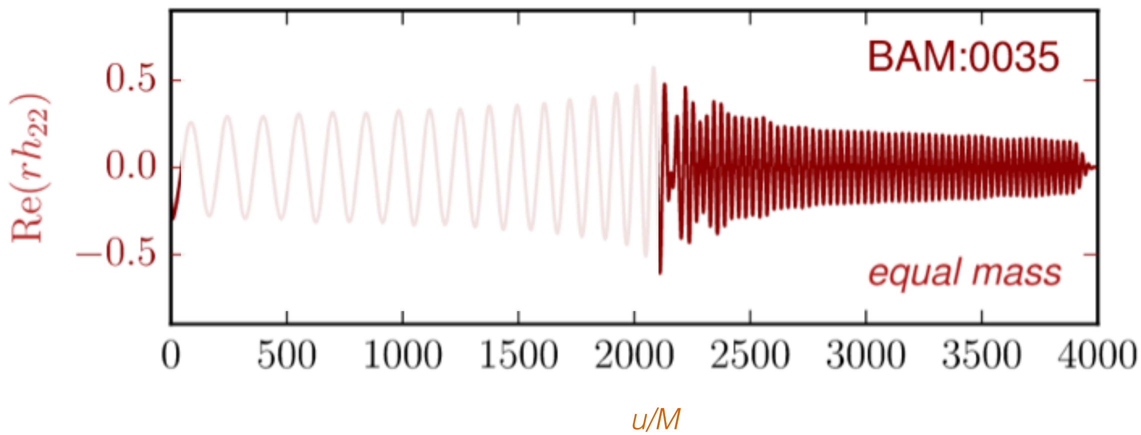

Postmerger

Inspiral phase only probes cold EoS

Thermal effects not accessible

Fate of postmerger remnant

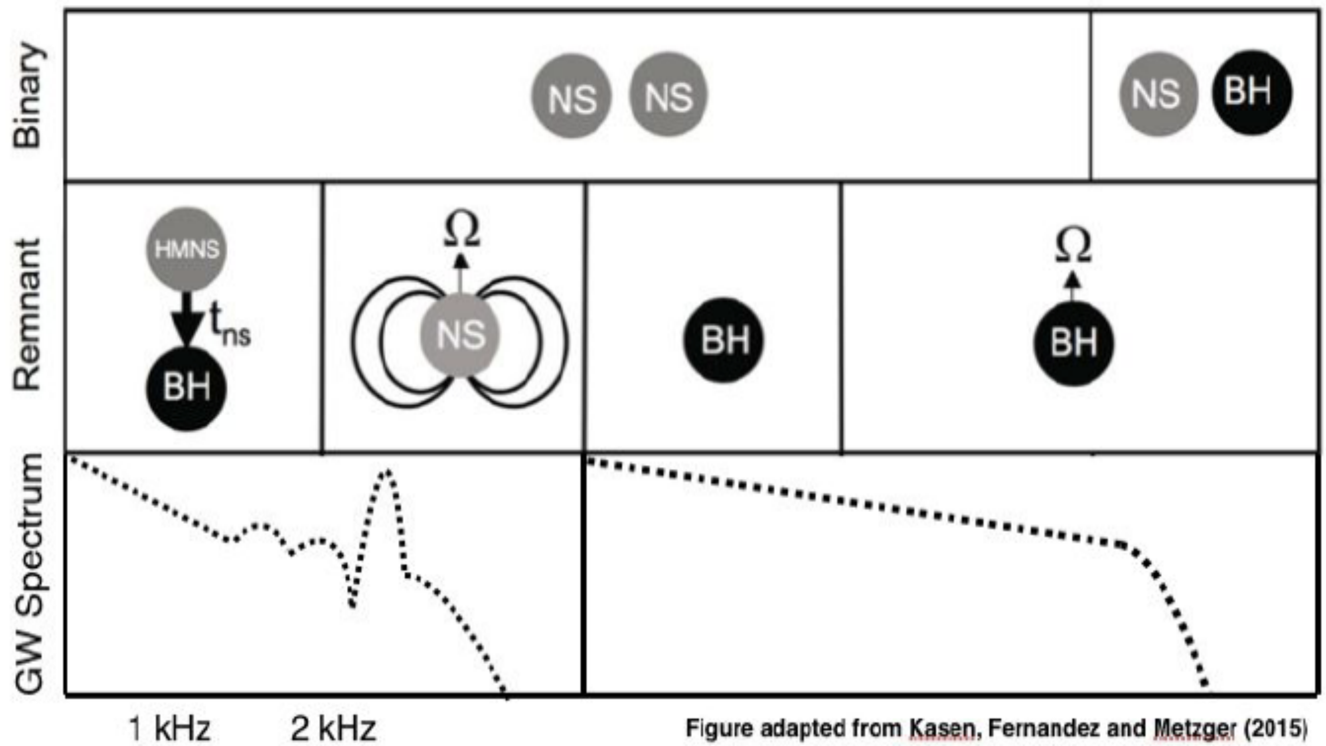

Possible outcome:

- Prompt collapse (BH ringing > 6 kHz)
- HMNS (t_{GW}~few-10 ms)
- SMNS (t_{GW}~10-100 ms)
- Stable remnant (t_{GW}~100 ms, minutes, weeks+)

HMNS: “Hypermassive” star. Remnant supported by differential rotation and thermal gradients.

SMNS: “Supramassive” star. Mass small enough to be supported by rigid rotation.

Fate of postmerger remnant

BNS merger → HMNS → BH+torus

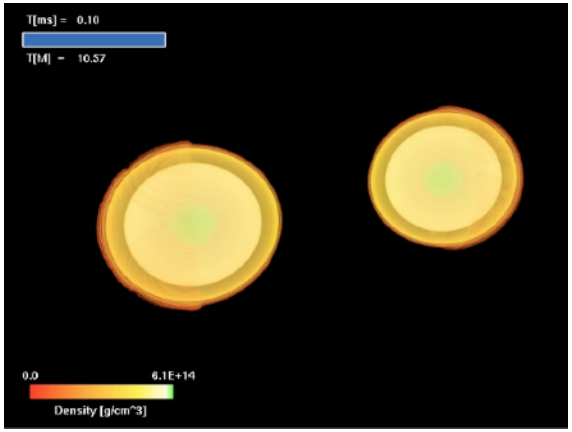

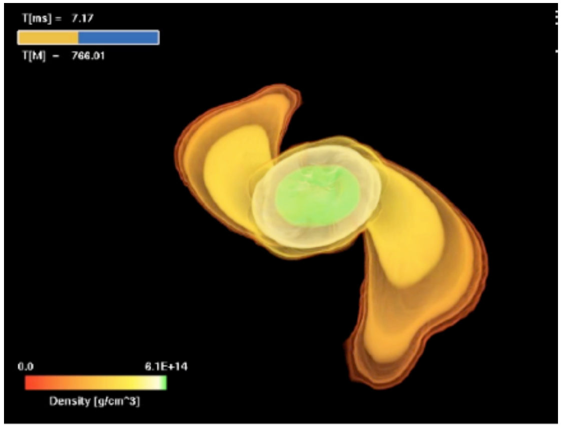

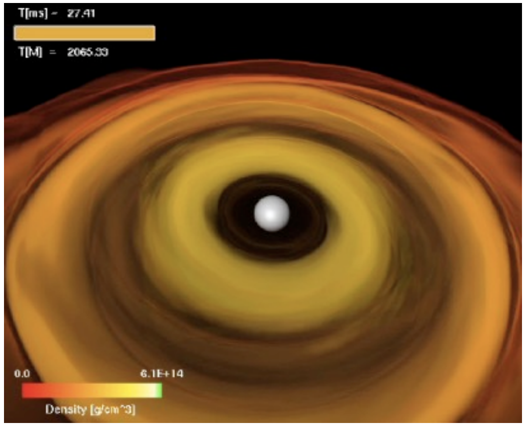

Credit: AEI/Frankfurt

Variations on this general trend are produced by:

- differences in the total mass for the same EOS: a binary with smaller mass will produce a HMNS which is further away from the stability threshold and will collapse at a later time.

- differences in the EOS for the same mass: a binary with an EOS allowing for a larger thermal internal energy (ie hotter after merger) will have an increased pressure support and will collapse at a later time.

Searches of postmerger signals

Search for post-merger GW from the remnant of the binary neutron star merger GW170817 (LVK, Abbott+ 2017)

Search for signals of short duration ($\lesssim$1 s) (cWB; Klimenko+ 2016) and intermediate duration ($\lesssim$500s) (STAMP Thrane+ 2011 y cWB) in the LIGO/Virgo data, including emission from HMNS or SMNS, respectively.

No GW signal from post-merger remnant found.

Upper limits (root-sum-square) of the amplitude, between 1-4 kHz, at a 50% detection efficiency

Short signal: $h_{\rm rss}^{50\%} = 2.1 \times 10^{-22}\,{\rm Hz}^{-1/2}$

Intermediate signal:

$h_{\rm rss}^{50\%} = 8.4 \times 10^{-22}\,{\rm Hz}^{-1/2}$ (ms magnetar model)

$h_{\rm rss}^{50\%} = 5.9 \times 10^{-22}\,{\rm Hz}^{-1/2}$ (bar-mode model)

Post-merger emission from a GW170817-like event may be detected when LIGO/Virgo reach design sensitivity or with 3G detectors (ET, CE).

3G Detectors

Einstein Telescope

Cosmic Explorer

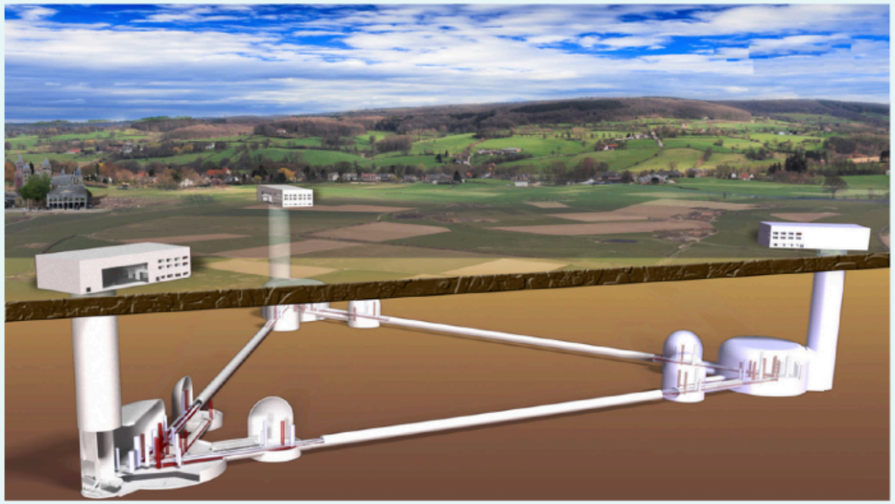

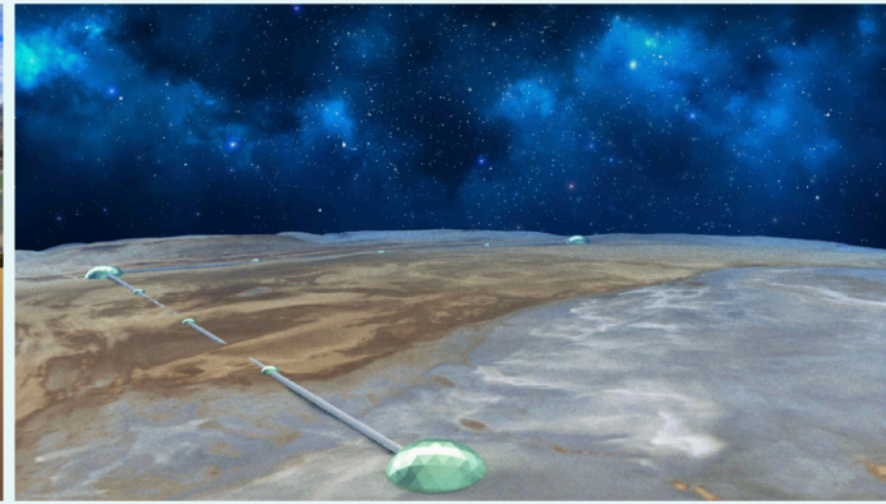

Einstein Telescope conceived to be six, V-shaped, underground interferometers, formed out of 10 km sides of an equilateral triangle

http://www.et-gw.eu

Cosmic Explorer conceived to be an L-shaped, overground interferometer, with 40 km arms

https://dcc.cosmicexplorer.org/P2100003/public

GWIC 3G reports https://gwic.ligo.org/3Gsubcomm/

3G Detectors

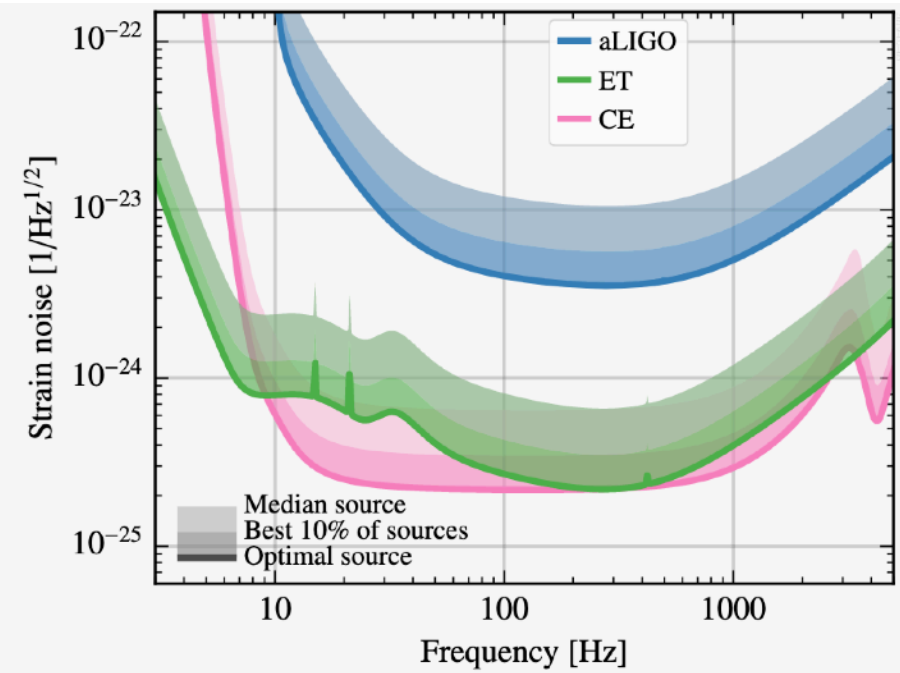

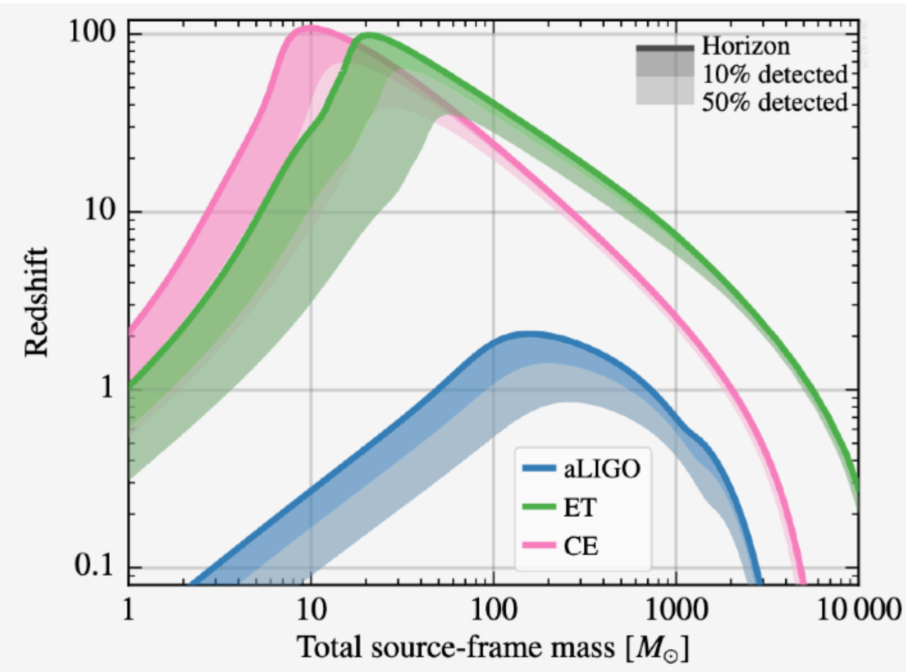

Sensitivity of ET and CE compared to Advanced LIGO

Reach for equal-mass non spinning binaries for 3G Observatoires

GWIC 3G reports https://gwic.ligo.org/3Gsubcomm/

3G Detectors

With ET and CE, GW observatories will leap from monitoring only the nearby Universe to surveying the entire Universe for BH mergers

Redshift reach of LIGO Voyager, ET, and CE. Shown are the redshifts for:

- BNS mergers
- BBH mergers

Assumptions:

- Madau-Dickinson SFR
- Time from binary formation to merger is 100 Myr

Most binaries merge at z~2

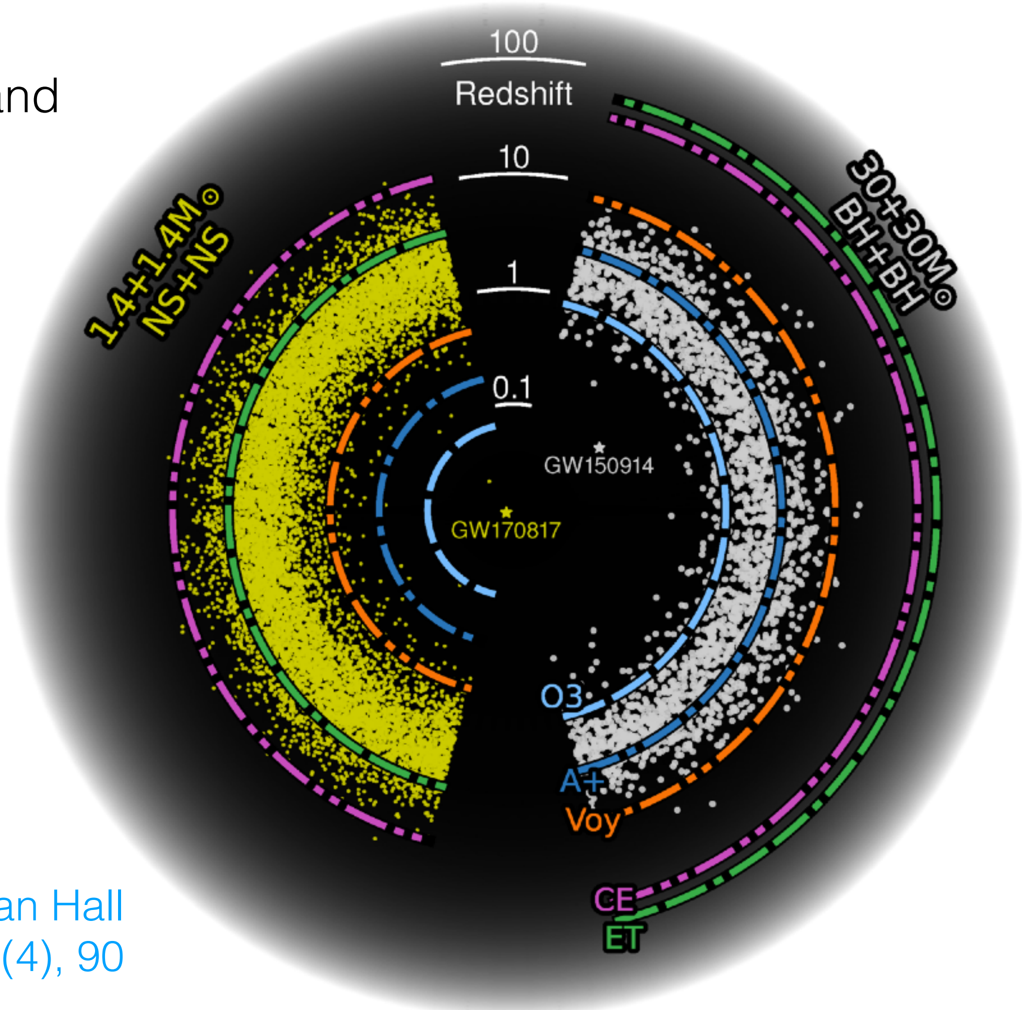

Evan Hall
Galaxies **2022**, 10(4), 90

Characterisation of the properties of postmerger signal

HMNS Fourier spectrum (h_{eff} @ 100 Mpc)

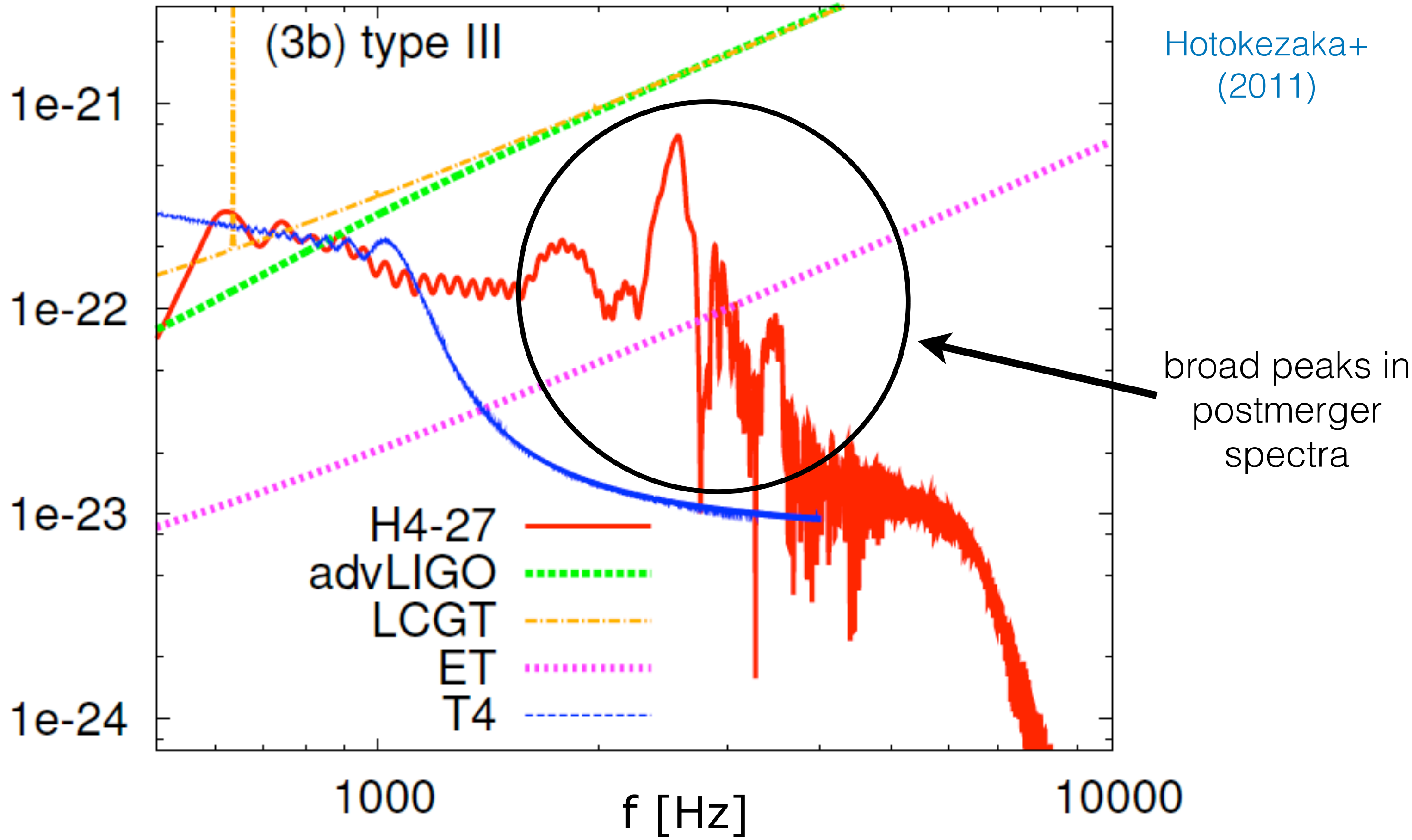

Hotokezaka+ (2011)

2-4 kHz peaks detectable by 3G detectors or 2G detectors if source close enough (20 Mpc).

Characterisation of the properties of postmerger signal

Postmerger phase has rich GW phenomenology; good prospects for constraining EoS.

HMNS asteroseismology: interpretation of the characteristics of oscillation modes of the postmerger remnant in terms of the physical properties of the stellar interior.

Goal: use GW spectra to find **quasi-universal relations** between oscillation frequencies (spectra peaks) and NS properties (mass, radius, tidal deformability)

NR simulations have revealed that a number of peculiar frequencies are related with the properties of the binary through quasi-universal relations.

Relations suggested for:

1. **the GW frequency at merger** (e.g. Read+ 2013; Bernuzzi+ 2014; Takami+ 2015; Rezzolla & Takami 2016; Most+ 2019; Bauswein+ 2019; Weih+ 2020; Gonzalez+ 2022; Topolski+ 2024; Guerra+ 2024)

2. **the dominant peak frequency in the postmerger spectrum** (e.g. Oechslin & Janka 2007; Bauswein & Janka 2012; Read+ 2013; Rezzolla & Takami 2016; Gonzalez+ 2022; Topolski+ 2024, Guerra+ 2024)

3. **other frequencies** identifiable in the transient period right after the merger (Bauswein & Stergioulas 2015; Takami+ 2015; Rezzolla & Takami 2016)

HMNS asteroseismology

Many attempts to empirically fit HMNS mode frequencies vs Love number: Bauswein & Stergioulas (2013), Read+ (2013), Takami+ (2015), Rezzolla & Takami (2016), Vretinaris+ (2019), Lioutas+ (2021), …

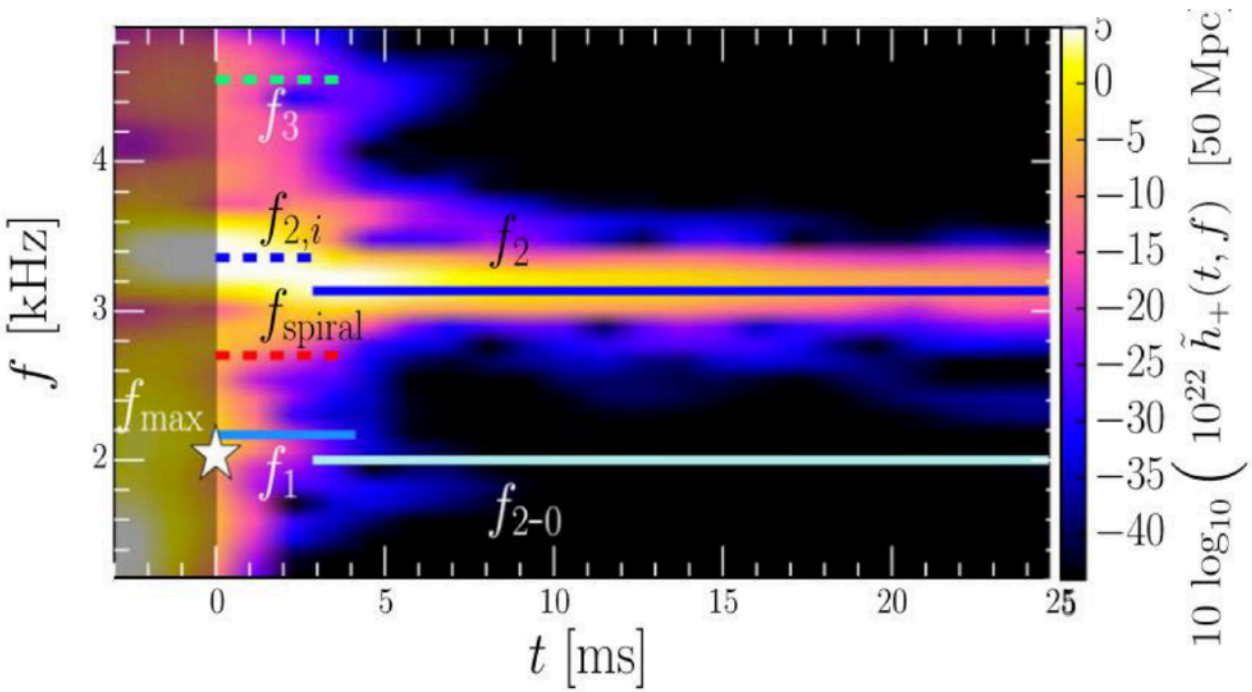

- $$\log_{10}\left(\frac{f_{\rm max}}{\rm kHz}\right) \approx a_0 + a_1(\kappa_2^T)^{1/5} - \log_{10}\left(\frac{2\overline{M}}{M_\odot}\right)$$
  $$a_0 = 4.186, \qquad a_1 = -0.195.$$
- $$f_{2,i} \approx 6.401 - 1.299(\kappa_2^T)^{1/5}\ \text{kHz},$$
- $$f_2 \approx 5.832 - 1.118(\kappa_2^T)^{1/5}\ \text{kHz}.$$

Quasi-normal modes of oscillation of stars

Kokkotas & Schmidt (1999)

Polar fluid modes most important for GW emission:

- **Fundamental mode (f-mode)**: exists only for non-radial oscillations and describes surface waves. Due to the interface between the star and its surroundings. Eigenfunction has no nodes inside the star.

$$f \propto \sqrt{\bar{\rho}} \propto \sqrt{M/R^3} \qquad f \sim 2\,\mathrm{kHz},\ \ \tau < 1\,\mathrm{s}$$

- **Pressure modes (p-modes)**: exist for both radial and non-radial oscillations. Infinitely many of them. Pressure is the restoring force. Oscillations nearly radial. Frequencies depend on the travel time of acoustic waves across the star (standing sound waves).

$$f > 4\,\mathrm{kHz},\ \ \tau > 1\,\mathrm{s}$$

- **Gravity modes (g-modes)**: only exist for finite temperature stars. Infinitely many of them. Buoyancy is the restoring force. Oscillations nearly tangential.

$$f < 500\,\mathrm{Hz},\ \ \tau > 5\,\mathrm{s}$$

Axial fluid modes:

- Rotation modes (r-modes). Subclass of inertial modes.

Polar and axial spacetime modes:

- Wave or curvature modes (w-modes).

$$f > 6\,\mathrm{kHz},\ \ \tau \sim 0.1\,\mathrm{ms}$$

GW asteroseismology of pulsating NS

Idea already put forward in seminal work by Andersson & Kokkotas (1998).

Computed linear eigenfrequencies of the oscillation modes of NS most important for GW astronomy, the f-mode, the first pressure p-mode and the first GW w-mode.

Used NS models with twelve realistic EoS.

A set of "empirical relations" between the mode-frequencies and the parameters of the star (the radius R and the mass M) was inferred.

For example, for the f-mode:

$$\omega_{\rm f} \sim 0.78 + 1.635 \left(\frac{M}{1.4 M_\odot}\right)^{1/2} \left(\frac{10\,{\rm km}}{R}\right)^{3/2}$$

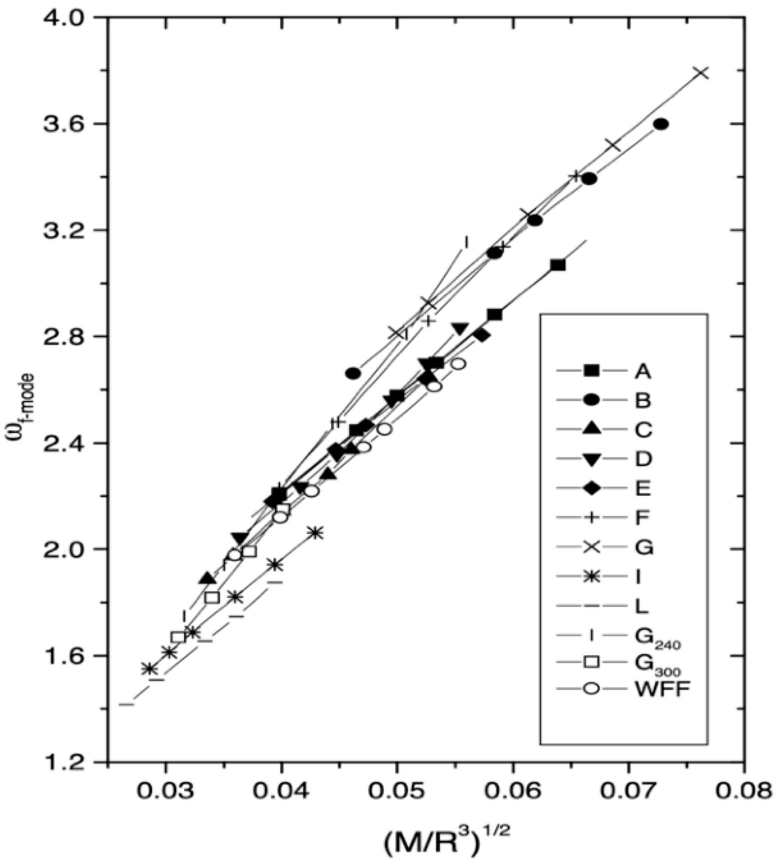

Proof-of-principle that those empirical relations can be used to extract the details of the star from observed oscillation modes.

Oscillation modes in HMNS (early postmerger)

GW signal divided in three distinct phases: inspiral, merger, postmerger oscillations

Stergioulas+ (2011)

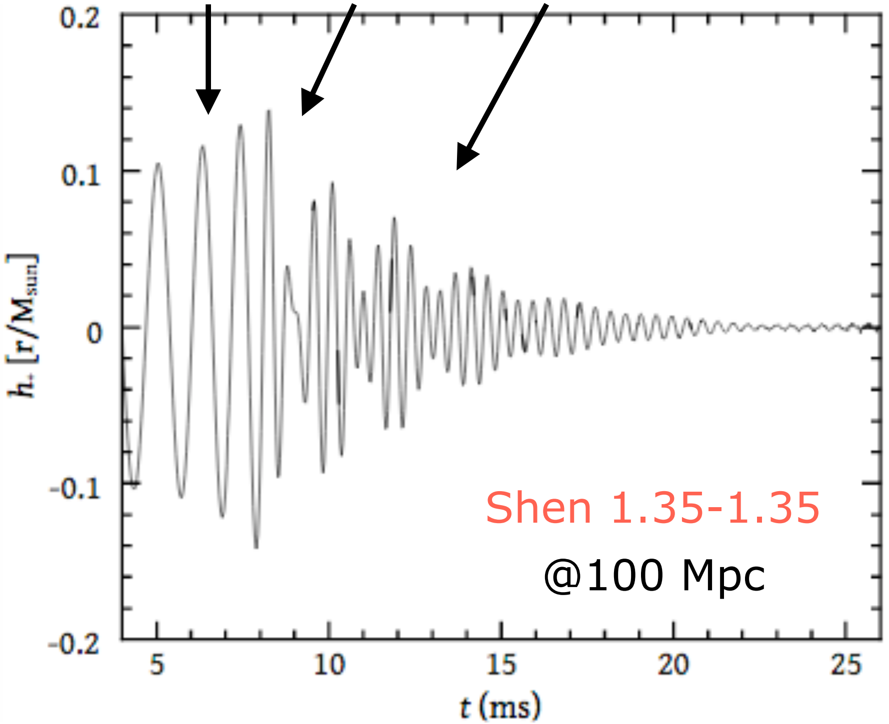

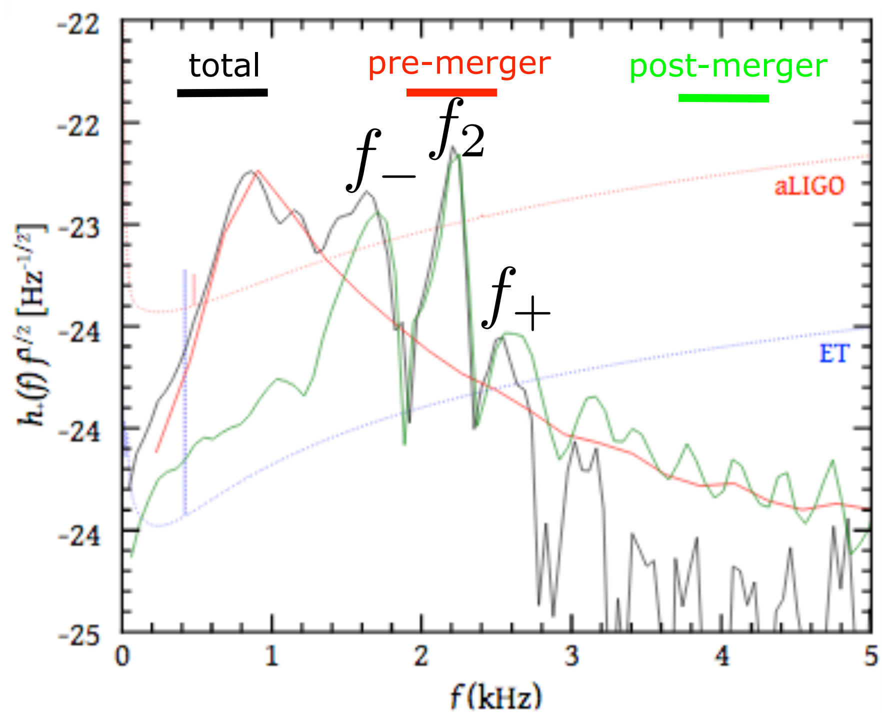

Triplet of frequencies identified in GW spectrum.

Future GW observations may extract f_2 & f_0

GW **asteroseismology** with post-merger remnant to **constrain the EOS.**

$f_{\rm peak} = f_2$ fundamental l=m=2 f-mode oscillation

$f_- = f_2 - f_0$

$f_+ = f_2 + f_0$

quasilinear combination tones

Detectabilty postmerger signal - `Bayeswave`

`Bayeswave` (Cornish & Littenberg 2015) provides a robust method to characterize the GW emission from the remnant of a BNS merger.

Bayesian GW data analysis pipeline developed within the LVK Collaboration.

`docs.ligo.org/lscsoft/bayeswave`

`Bayeswave` employs a morphology-independent approach to reconstruct the postmerger GW signal through a sum of appropriate basis functions (sine-Gaussians wavelets) and provide the full posterior probability distribution of the underlying waveform.

`Bayeswave` has been applied on simulated data from NR simulations of BNS mergers injected into a network of advanced ground-based detectors

Clark+ 2014, 2016; Chatziioannou+ 2017; Bose+ 2018; Miravet-Tenés+ 2023, 2024

Results demonstrate the GW signal reconstruction capabilities of the pipeline. Posterior distributions for the GW peak frequency and for the NS radius.

Detectabilty postmerger signal - `Bayeswave`

Reconstruction of waveform and spectrum

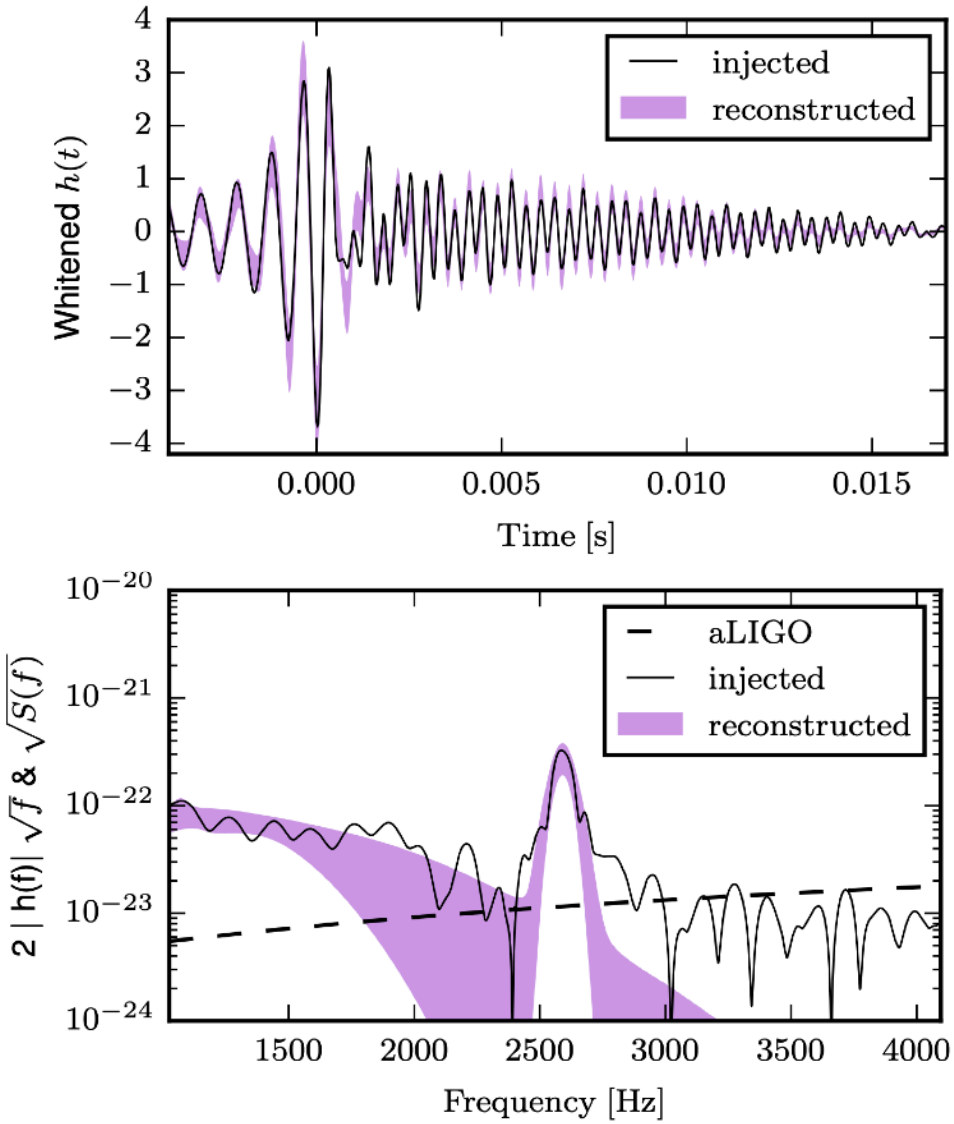

Waveform from a NR simulation of two nonspinning, (1.35, 1.35)$M_\odot$ NS with DD2 EoS.

Injected at a post-merger SNR of 5 (roughly corresponds to a distance of 20Mpc).

Shaded region denote 90% CI of the reconstruction.

Chatziioannou+ 2017

Detectabilty postmerger signal - `Bayeswave`

Quality of reconstruction measured by the overlap between signal *s* and model *h*

$$\mathcal{O} \equiv \frac{\langle s, h \rangle}{\sqrt{\langle s, s \rangle}\sqrt{\langle h, h \rangle}} \qquad \langle a, b \rangle \equiv 2 \int_0^\infty \frac{a(f)b^*(f) + a^*(f)b(f)}{S_h(f)} df$$

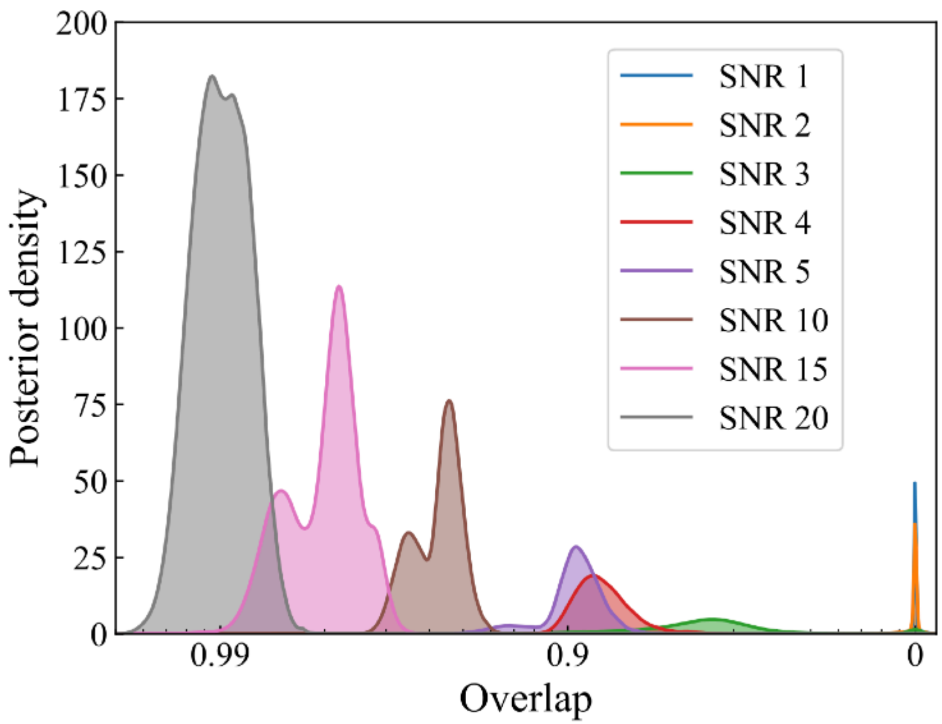

Chatziioannou+ 2017

$\mathcal{O} = 1$ perfect match between injected and reconstructed signals

$\mathcal{O} = 0$ no match

Detectabilty postmerger signal - **`Bayeswave`**

Posterior density function of the GW peak frequency

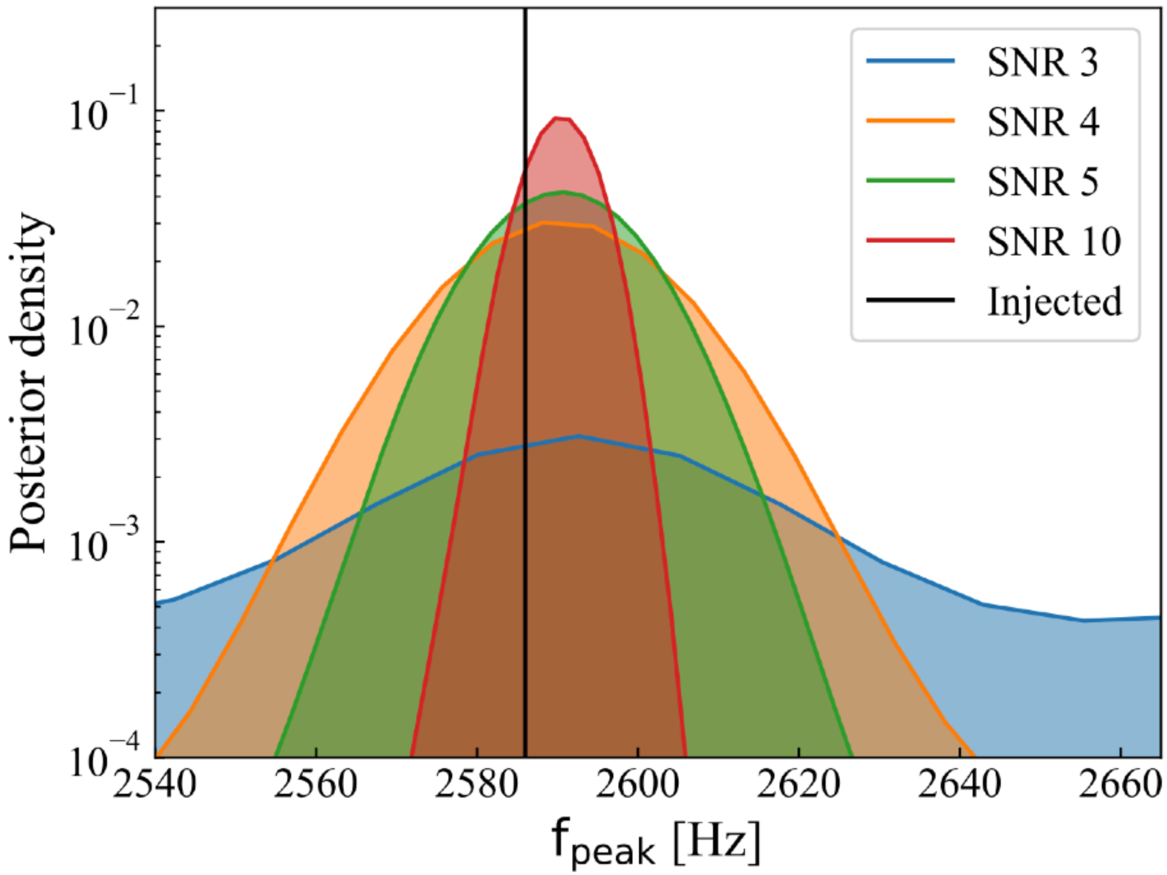

Chatziioannou+ 2017

As SNR increases, **`Bayeswave`** achieves a more accurate reconstruction of the signal and the posterior peaks at the correct value for f_{peak}.

Detectabilty postmerger signal - `Bayeswave`

Bauswein+ (2012): peak frequency of (1.35−1.35)$M_\odot$ BNS merger correlates with the radius of a 1.6$M_\odot$ nonrotating NS in an EoS-independent manner (density regimes are comparable). Similar relations found for other binary masses and other radii ($R_{1.35}$ or $R_{1.8}$) (Bauswein+ 2012, 2016)

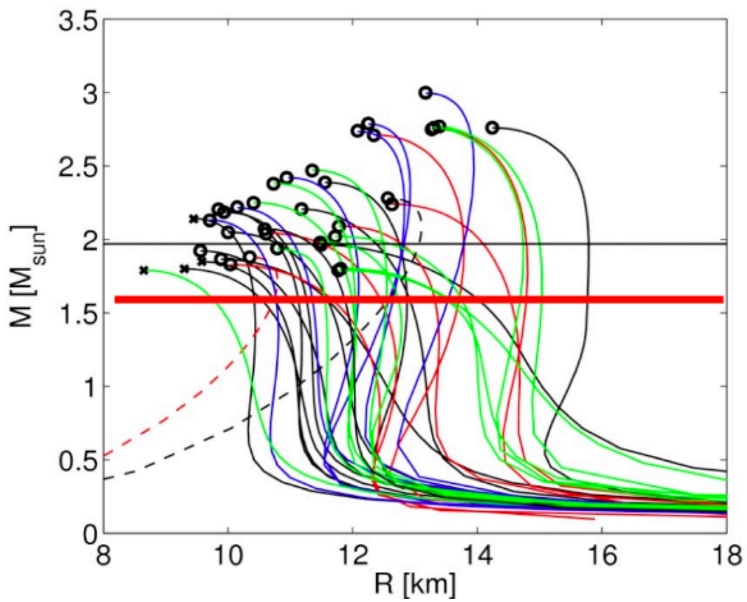

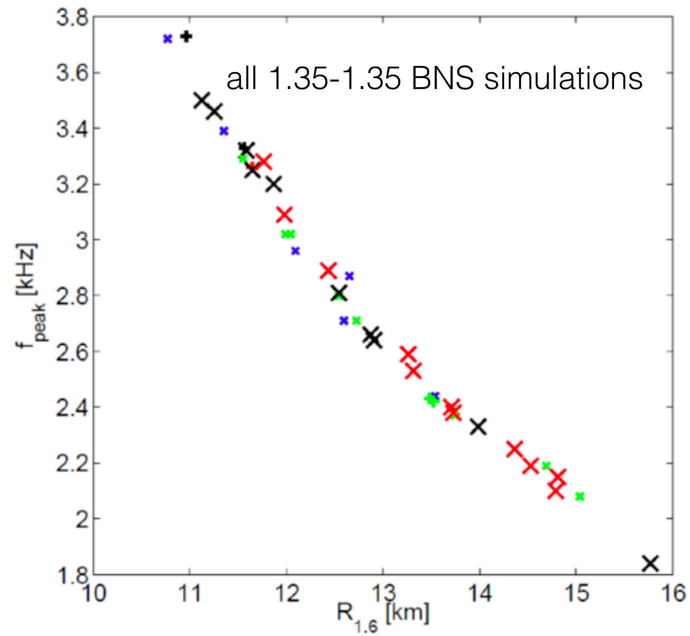

Therefore, a potential measurement of f_{peak} from postmerger signal can be used to obtain an estimate on $R_{1.6}$, a quantity that can be used to directly constrain the EoS.

The smaller the scatter (<200 m) the smaller the error in radius measurement.

Detectabilty postmerger signal - `Bayeswave`

Inference on the radius: posteriors for the f_{peak} converted to posteriors for $R_{1.6}$.

For different binary total mass *M*, the deviation from perfect universality in the $f_{peak}/M - R_{1.6}$ relation is taken into account. Systematic uncertainties dealt with through marginalisation.

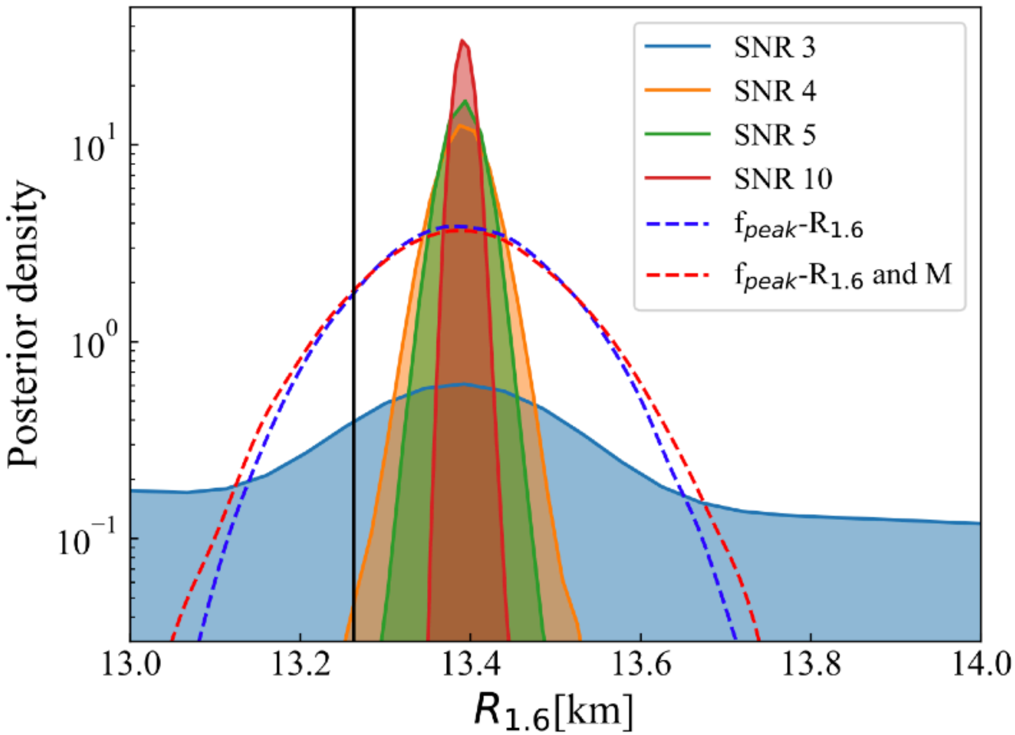

Shaded regions: posteriors for best-fit model (systematic uncertainties ignored)

Dashed lines: marginalised posteriors including systematic uncertainties in measurements in $f_{peak}/M - R_{1.6}$ and total mass M.

Chatziioannou+ 2017

Measurement of $R_{1.6}$ to within (300–700) m at the 90% CL.

The statistical error in the NS radius measurement from the postmerger signal comparable to the corresponding error from the inspiral signal.

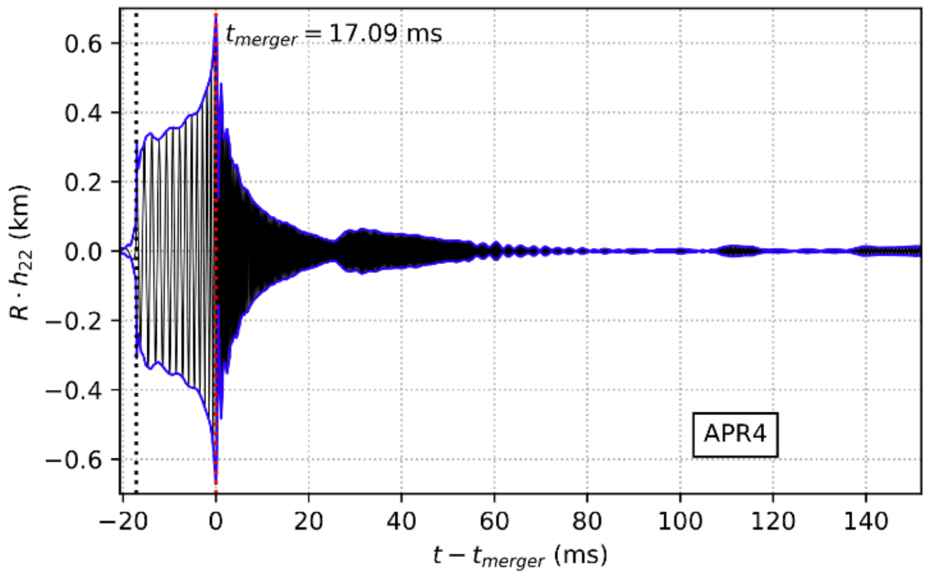

Late time postmerger

Late postmerger: convective excitation of inertial modes

De Pietri+ (2018, 2022) reported results on the **longest term simulations** of BNS mergers thus far performed (up to 140 ms post-merger).

De Pietri+ (2018)

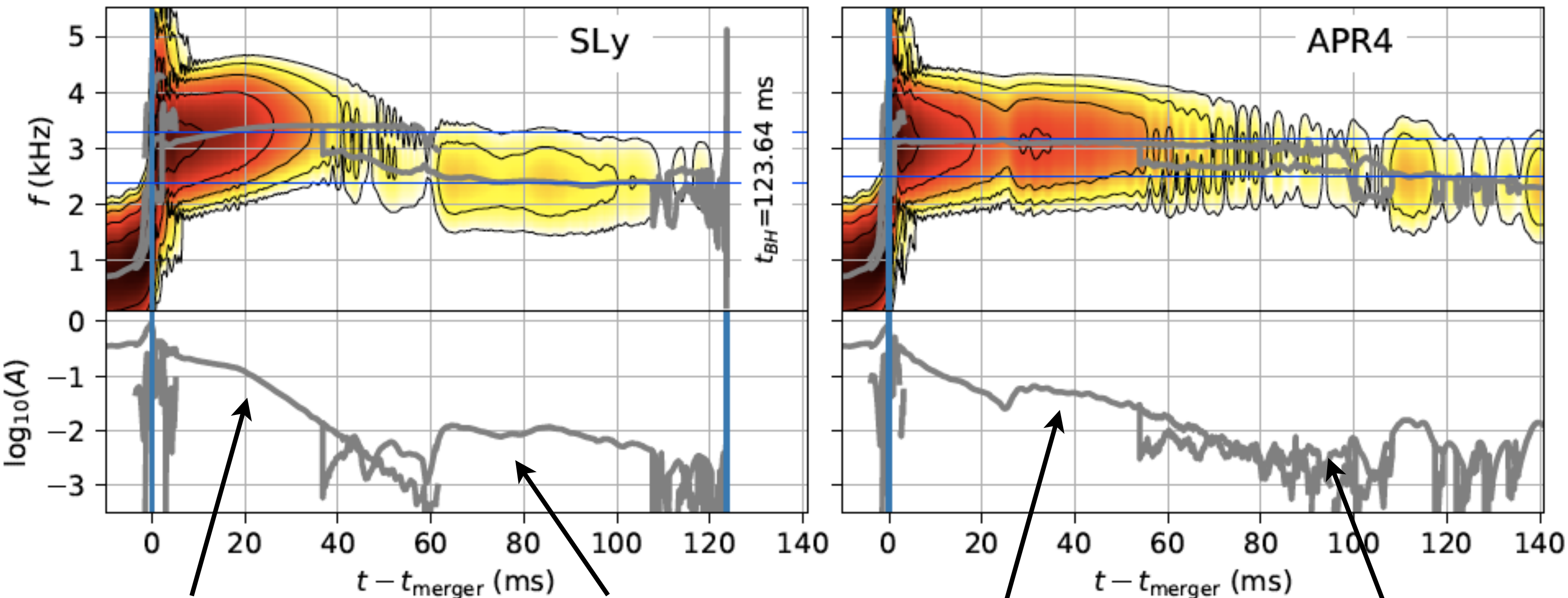

f_2-mode inertial mode f_2-mode inertial mode

Early post-merger GW emission dominated by the f-mode.

Late post-merger GW emission dominated by a low-frequency (gravito-)inertial mode (due to convection).

Convective excitation of inertial modes

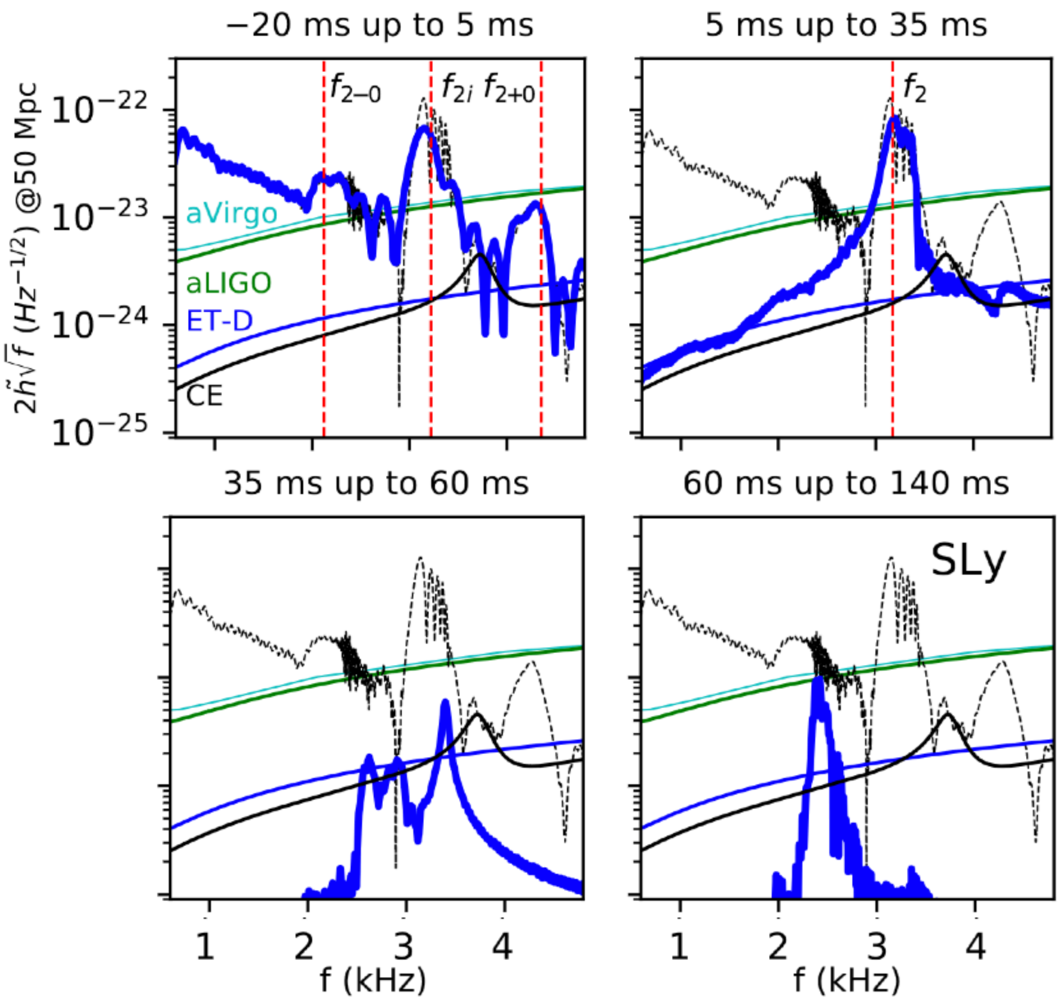

De Pietri+ (2018)

Early postmerger GW emission dominated by the f_2-mode.

Late postmerger emission dominated by a low-frequency (gravito-)inertial mode (due to convection).

Results shown for SLy EoS only. Holds for all EoS models.

Sign of Schwarzschild discriminant (>0 unstable=dark)

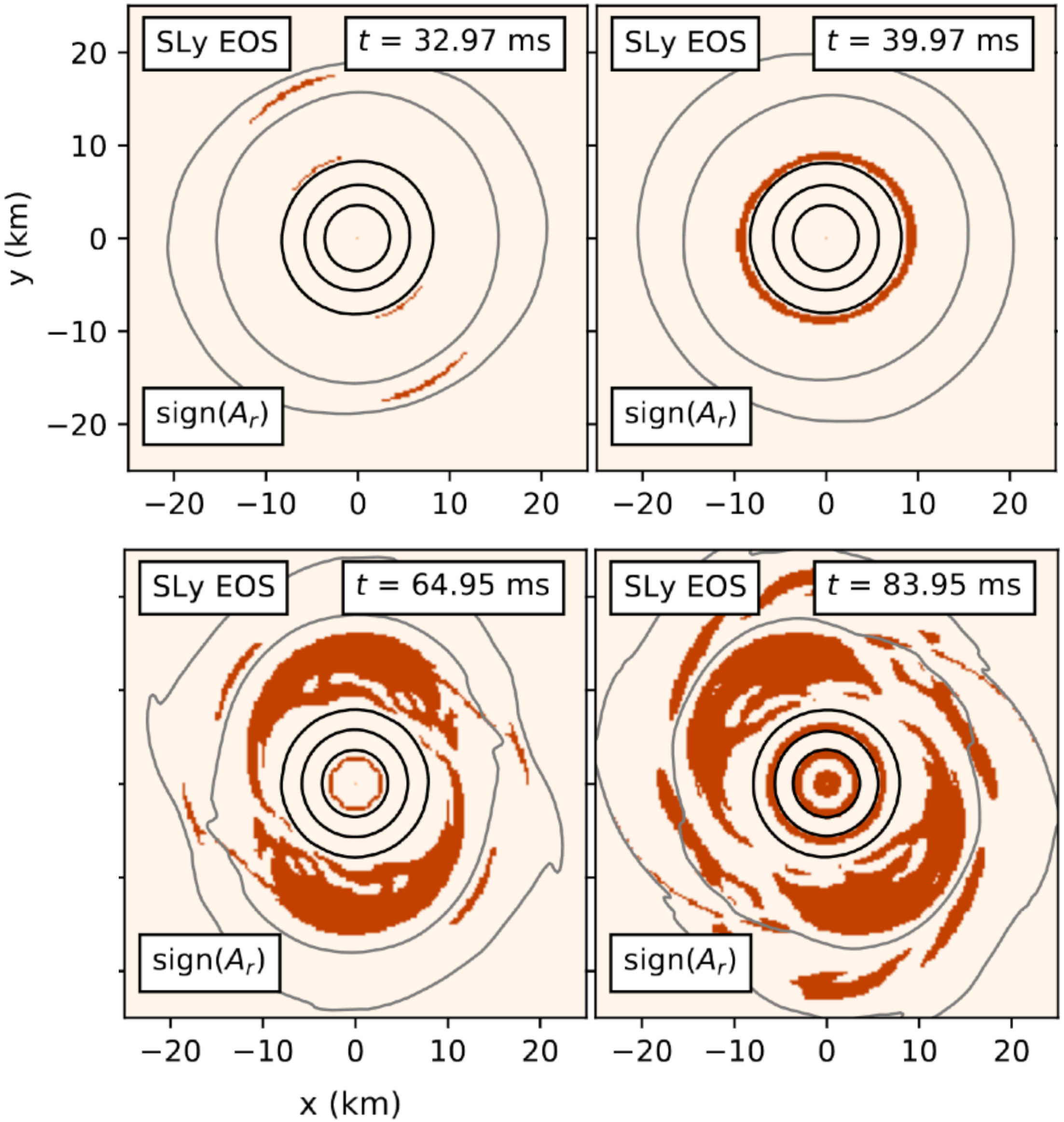

$$A_\alpha = \frac{1}{\varepsilon + p}\nabla_\alpha \varepsilon - \frac{1}{\Gamma_1 p}\nabla_\alpha p$$

$$\Gamma_1 = \Gamma_{\rm th} + (\Gamma_i - \Gamma_{\rm th})\frac{K_i \rho^{\Gamma_i}}{p}$$

About 30-50 ms after merger, parts of the HMNS become convectively unstable, exciting inertial modes.

Might be potentially detected by 3G detectors.

Opportunity to infer rotational and thermal properties of BNS remnants.

Treatment of thermal effects in postmerger

hybrid EoS vs tabulated EoS

Thermal conditions of BNS mergers

Late inspiral phase: neutron stars are **cold**.
Neutron stars with age > 10^7 years have undergone long-term cooling by neutrinos and photons.

$$\mathrm{T} < 10^5\,\mathrm{K} \sim 10\,\mathrm{eV} \ll E_\mathrm{F} \sim 100\,\mathrm{MeV}$$

Hence, neutron stars can be modelled by cold EOS.
Problem: such EOS is still unknown; need for a systematic survey.

Merger phase: neutron stars are **hot**. Shock heating increases temperature to about

$$\mathrm{kT} \sim 0.1 - 0.2\,E_\mathrm{F} \sim 10\,\mathrm{MeV}$$

New effects likely to play important dynamical role: finite temperature effects, lepton fraction, neutrino thermal pressure, neutrino cooling.

Neutron stars modeled by thermal EOS.
Problem: systematic survey as well; few EOS available, more needed.

Dependence on the nuclear EOS

$$P(\rho, \varepsilon) = P_{\rm cold}(\rho) + P_{\rm th}(\rho, \varepsilon)$$

Piecewise-polytropic EOS for the cold part (Read et al 2009)

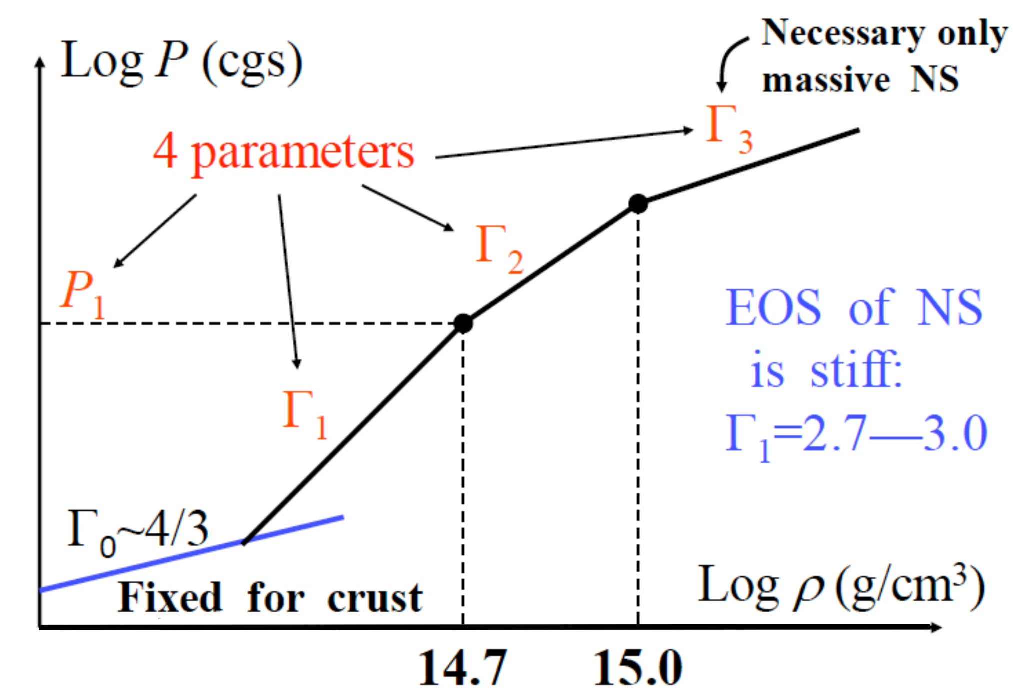

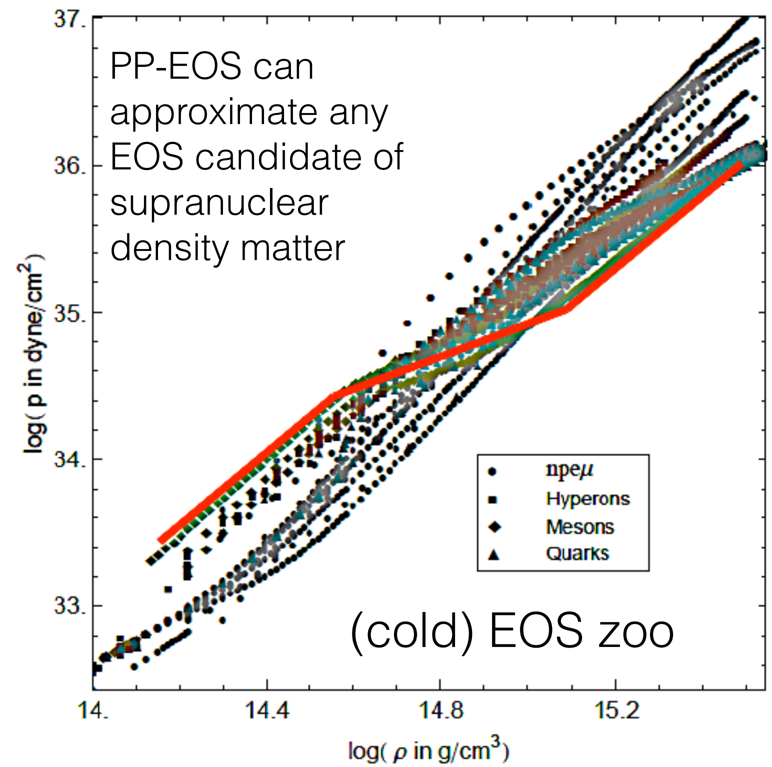

Thermal part of the pressure (shock heating) for hot, merged NS (T~10MeV) given by

$$P_{\rm th} = (\Gamma_{\rm th} - 1)(\varepsilon - \varepsilon_{\rm cold})\rho, \quad \Gamma_{\rm th} = 1.357 - 1.8$$

Thermal conditions of BNS mergers

Finite temperature adds **further pressure support** that may change the internal structure of the postmerger remnant and its subsequent evolution.

Lim & Holt (2019) showed that above $0.5n_0$ ($n_0 \approx 0.16$ fm^{-3}), $\Gamma_{\rm th}$ strongly depends on the nucleon effective mass.

Hence, hybrid approach may overestimate the thermal pressure by a few orders of magnitude (Raithel+ 2021) and may induce significant changes in the GW frequencies (Bauswein+ 2010, Figura+ 2021)

To overcome this limitation, some BNS simulations incorporate thermal effects through full finite-temperature EOS:

- CFC gravity: Oechslin+ 2007, Bauswein+ 2010
- full GR: Sekiguchi+ 2011, Espino+ 2022, Fields+ 2023, Werneck+ 2023, Guerra+ 2023

Main questions we are interested in addressing:

Q1: is treatment of thermal effects imprinted in the GW spectra of the HMNS signal?

Q2: what are the differences in the spectra of finite-temperature models compared to piecewise-polytropic (hybrid) models?

Comparison between hybrid and tabulated EoS treatment

- equal-mass BNSs in a quasiequilibrium circular orbit generated using LORENE
- binaries consist of two identical irrotational NSs modeled by
  1. **hybrid** EOS (SLy, APR4, H4 & MS1): 7-piece PWP + thermal part $\Gamma_{th} = 1.8$.
  2. corresponding **tabulated** models. Tables by Schneider–Roberts–Ott (2017) freely available at stellarcollapse.org

Case		T	M	$\mathcal{C}$	Λ	M_{ADM}	J_{ADM}	Ω
$SLy4_{TAB}$	SLy4	0.01	1.28	0.13	304.75	2.54	6.63	1.77
$DD2_{TAB}$	DD2	0.01	1.29	0.11	700.24	2.56	6.73	1.77
$HShen_{TAB}$	HShen	0.01	1.30	0.10	1170.90	2.58	6.82	1.78
$LS220_{TAB}$	Ls220	0.01	1.29	0.12	511.89	2.55	6.68	1.77
$SLy4_{PWP}$	SLy4	-	1.23	0.13	304.75	2.54	6.62	1.77
$DD2_{PWP}$	DD2	-	1.25	0.11	700.24	2.56	6.73	1.77
$HShen_{PWP}$	HSHen	-	1.26	0.10	1170.90	2.58	6.82	1.78
$LS220_{PWP}$	LS220	-	1.24	0.12	511.89	2.55	6.69	1.77

Simulations performed using the NR open-source `EinsteinToolkit` (Löffler+ 2012).

einstein toolkit

einsteintoolkit.org

illinoisgrmhd.net

Initial Data

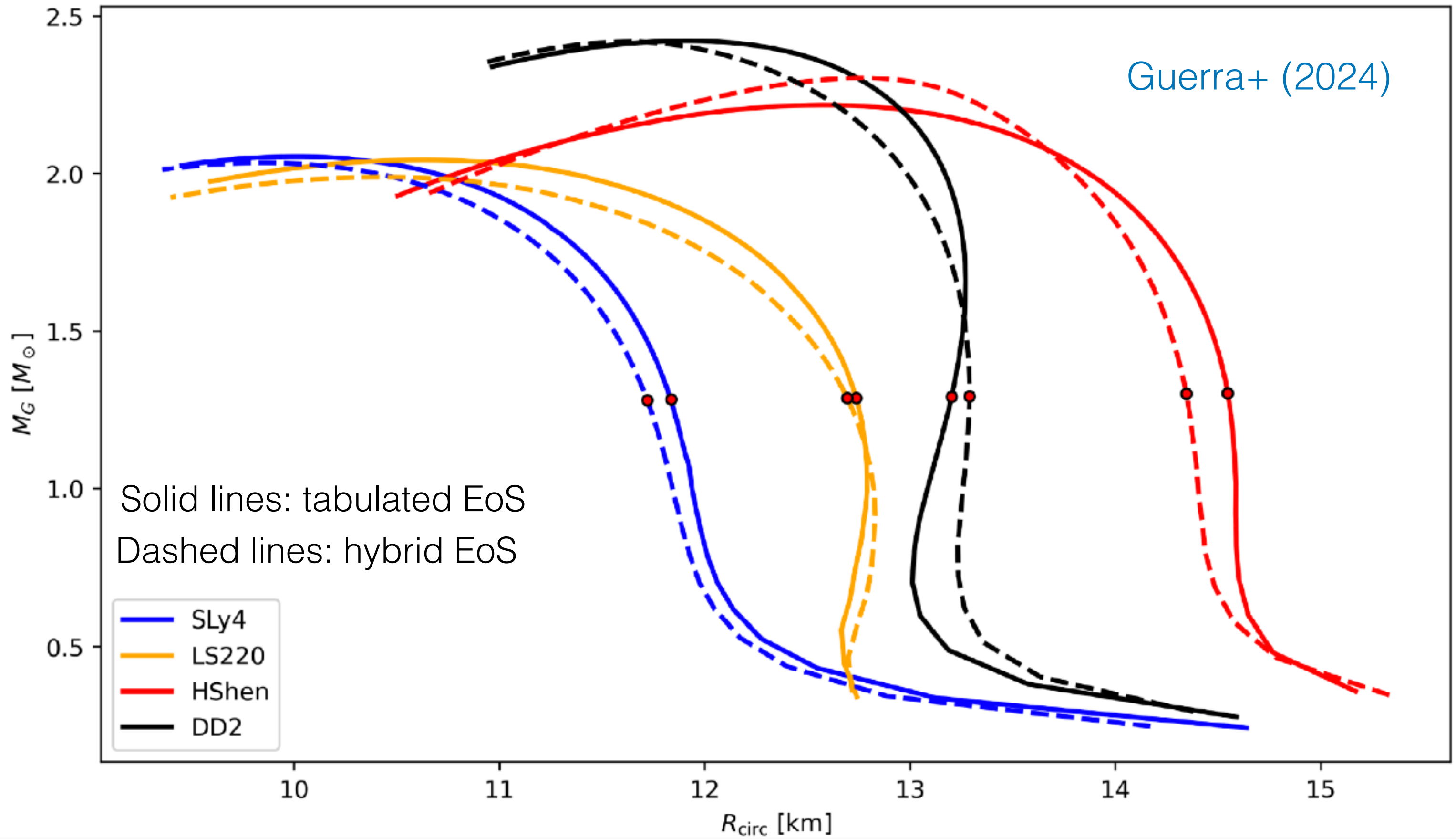

[Soft EoS]

SLy4: Chabanat+ (1998)

LS220: Lattimer & Swesty (1991)

[Stiff EoS]

DD2: Typel+ (2010)

HShen: Shen+ (2011)

Long-term postmerger evolutions illinoisgrmhd.net

Postmerger evolution of rest-mass density and internal energy for HShen EoS

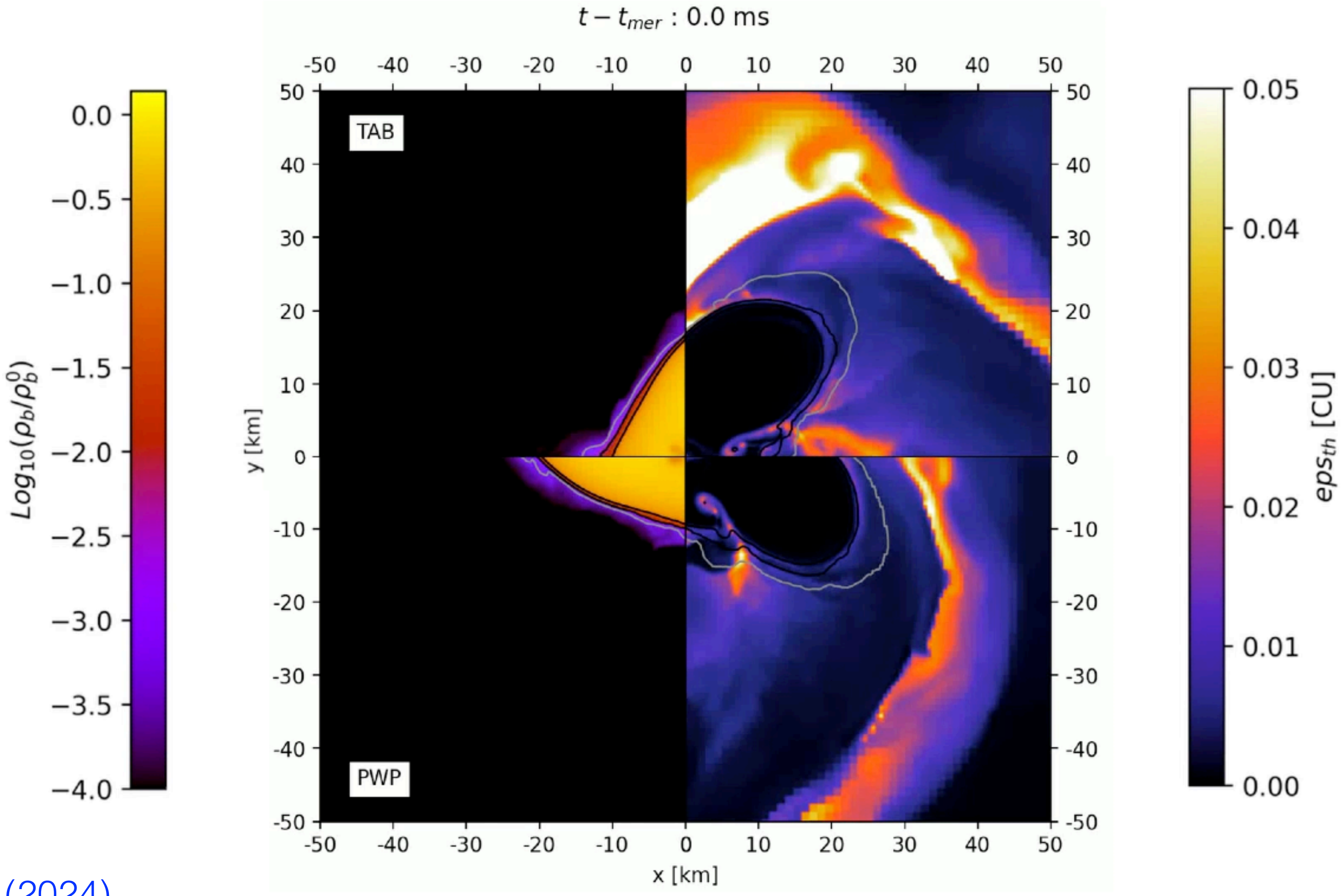

Guerra+ (2024)

Top half: tabulated model
Bottom half: hybrid model

Left half: rest-mass density
Right half: internal energy

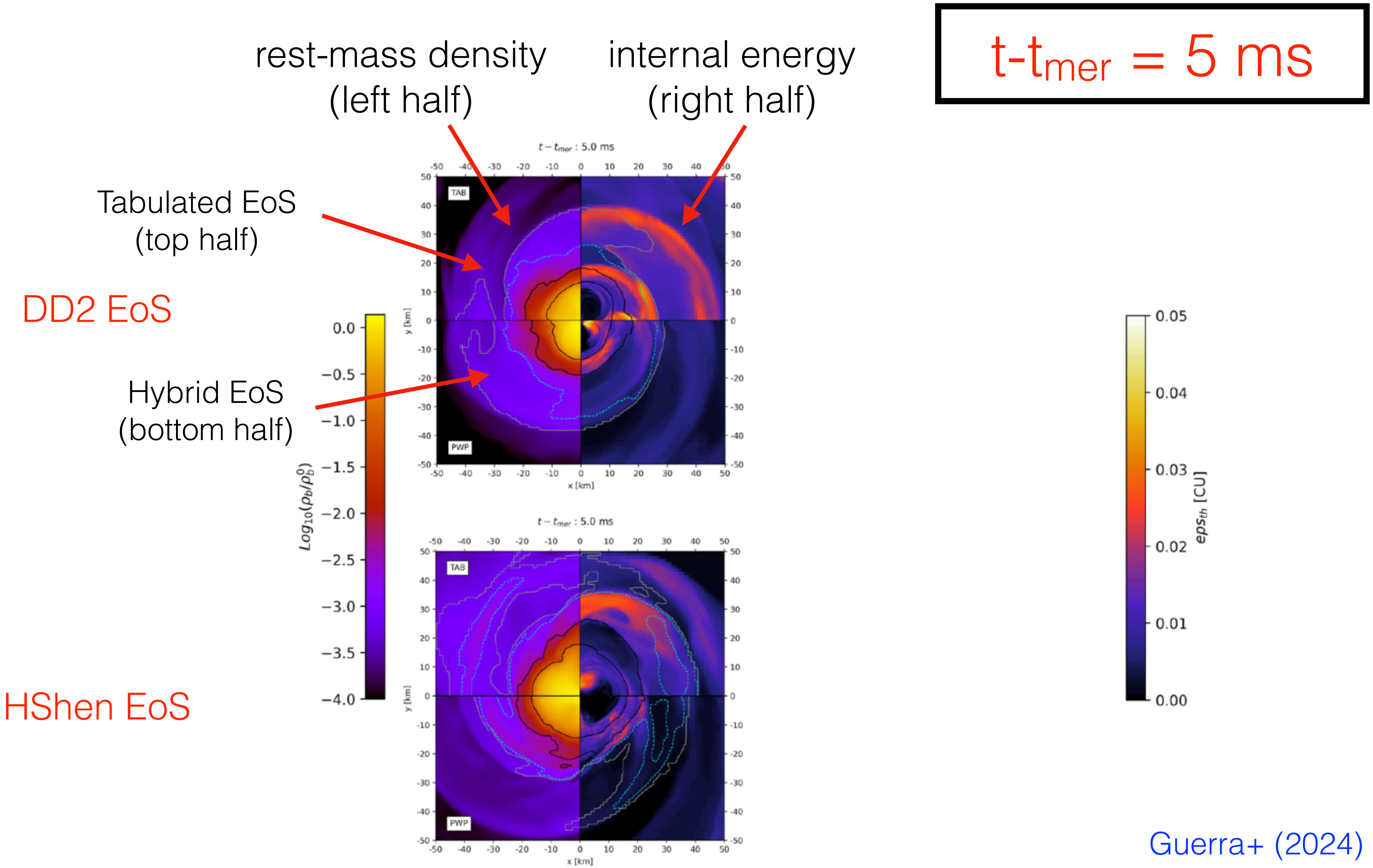

Guerra+ (2024)

A few ms after merger, the production of heat (increase in T) much more significant in tabulated EoS models. Similar density distribution in both (hybrid and tabulated) models.

$t\text{-}t_{mer}$ = 140 ms

rest-mass density (left half)

internal energy (right half)

Tabulated EoS (top half)

Hybrid EoS (bottom half)

DD2 EoS

HShen EoS

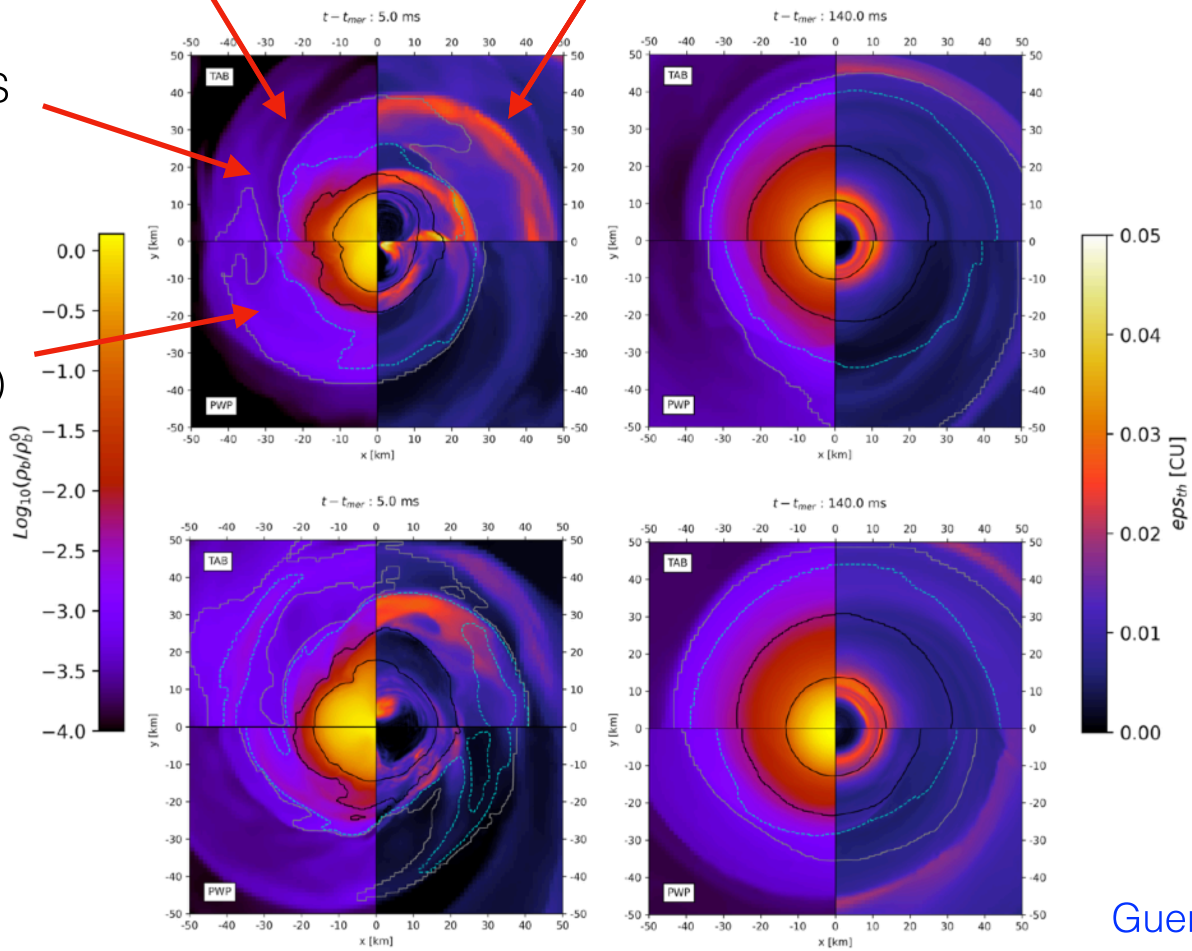

Guerra+ (2024)

At late time, bulk radius of HMNS smaller for PWP models (higher compactness) and for both EoS (~10 km decrease for HShen). Ring of higher T surrounding HMNS for thermal models.

Evolution of the lapse function: LS220

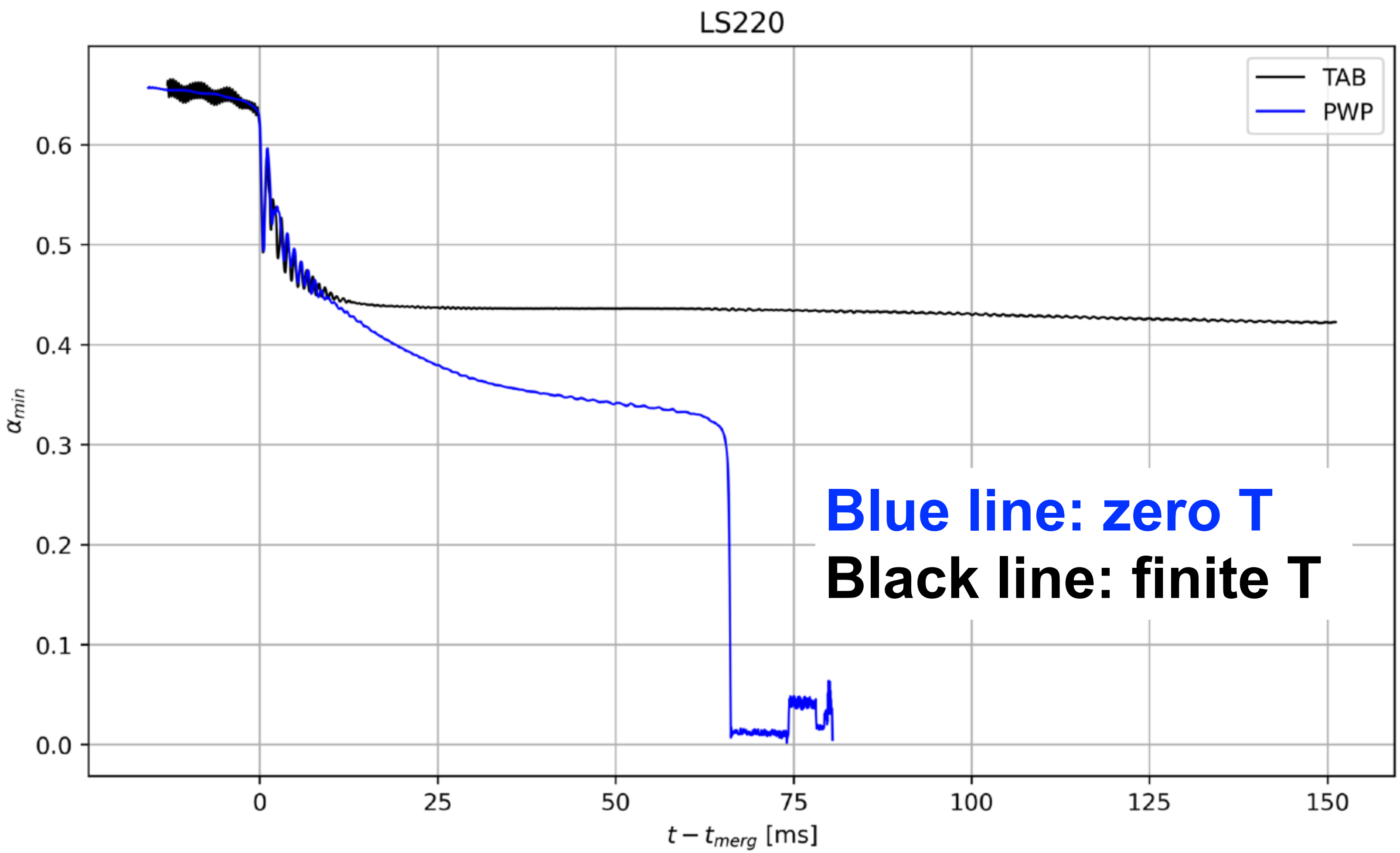

Most important dynamical difference found for LS220 EoS:

- Finite T model produces a stable HMNS
- Zero T model collapses to a BH

Differences on waveforms

Guerra+ (2024)

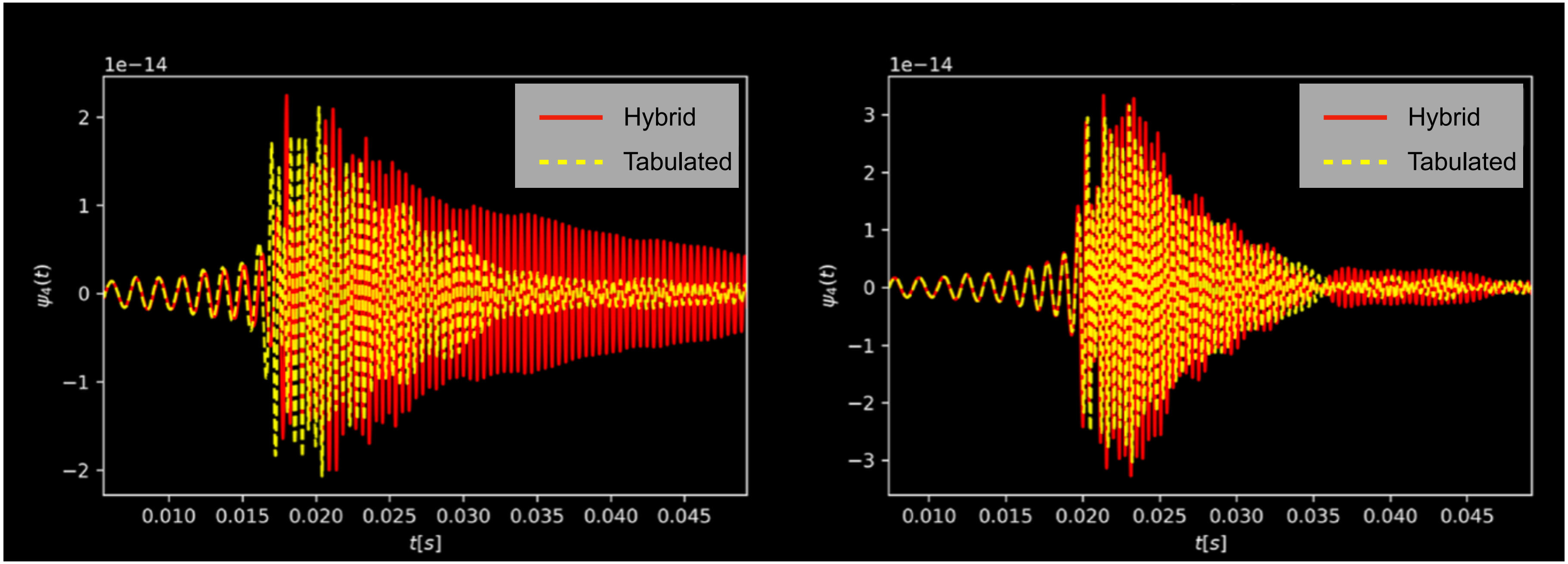

HShen DD2

Most significant differences in postmerger waveform found for HShen EoS.
HMNS oscillations damped more rapidly for tabulated EoS model.

GW spectra: HShen (top) & SLy4 (bottom)

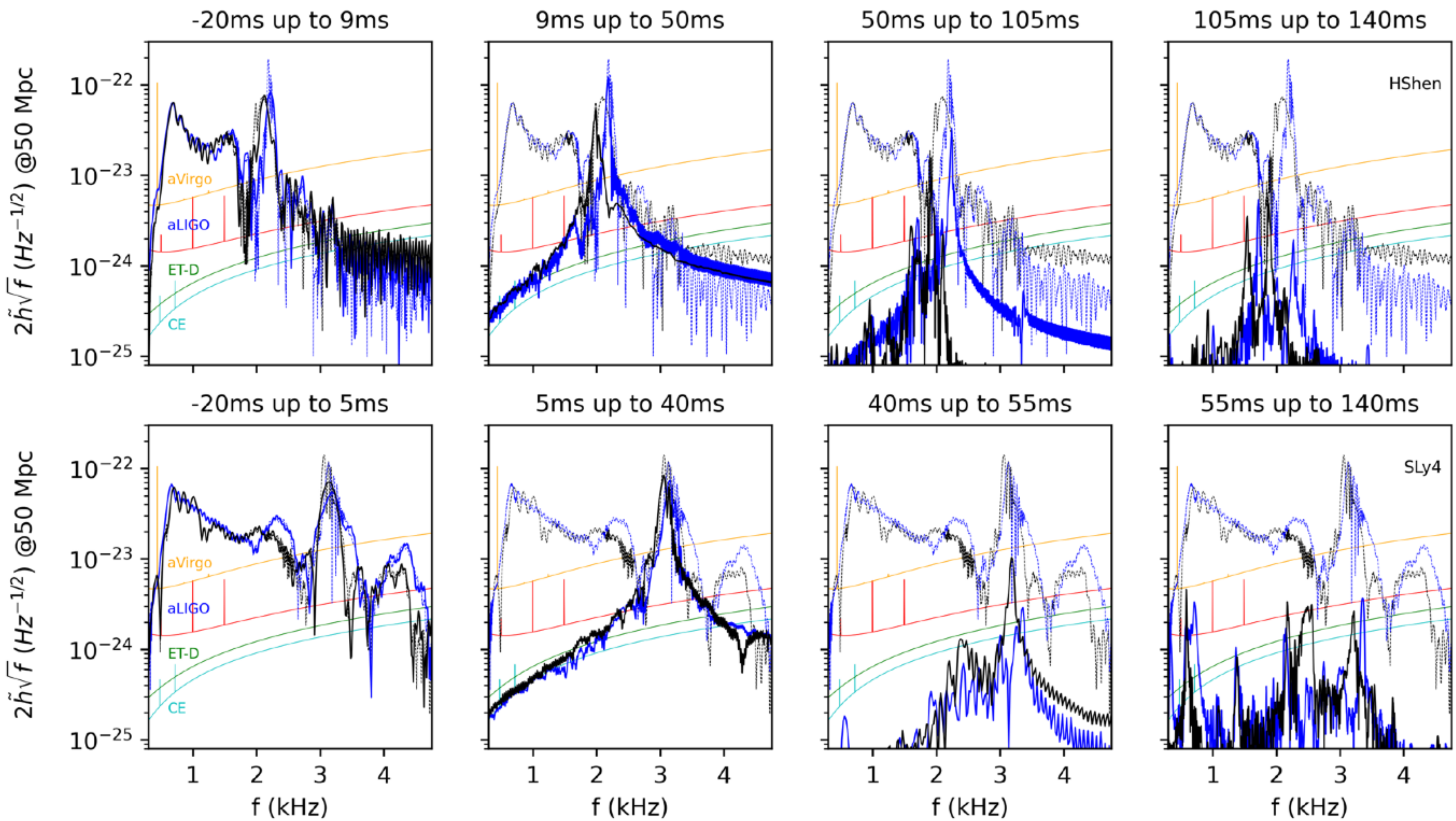

Blue curves: PWP. Black curves: TAB

Dashed lines: full PSD. Solid lines: windowed PSD

Peaks for f_2, f_{2i}, $f_{inertial}$ shifted to lower frequencies for tabulated EoS models.

HMNS asteroseismology - treatment of thermal effects

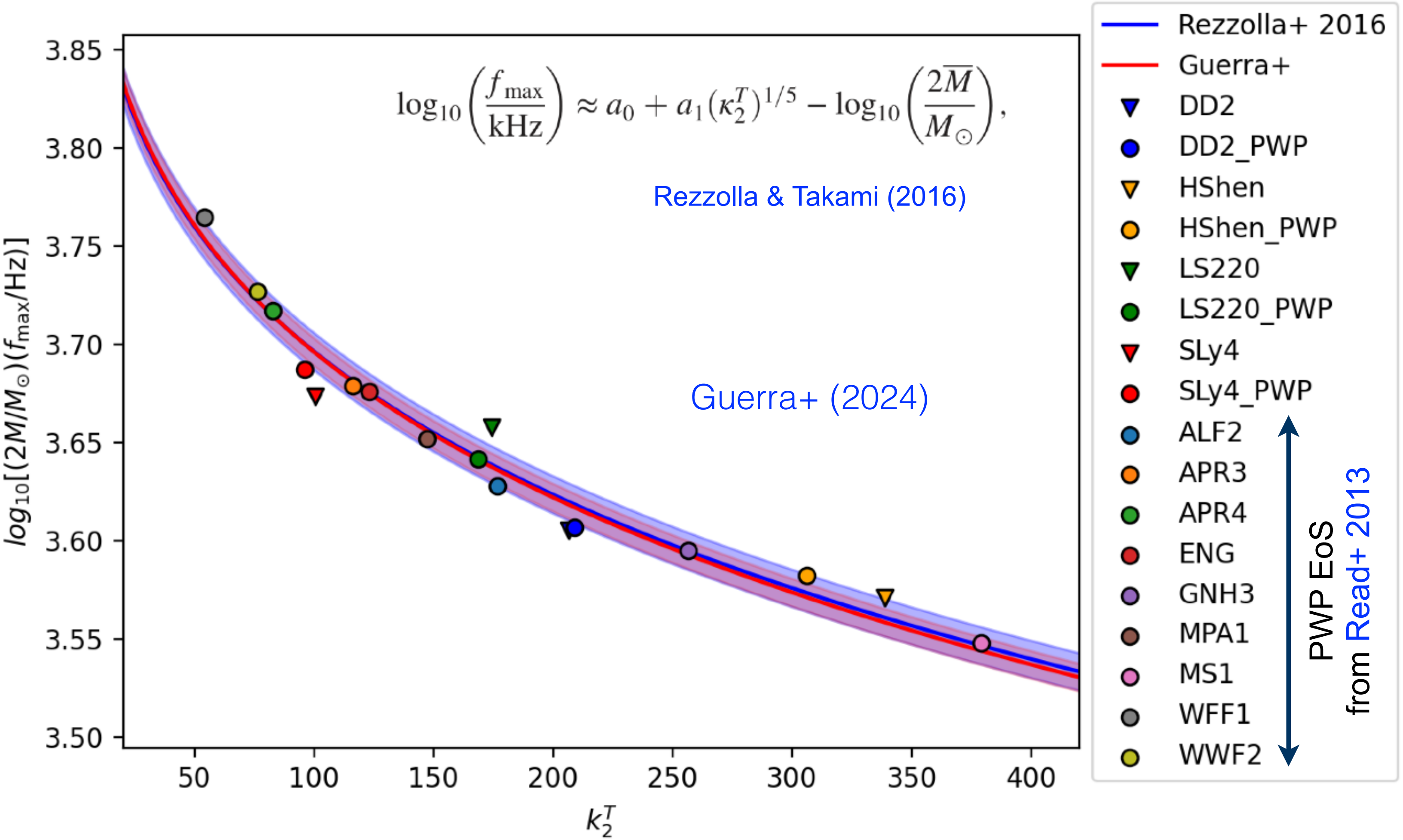

Hybrid models (circles):
similar STD for both fits (0.0095, blue shaded region)

Tabulated models (triangles):
Smaller STD (0.007; purple shaded region)

Detectability of thermal EoS treatment - `Bayeswave`

Network overlap of early post-merger signal (f_2-mode)

Miravet-Tenés+ (2024)
2401.02493

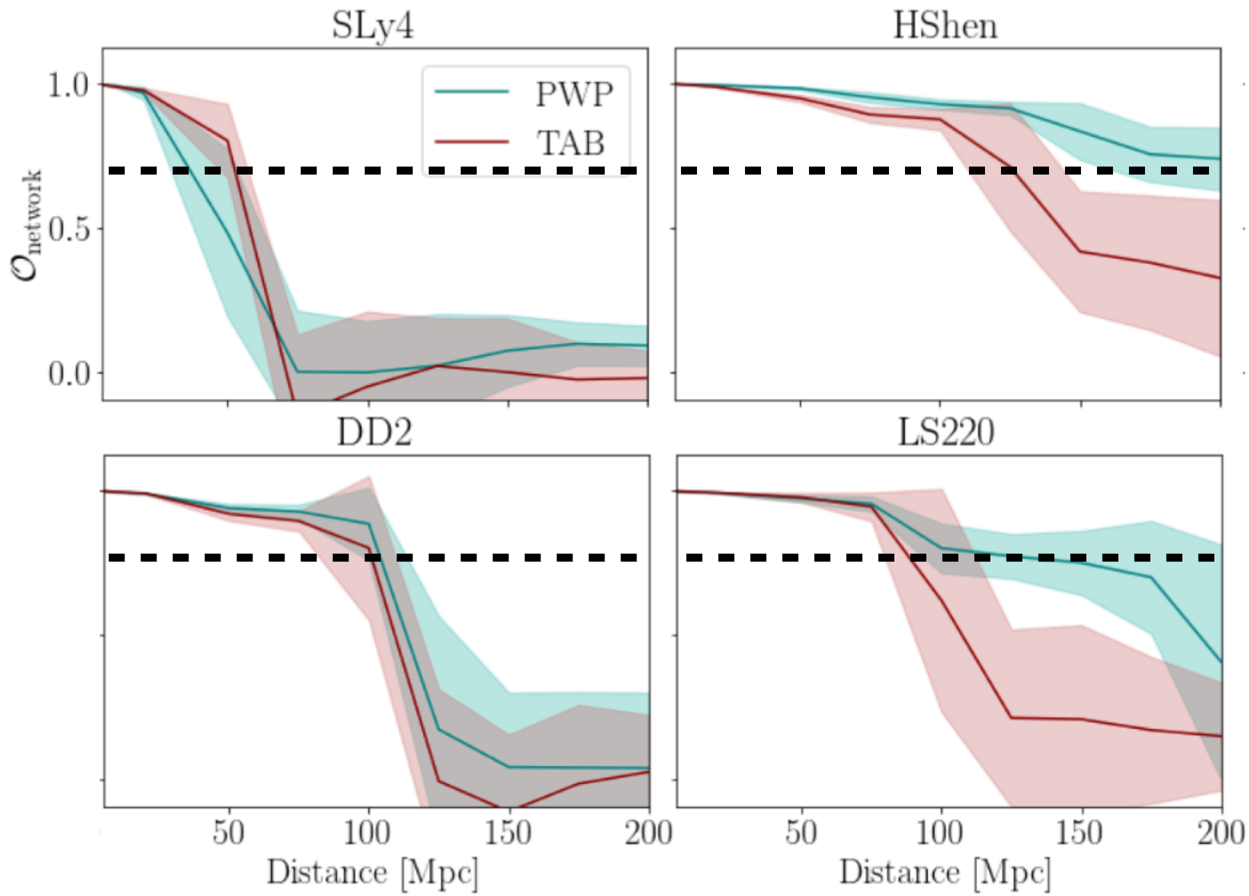

No large differences between hybrid and tabulated models.

ET overlap > 0.7 for all EoS except SLy4 even @100 Mpc.

Detectability of thermal EoS treatment - `Bayeswave`

Network overlap of late post-merger signal (inertial mode)

Miravet-Tenés+ (2024)
2401.02493

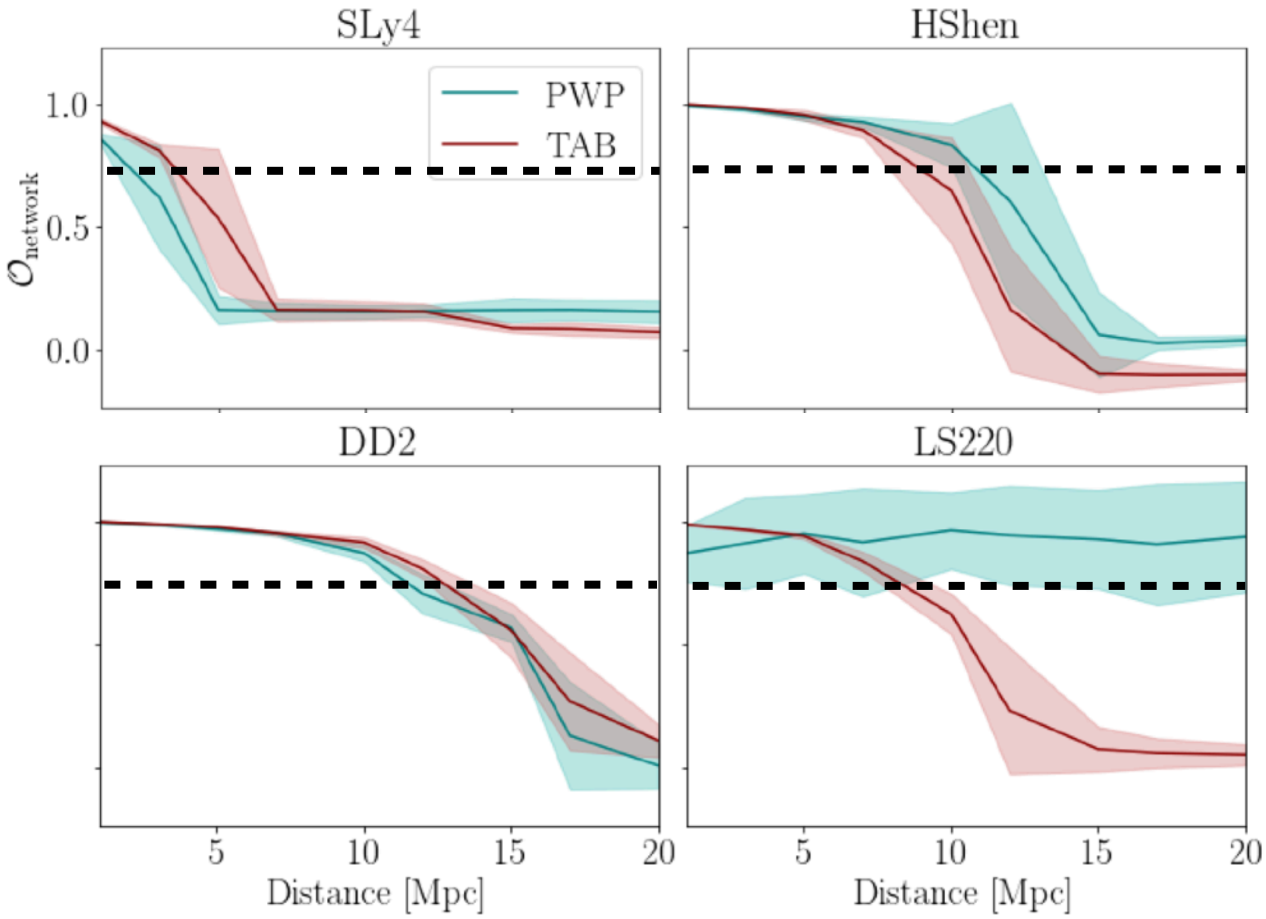

Inertial modes reconstructed properly up to **significantly closer distances** than the fundamental quadrupolar mode (10s of Mpc vs 100s of Mpc).

Inference on the f_2 peak

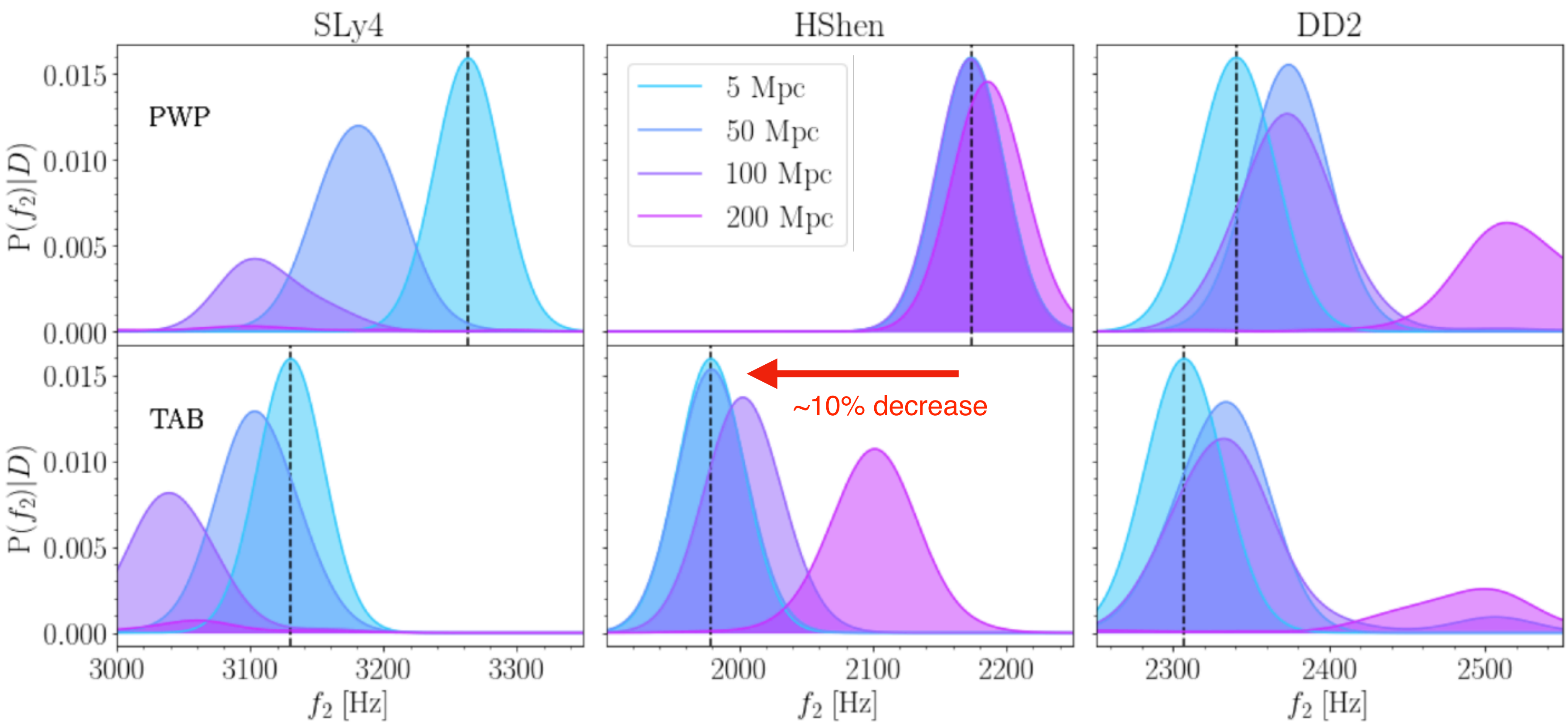

Posterior probability of the peak frequency of the f_2 mode, for different distances and PWP and TAB EoS. [Dashed vertical line: injected value]

HShen EoS shows the best results up to ~100-200 Mpc, for both types of models.

Inference on the tidal deformability

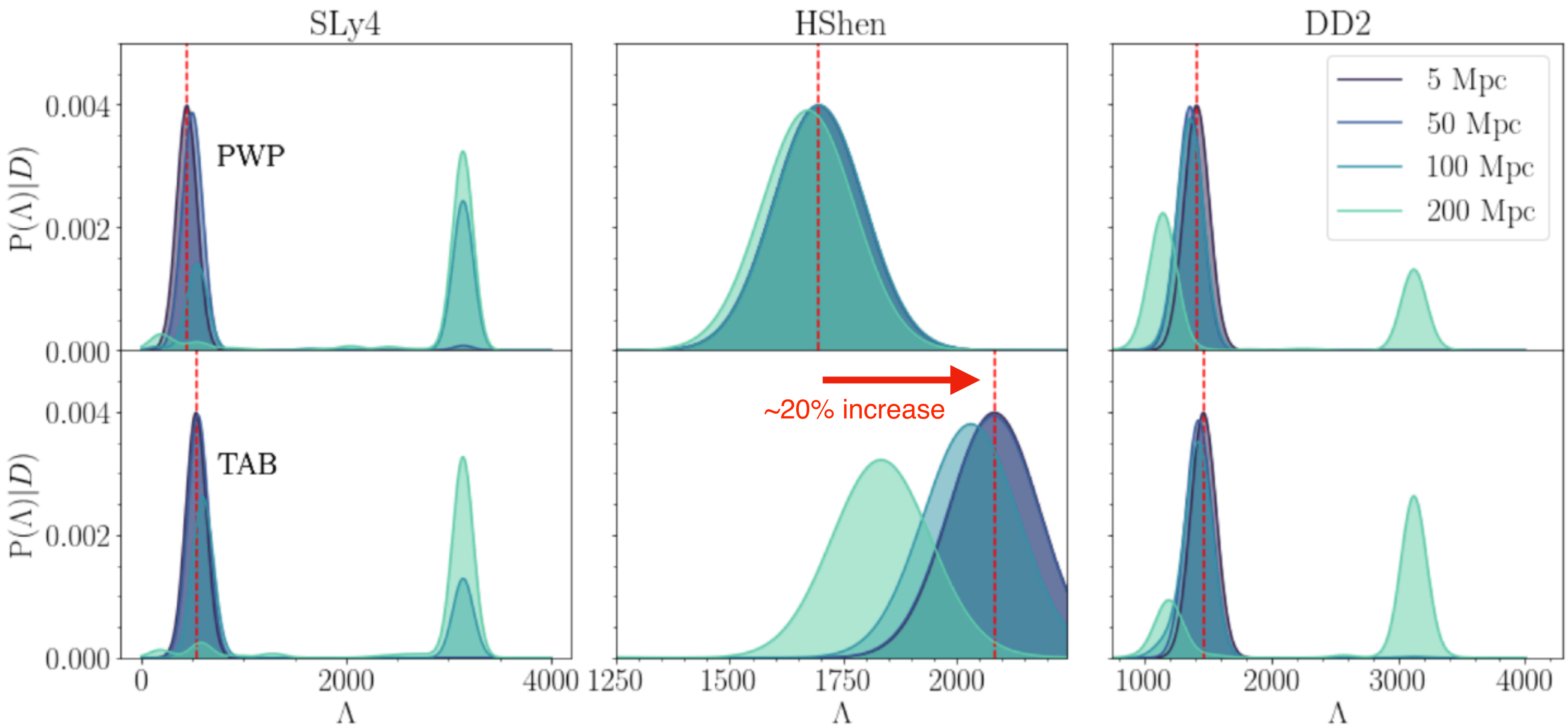

Posterior probability of tidal deformability obtained from the f_2 mode, for different distances and PWP and TAB EoS. [Dashed red vertical line: injected value].

Largest **differences between hybrid and tabulated models** found for HShen.

Detectability of thermal effects treatment

EOS	$\log \mathcal{B}^{\rm Th}_{\rm Cold}$
HShen	16.2
Sly	10.1
LS220	9.7
DD2	5.6

Log of relative Bayes Factors between tabulated and hybrid models (inclination 0.3, distance 100 Mpc)

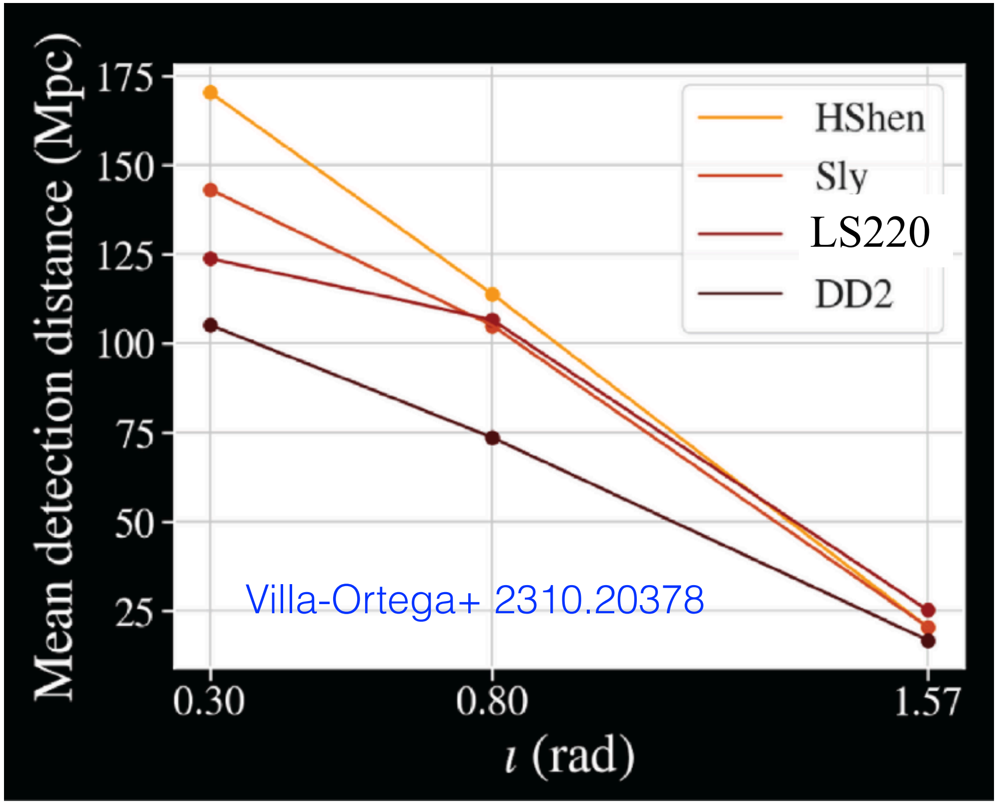

Mean detection distances (averaged over sky angles) for a mean Bayes Factor $\log \mathcal{B}^{\rm th}_{\rm cold} \sim 5$

Thermal EoS treatment detectable with $\log \mathcal{B}^{\rm th}_{\rm cold} \geq 5$ at average distances of ~ 50Mpc for source inclinations $\iota \leq 0.8$ regardless of the EoS.

Non-convex dynamics in BNS mergers

G. Rivieccio, D. Guerra, M. Ruiz & JAF (2024)
arXiv:2401.06849

QCD phase diagram

QCD phase diagram determines the form of hadronic matter depending on temperature and matter density.

(Credit: GSI Helmholtzzentrum für Schwerionenforschung GmbH, Darmstadt/Germany)

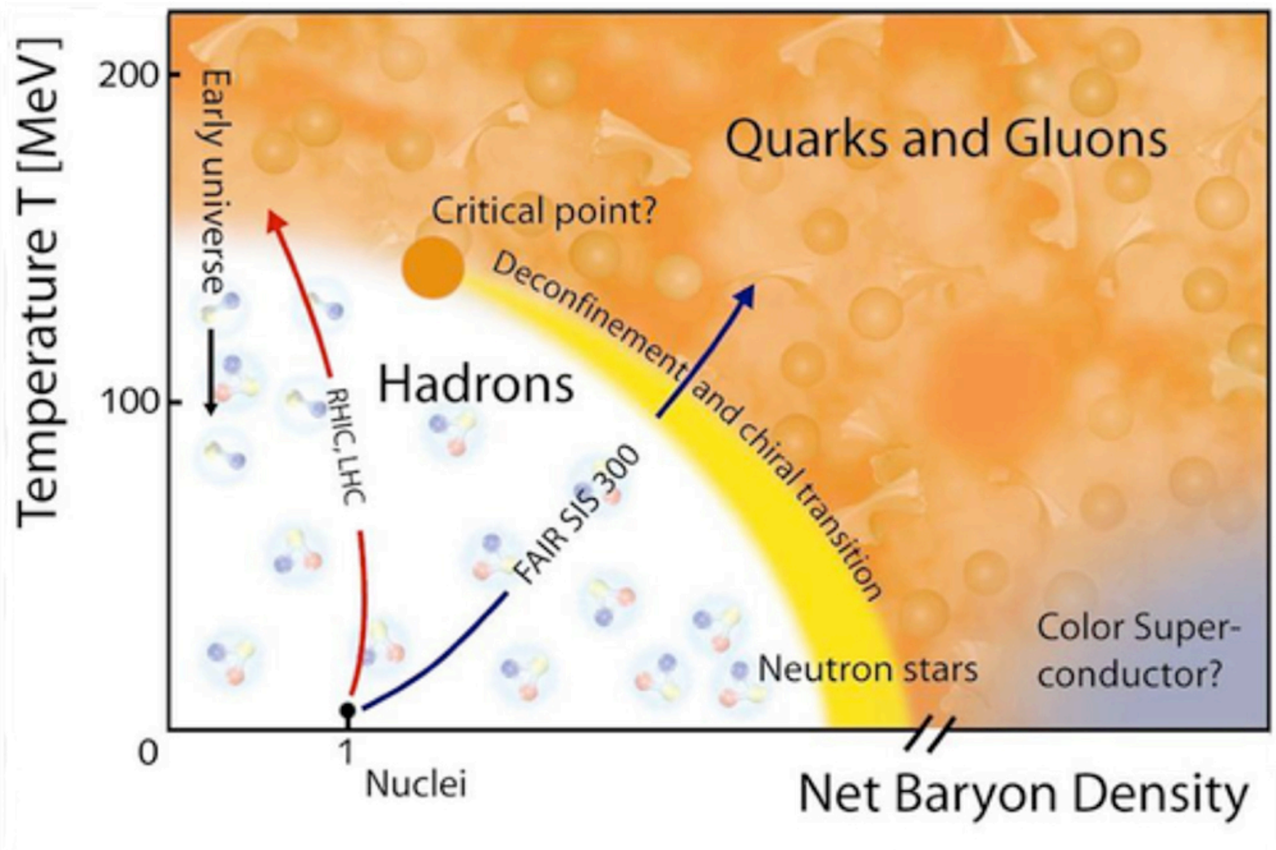

Is there a first order transition (from ordinary nuclear matter to a quark gluon plasma) and a critical point at finite density?

BNS mergers with hadron-quark phase transitions

Bauswein+ (2019) identified an observable imprint of a first-order hadron-quark PT at supranuclear densities on the GW emission of BNS mergers.

Dominant postmerger GW frequency f_{peak} may exhibit a significant deviation from an empirical relation between f_{peak} and tidal deformability if a first-order PT leads to the formation of a stable extended quark matter core in the postmerger remnant.

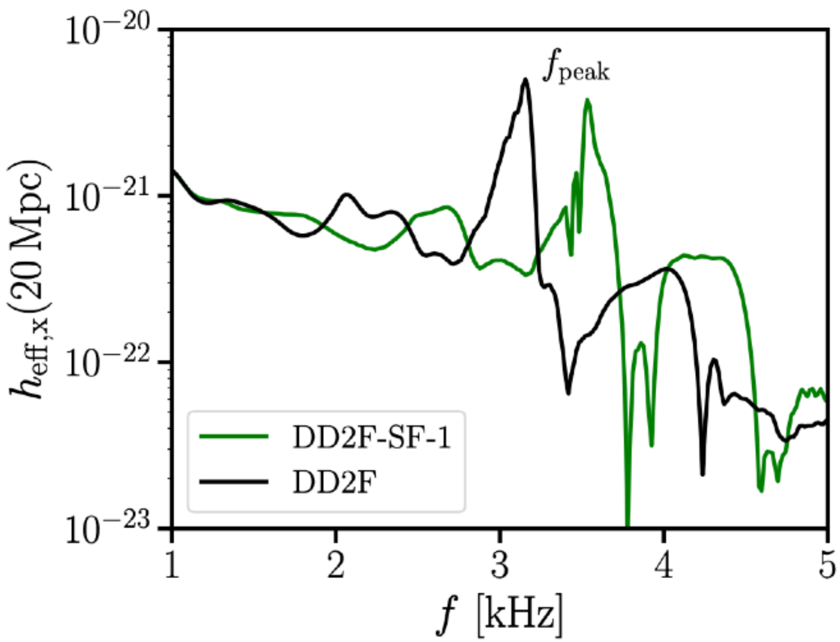

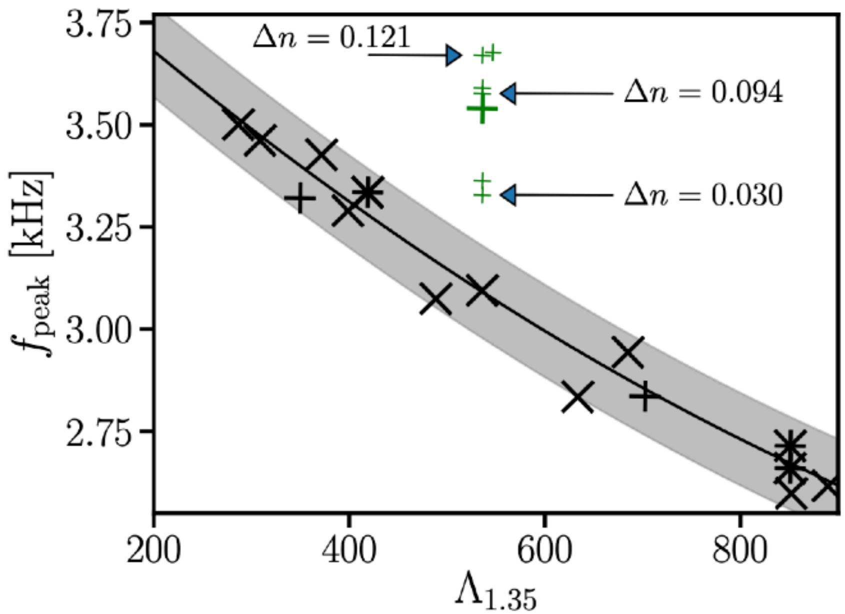

Green + : DD2F-SF EoS (PT to deconfined quarks)

Black markers: purely hadronic EoS

EoS from Wroclaw group (Fischer+ 2018, Bastian+ 2018)

(Bauswein+ 2019)

Q1: Could this shift in frequency be explained by a different reason?

Q2: Could the anomalous dynamics be triggered by a non-convex EoS?

In classical fluid dynamics, the convexity of the system is determined by the EoS, (Menikoff & Plohr 1989; Godlewski & Raviart 1996), more specifically, by the so-called fundamental derivative:

$$\mathcal{G}_{(C)} \equiv -\frac{1}{2} V \frac{\frac{\partial^2 p}{\partial V^2}}{\frac{\partial p}{\partial V}} \qquad \mathcal{G}_{(C)} = 1 + \frac{\partial \log c_s}{\partial \log \rho} = \frac{1}{2}\left(1 + \Gamma_1 + \frac{\partial \log \Gamma_1}{\partial \log \rho}\right)$$

(all derivatives computed at constant entropy)

Γ_1 adiabatic index. Characterizes stiffness of EoS at a given density, showing a local maximum above nuclear matter density.

Pioneer work on EoS-driven, non-convex thermodynamics made by Bethe (1942), Zel'dovich (1946), and Thompson (1971). The latter introduced the concept of fundamental derivative. Fluids attaining negative values of the fundamental derivative are called Bethe-Zel'dovich-Thompson fluids, or BZT fluids (e.g. van der Waals EoS; see Voss 2005).

For relativistic fluid dynamics, Ibáñez+ (2013) found a quantity analogous to the classical fundamental derivative, the relativistic fundamental derivative.

$$\mathcal{G}_{(R)} = \mathcal{G}_{(C)} - \frac{3}{2}\, c^2_{s(R)}$$

“Exotic” fluid dynamics

The fundamental derivative measures the convexity of the isentropes in the $p - \rho$ plane.

- If $\mathcal{G} > 0$, isentropes in the $p - \rho$ plane are convex, leading to expansive rarefaction waves and compressive shocks (Thompson 1971). This is the usual regime in which many astrophysical scenarios develop.
- However, some EoS may display regimes in which $\mathcal{G} < 0$ and the EoS is non-convex. The non-convexity of isentropes in the $p - \rho$ plane yield e.g. compressive rarefaction waves and expansive shocks.

These “exotic” phenomena have been observed experimentally

Cinnella & Congedo (2007)
Cinnella+ (2011).

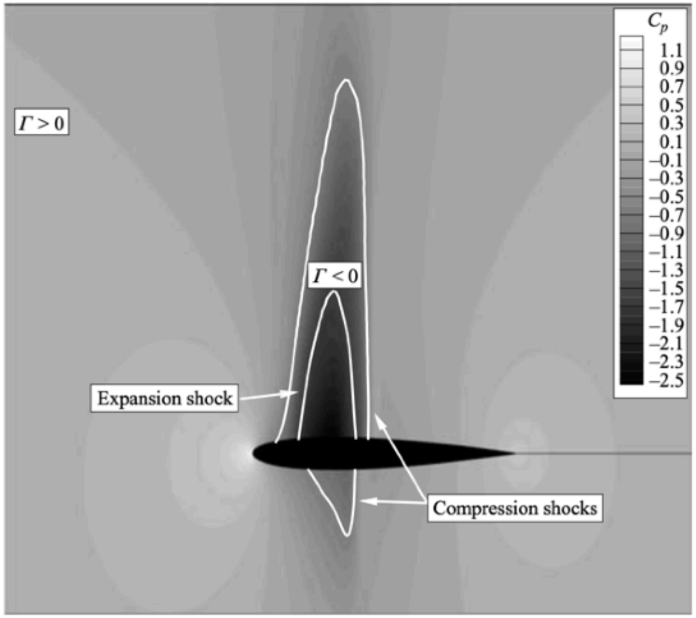

FIGURE 11. Pressure coefficient contours and $\Gamma = 0$ contours for operating conditions $p_\infty / p_c = 1.05$, $\rho_\infty / \rho_c = 0.877$, $\Gamma_\infty = 1.31$ (low-pressure transonic BZT regime).

At densities higher than nuclear saturation density n_0 nuclear/hadronic matter undergoes a phase transition into a quark-gluon plasma.

The HotQCD Collaboration (Bazavov+ 2014) and the Wuppertal-Budapest Collaboration (Borsányi+ 2014) have shown that the EoS energy density in the crossover region is about 1.2–3.1n_0. Within this temperature range $[145 \leq T(\mathrm{MeV}) \leq 163]$ the sound speed is non-monotonic.

Similar conclusions achieved by Badaque & Steiner (2015)

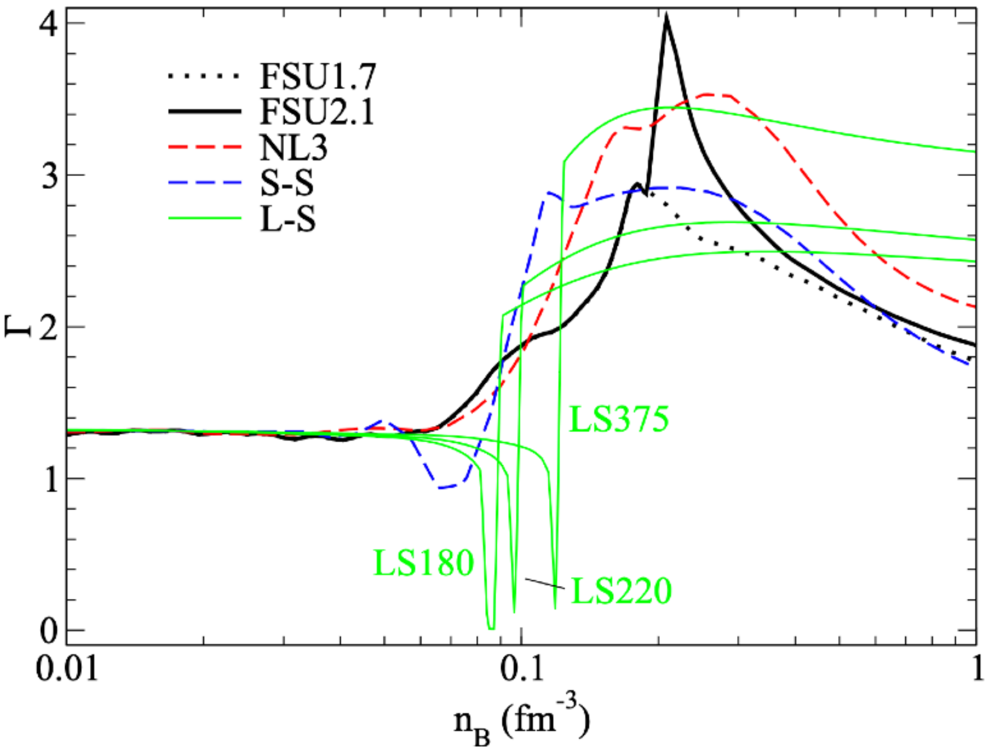

Non-monotonicity of sound speed can also result from the behaviour of the adiabatic index (see Haensel & Potekhin 2004).

Shen+ (2011)

non-monotonic behaviour of adiabatic index for various EoS broadly used in numerical simulations of core collapse supernovae and BNS mergers.

The non-monotonicity of the adiabatic index (sound speed) should be considered as a genuine feature of matter at a few times nuclear saturation density.

Under such conditions, and particularly if there are phase transitions to exotic components, the fundamental derivative could be negative, implying that the EoS be non-convex in that regime. This would lead to non-convex dynamics.

Following Ibáñez+ 2018 and Aloy+ 2018 we illustrate the effects a non-convex EoS may produce on the dynamics of BNS mergers with a phenomenological EoS. This toy-model EoS mimics the loss of convexity resulting from a non-monotonic behavior of the adiabatic index with density.

$$p = (\Gamma - 1)\rho\epsilon \qquad \Gamma = \gamma_0 + (\gamma_1 - \gamma_0)e^{-\frac{(\rho-\rho_1)^2}{\sigma^2}}$$

4 free parameters: $\gamma_0, \gamma_1, \sigma, \rho_1$

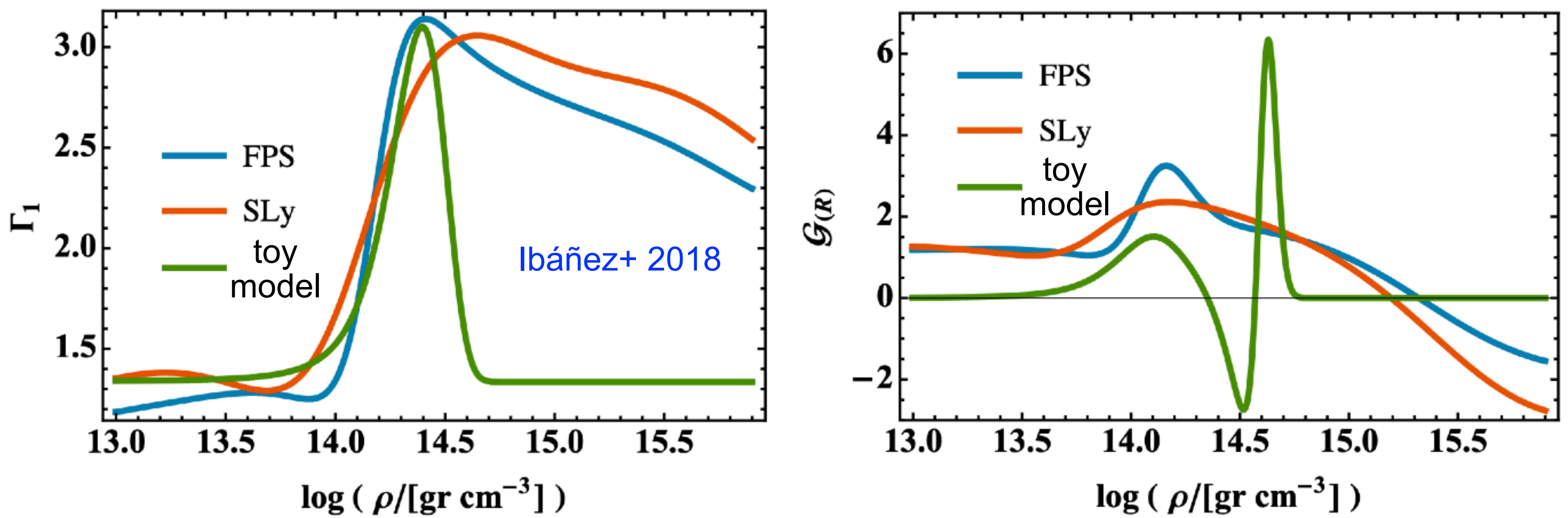

Example Riemann problem: relativistic blast wave collision

Ibáñez+ 2018

Convex dynamics
(Ideal gas EoS)

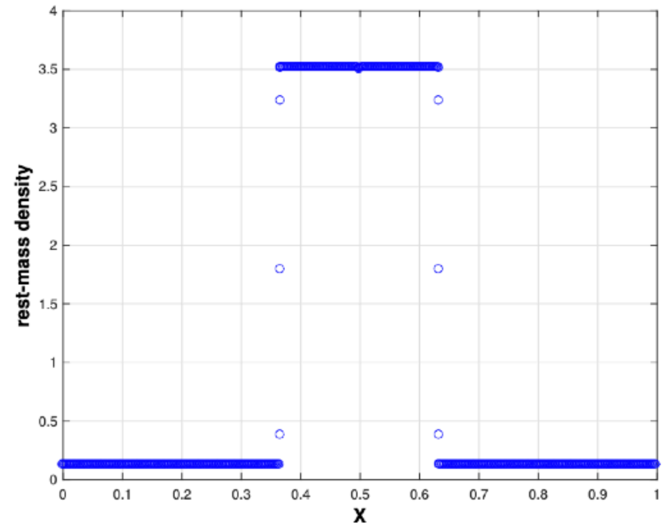

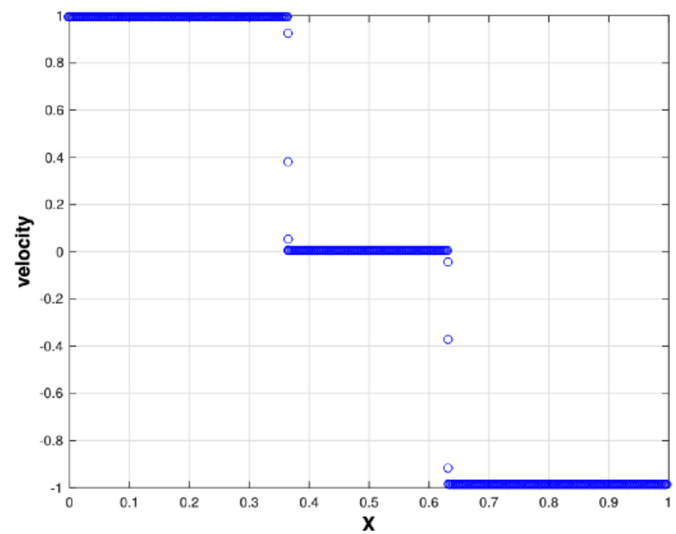

Example Riemann problem: relativistic blast wave collision

Ibáñez+ 2018

Non-convex dynamics (toy model EoS)

Convex dynamics (Ideal gas EoS)

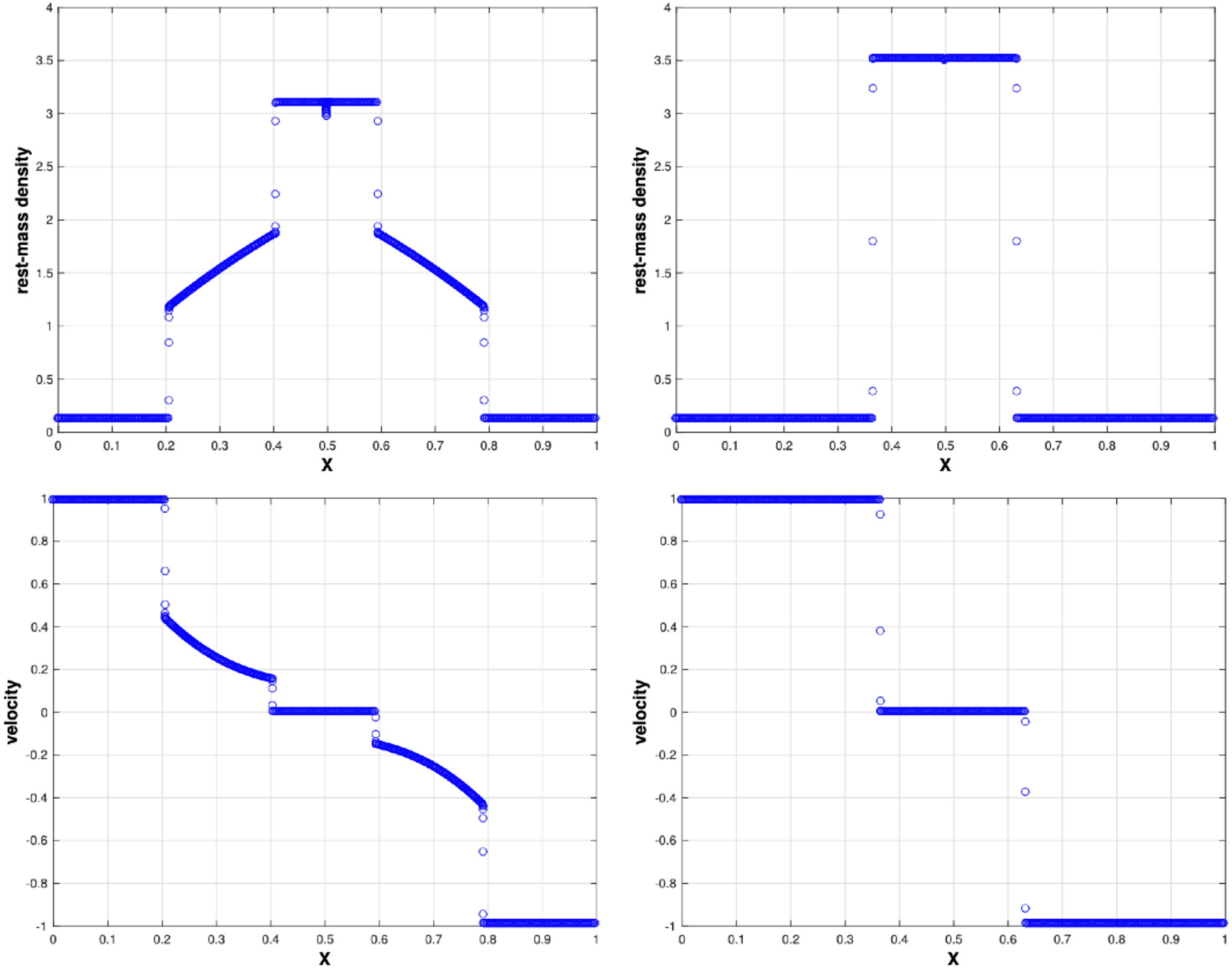

The $p-\rho$ plane for a representative BNS simulation

$$p = (\Gamma - 1)\rho\epsilon$$

$$\Gamma = \gamma_0 + (\gamma_1 - \gamma_0)e^{-\frac{(\rho-\rho_1)^2}{\sigma^2}}$$

$$\gamma_0 = 1.8$$
$$\gamma_1 = 3.0$$
$$\rho_1 = 0.91 \times 10^{15}(\text{cgs})$$
$$\sigma = 0.35\rho_1$$

Blue: convex dynamics

$(\mathcal{G}_{\rm C} > 0, \mathcal{G}_{\rm R} > 0)$

Red: convex (classical)
non-convex (relativistic)

$(\mathcal{G}_{\rm C} > 0, \mathcal{G}_{\rm R} < 0)$

Green: non-convex dynamics

$(\mathcal{G}_{\rm C} < 0, \mathcal{G}_{\rm R} < 0)$

Black: sound speed out of bounds

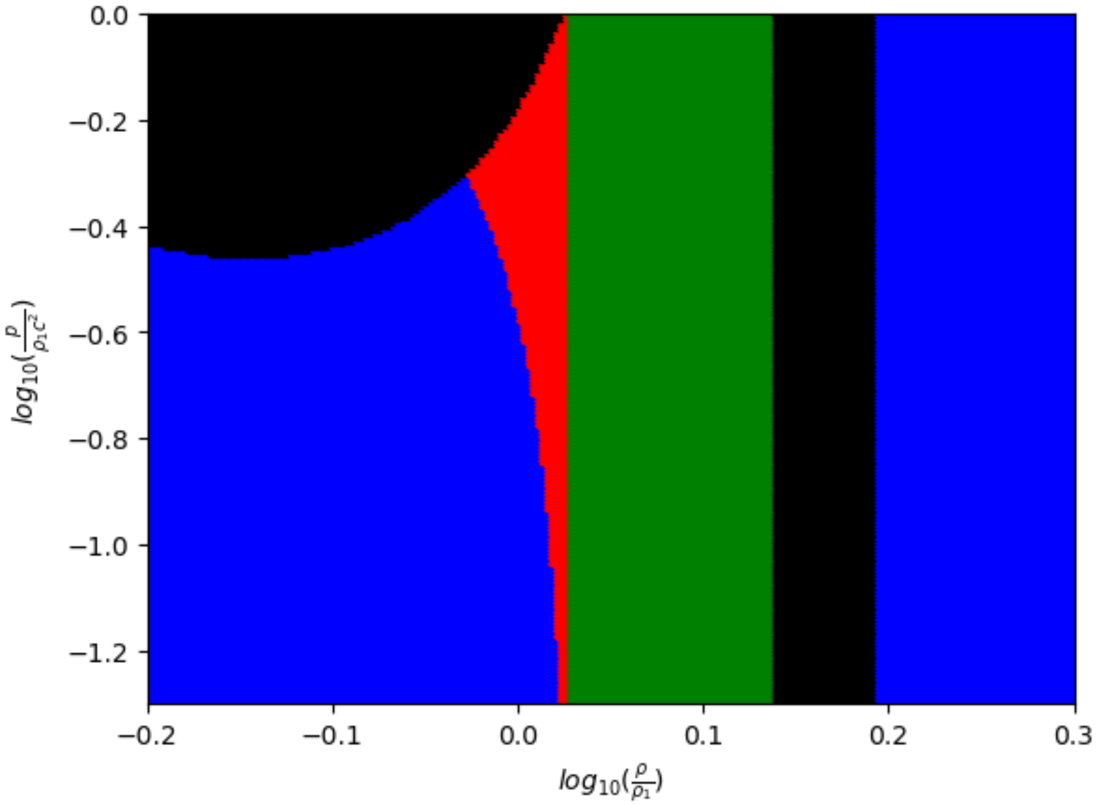

Non-convex BNS simulation

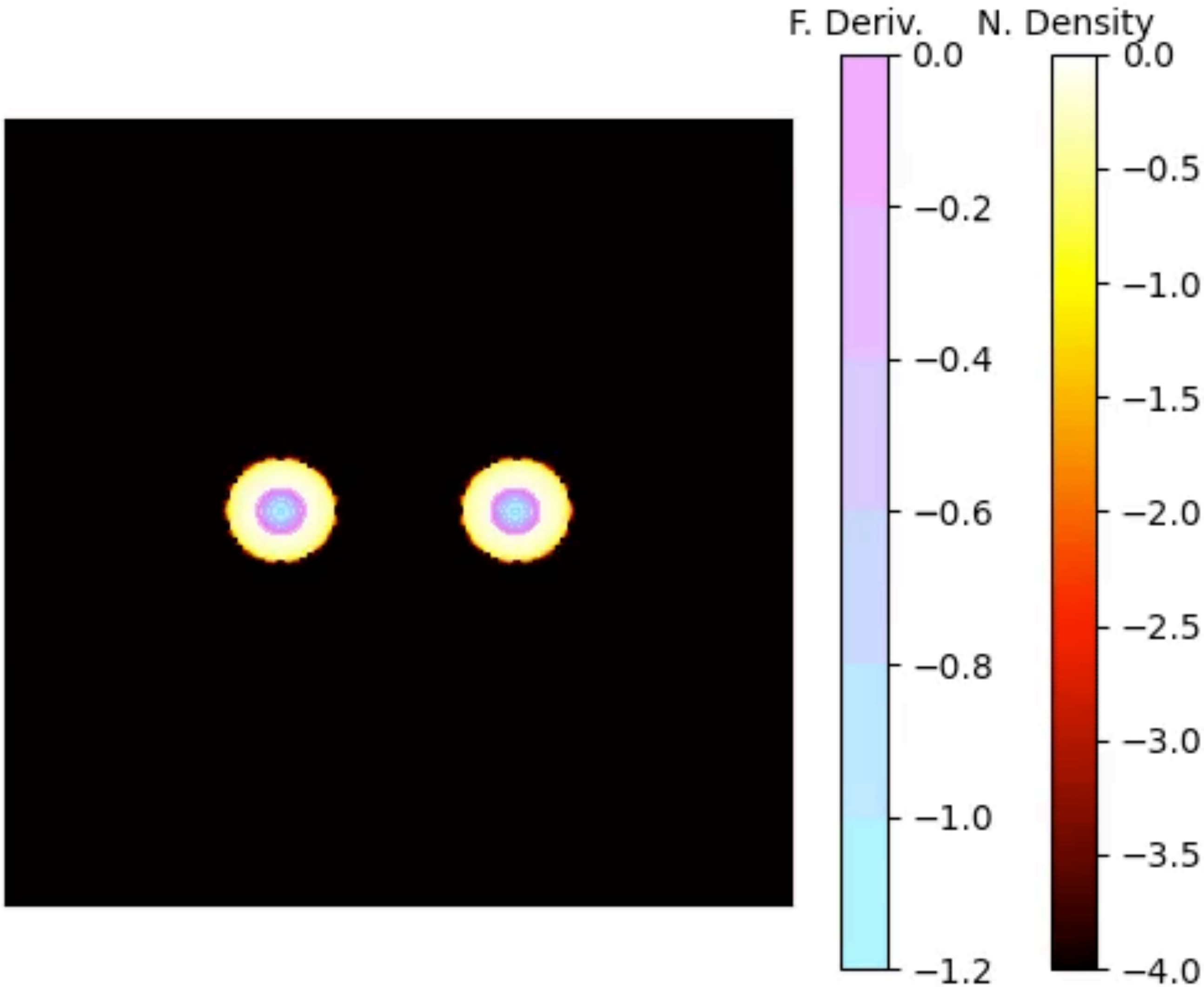

Empirical universal relations affected by non-convex dynamics

Set of models considered

EOS	$M[M_\odot]$	$\mathcal{C}$	Λ	$M_{\rm ADM}[M_\odot]$	$J_{\rm ADM}[M_\odot^2]$	Ω
WFF1	1.26	0.18	406.07	2.50	6.45	1.76
WFF2	1.27	0.17	1115.06	2.52	6.54	1.76
APR4	1.28	0.17	440.75	2.52	6.56	1.77
SLy4	1.28	0.16	512.57	2.54	6.62	1.77
APR3	1.28	0.16	620.00	2.53	6.61	1.77
ENG	1.28	0.16	636.35	2.53	6.60	1.77
MPA1	1.28	0.15	784.52	2.54	6.64	1.77
LS220	1.29	0.15	899.69	2.55	6.69	1.77
ALF2	1.29	0.15	941.42	2.54	6.66	1.77
DD2	1.29	0.13	1115.1	2.56	6.73	1.78
HShen	1.30	0.14	1633.39	2.58	6.82	1.78
GNH3	1.30	0.13	1371.15	2.58	6.81	1.78
MS1	1.30	0.13	2020.75	2.58	6.83	1.79

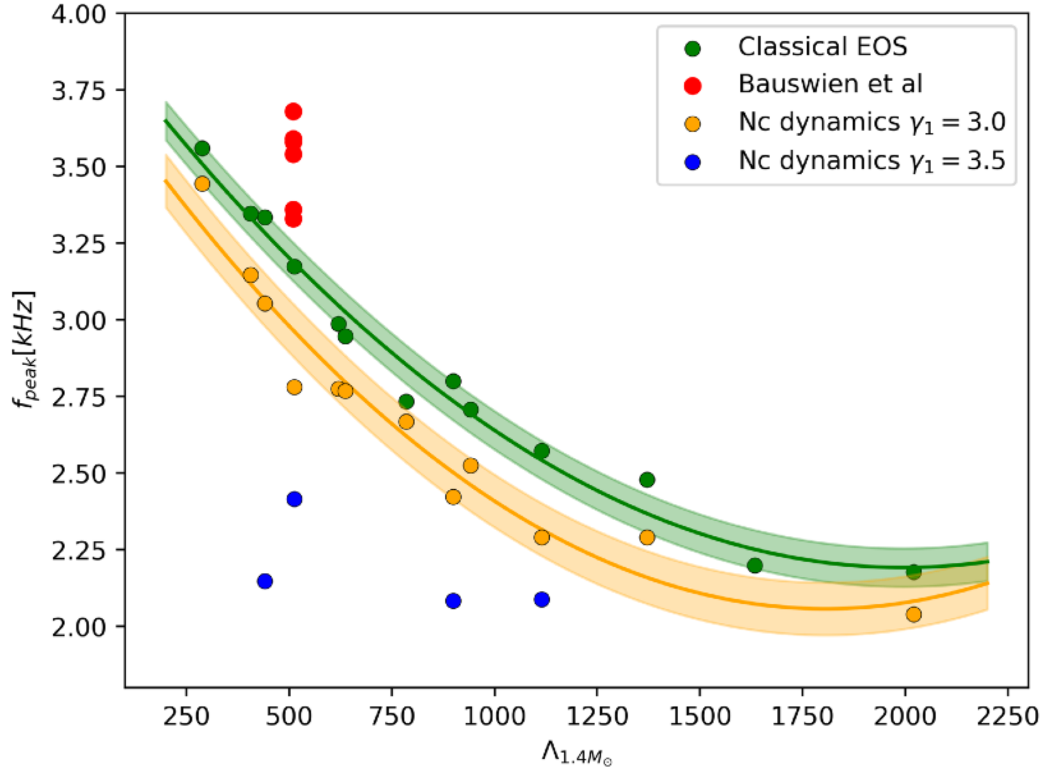

Significant shifts in frequency observed for f_2 mode.

They can be as large as ~ 500 Hz for some choice of the parameters of the toy model EoS.

Do these findings hold for realistic EoS?

Going further

Postmerger dynamics and waveforms can also be affected by

- Effect of B-field amplification
- Effect of viscosity
- Neutrinos

Waveform generation (both inspiral and postmerger) and parameter estimation to be aided by AI and Deep Learning.

Thank you for your attention!

Main collaborators:

Davide Guerra (PhD student @ UV)
Miquel Miravet-Tenés (PhD student @ UV)
Giuseppe Rivieccio (PhD student @ UV)
Milton Ruiz (senior post-doc @ UV)
Pablo Cerdá-Durán (faculty @ UV)

Roberto De Pietri (faculty @ Parma University)
Nikolaos Stergioulas (faculty @ AUTH)

Acknowledgements:

Spanish Research Agency (PID2021-125485NB-C21)
Prometeo Grant Generalitat Valenciana (CIPROM/2022/49)
EU RISE and SE programs (H2020-MSCA-RISE-2017 (FunFiCO-777740) and HORIZON-MSCA-2021-SE-01 (NewFunFiCO-101086251))
Allocations from the Spanish Supercomputing Network (MareNostrum and others)